POLITECNICO DI TORINO

Master's Degree in Mechanical Engineering

Master's Degree Thesis

Development of a Virtual Test Rig for the Assessment of the Fuel Economy Potential of an Innovative Plug-in Hybrid Electric Vehicle

Supervisors:
Prof. Luciano Rolando
Prof. Federico Millo

Candidate:
Lorenzo Carniel

Academic Year 2025/26

“Scientists discover the world that exists;

engineers create the world that never was.”

Theodore von Kármán

Acknowledgements

First, I would like to express my deepest gratitude to Professor Federico Millo and Professor Luciano Rolando for making this project possible and for their constant availability throughout these months. A special acknowledgement goes to Mario Milite and the entire “e3” group for their guidance, expertise, and the positive attitude they always showed.

My sincere thanks also go to my family, my parents, grandparents, and my brother, for their unwavering support throughout my academic career and beyond.

Finally, I would like to thank all my friends and everyone with whom I have shared this journey for the encouragement, and unforgettable moments we experienced together.

Abstract

The increasingly stringent regulations regarding greenhouse gas and pollutant emissions imposed by the European Union through both the Fit-for-55 package and the Euro 7 standard require the rapid development of innovative and environmentally sustainable propulsion systems. Among the wide range of possible solutions, high-efficiency internal combustion engines and their integration into hybrid powertrain architectures represent a viable pathway, at least in the short term.

Within this framework, the Horizon 2020 PHOENICE project was developed with the aim of demonstrating the potential of a plug-in hybrid electric vehicle to reduce both pollutant emissions and fuel consumption. The adoption of innovative technologies, such as highly diluted charge operation, an electrified turbocharging system and an innovative in-cylinder charge motion, enables indicated efficiency values of up to 47%. In addition, the implementation of a state-of-the-art aftertreatment system allows pollutant emissions to be reduced in compliance with the Euro 7 regulations.

To optimize the introduced technologies and maximize overall performance, such an innovative project requires predictive and physics-based models with varying degrees of accuracy, both 1D and 0D map-based. Initially, the research activity focused on the development of the existing 1D simulation platform. Thanks to 3D CFD simulations, it was possible to improve the predictive capabilities of the engine model, particularly in terms of turbulence prediction, which has a significant impact on combustion due to the innovative charge motion configuration combined with the adoption of aggressive Miller strategies. The core of this research activity, however, was the development of a virtual test rig aimed at evaluating fuel consumption and optimizing the vehicle operating strategy. To further extend the scope of the project analyses, an Equivalent Consumption Minimization Strategy was implemented, capable of determining a local optimum for energy management at each instant of the driving cycle.

The results obtained demonstrate that the adopted control strategy is capable of optimizing energy utilization and, consequently, reducing both fuel consumption and emissions. Furthermore, the developed model enables the analysis to be extended to different driving cycles and operating conditions, thereby broadening the scope and applicability of the project.

Table of Contents:

Acknowledgements IV

Abstract V

Table of Contents: VI

Table of Figures VIII

Table of Tables X

List of Acronyms XII

1 Introduction 1

1.1 The Legislative Framework 1

1.2 European Commission Proposals 1

1.3 The Role of the Research 3

1.4 The PHOENICE Project 4

1.5 The scope of the thesis 5

2 The PHOENICE Project 7

2.1 Introduction 7

2.2 The Engine Technical Specifications 7

3 Methodology 10

3.1 Introduction 10

3.2 Data 10

3.2.1 Politecnico di Torino Dataset 11

3.2.2 IFPEN Dataset 12

3.3 Engine Digital Twin Refinement 13

3.3.1 TPA Model 13

3.3.2 Intake Ports Flow Analysis 19

3.4 Vehicle Virtual Test Rig 25

3.4.1 Hybrid Drivetrain Implementation in GT-SUITE 26

3.4.2 ECMS Controller Setup 28

3.5 Conclusions 35

4 Digital Twin Refinement Results 37

4.1 Introduction 37

4.2 TPA Model Results 37
4.3 Intake Flow Analysis Results 56
4.4 Conclusions 63
5 Vehicle Virtual Test Rig Results 65
5.1 Introduction 65
5.2 ECMS Implementation Results 66
5.3 Conclusions 76
6 Conclusions 78
Bibliography 80

Table of Figures

Figure 1: Euro 7 exhaust emission limits for Passenger Cars of Category M1 and Light-Duty Vans of Category N1 [2] 2

Figure 2: PHOENICE Project innovation areas [17] 5

Figure 3: Main PHOENICE engine technologies [17] 8

Figure 4: Engine operating points 12

Figure 5: TPA model on GT-SUITE simulation platform 14

Figure 6: TKE profiles with and without fuel injection 15

Figure 7: Turbulence calibration parameters available on GT-SUITE 16

Figure 8: Baseline single-cylinder 3D model provided by Politecnico di Torino 20

Figure 9: Simplified model with the appropriate geometric modifications 21

Figure 10: Location of the first level of mesh refinement 22

Figure 11: Discharge Coefficient values provided by IFPEN 23

Figure 12: Model changes for the reverse discharge coefficient simulations 24

Figure 13: C-SUV class PHEV considered 25

Figure 14: P0 P4 hybrid architecture 25

Figure 15: Virtual Test Rig Baseline Layout 27

Figure 16: WLTC speed profile 28

Figure 17: Vehicle Main Model 31

Figure 18: Vehicle Surrogate Model 31

Figure 19: Default Penalty Function 34

Figure 20: Penalty Function for asymmetric setup 35

Figure 21: Pressure cycle for 4500 rpm x 16 bar BMEP 40

Figure 22: Trapped mass for 4500 rpm x 16 bar BMEP 41

Figure 23: Turbulence profiles for 4500 rpm x 16 bar BMEP 42

Figure 24: Pressure cycle for 2500 rpm x 10 bar BMEP 44

Figure 25: Trapped mass for 2500 rpm x 10 bar BMEP 44

Figure 26: Turbulence profiles for 2500 rpm x 10 bar BMEP 45

Figure 27: Pressure cycle for 2000 rpm x 6 bar BMEP 47

Figure 28: Trapped mass for 2000 rpm x 6 bar BMEP 47

Figure 29: Turbulence profiles for 2000 rpm x 6 bar BMEP......48
Figure 30: Spray/Jet Term Multiplier influence on TKE profiles......50
Figure 31: Optimized turbulence profiles for 4500 rpm x 16 bar BMEP......52
Figure 32: Optimized turbulence profiles for 2500 rpm x 10 bar BMEP......53
Figure 33: Optimized turbulence profiles for 2000 rpm x 6 bar BMEP......55
Figure 34: Mass Flow Rates for forward CDs......57
Figure 35: Forward CDs profiles......59
Figure 36: Mass Flow Rates for reverse CDs......61
Figure 37: Discharge coefficients profiles......63
Figure 38: WLTC speed profile for a C SUV-class PHEV......65
Figure 39: Simulated speed profile......66
Figure 40: Wheel Torque Request......67
Figure 41: Penalty Function for alpha=1......68
Figure 42: Battery SOC and vehicle operating mode......69
Figure 43: Starter Torque......70
Figure 44: ICE, P0 and P4 Brake Torque profiles......71
Figure 45: P0 Brake Torque and its limits......72
Figure 46: P4 Brake Torque and its upper limit......73
Figure 47: Gear Number profile......73
Figure 48: ICE Speed......74
Figure 49: ICE BMEP......74
Figure 50: ICE BSFC Map......75

Table of Tables

Table 1: PHOENICE Project targets.......5
Table 2: PHOENICE Engine Technical Specifications.......8
Table 3: Engine operating points provided by Politecnico di Torino.......11
Table 4: CR and HTM values in the TPA model.......15
Table 5: Updated engine operating points in the Politecnico di Torino dataset.......16
Table 6: Spray/Jet Term Multiplier optimal value.......17
Table 7: Integration window used in the optimization process.......18
Table 8: Parameters introduced into the Design Optimizer.......18
Table 9: Turbulence calibration parameters optimized values.......19
Table 10: Valve Lift values adopted in the analysis.......21
Table 11: Main properties for the second level of mesh refinement.......22
Table 12: Valve lifts and the corresponding model configurations.......23
Table 13: Vehicle Parameters.......26
Table 14: Vehicle State Signals.......29
Table 15: Optimal State Signals.......30
Table 16: Event Manager Setup.......30
Table 17: Backward State Optimization Control Inputs.......32
Table 18: Time Delays for the Backward State Optimization.......32
Table 19: Change Rate for the Backward State Optimization.......33
Table 20: Dependent Variables Limits for the Backward State Optimization.......33
Table 21: Asymmetric SOC values.......35
Table 22: Geometric and thermal calibration parameters.......38
Table 23: Turbulence calibration parameters initial values.......38
Table 24: First operating point.......39
Table 25: Second operating point.......43
Table 26: Third operating point.......46
Table 27: Spray/Jet Term Multiplier final value.......51
Table 28: Turbulence parameters optimized values.......51
Table 29: Valve lifts for CDs calculation.......56

Table 30: Mean Mass Flow Rate through the measurement region ... 58
Table 31: Forward CDs values ... 59
Table 32: Intake valves Mass Flow Rate values ... 62
Table 33: Intake valves discharge coefficients values ... 62
Table 34: Initial and final SOC values provided by IFPEN ... 67
Table 35: Equivalence factor and penalty function exponent calibrated values ... 67
Table 36: ECMS main parameters ... 69
Table 37: Fuel Consumption and CO_2 emissions ... 76

List of Acronyms

ASC	Ammonia Slip Catalyst
BDC	Bottom Dead Centre
BMEP	Brake Mean Effective Pressure
BMS	Battery Management System
BSFC	Brake Specific Fuel Consumption
CA	Crank Angle
CAD	Crank Angle Degree
CAI	Controlled Auto Ignition
CD	Charge Depleting
CDs	Discharge Coefficients
CFD	Computational Fluid Dynamics
CH_4	Methane
CO	Carbon Monoxide
CO_2	Carbon Dioxide
CR	Compression Ratio
CS	Charge Sustaining
DDCA	Dual Dilution Combustion Approach
EATS	Exhaust After Treatment System
e-AWD	Electric All Wheel Drive
ECMS	Equivalent Consumption Minimization Strategy
EGR	Exhaust Gas Recirculation
EHC	Electrically Heated Catalyst
EIVC	Early Intake Valve Closing
EV	Electric Vehicle
EVO	Exhaust Valve Opening
FMEP	Friction Mean Effective Pressure
GDI	Gasoline Direct Ignition
GPF	Gasoline Particulate Filter
GT-SUITE	Gamma Technologies Simulation Suite
HCCI	Homogeneous Charge Compression Ignition
HEV	Hybrid Electric Vehicle
HTM	Heat Transfer Multiplier

ICE	Internal Combustion Engine
IFPEN	Institut Français du Pétrole et des Énergies Nouvelles
IVC	Intake Valve Closing
LIVC	Late Intake Valve Closing
LP-EGR	Low Pressure Exhaust Gas Recirculation
LS	Normalized Length Scale
NH_3	Ammonia
NO_x	Nitrogen Oxides
PFP	Peak Firing Pressure
PHEV	Plug-in Hybrid Electric Vehicle
PM	Particulate Matter
PN	Particle Number
RDE	Real Driving Emissions
RSE	Root Square Error
SA	Spark Advance
SCR	Selective Catalytic Reduction
SOC	State of Charge
SOI	Start of Injection
SPCCI	Spark Controlled Compression Ignition
SUV	Sport Utility Vehicle
TDC	Top Dead Centre
THC	Total Hydrocarbons
TKE	Turbulent Kinetic Energy
TPA	Three Pressure Analysis
TWC	Three-Way Catalyst
VKA	Vehicle Kinematic Analysis
VNT	Variable Nozzle Turbine
VVA	Variable Valve Actuation
WLTC	Worldwide Harmonized Light Vehicles Test Cycle
WLTP	Worldwide Harmonized Light Vehicles Test Procedure
WOT	Wide Open Throttle

1 Introduction

1.1 The Legislative Framework

In recent years, the road transport sector has undergone a profound transformation driven by the growing need to reduce greenhouse gas emissions, improve air quality, and decrease dependence on fossil fuels. As one of the major contributors to climate change, this sector has become the focus of increasingly stringent environmental policies. In response, the European Commission has progressively introduced a comprehensive regulatory framework aimed at reducing the environmental impact of road transportation.

Within this context, the Euro 7 regulation, first proposed by the European Commission in November 2022 [1] and subsequently adopted in its final form in 2024 [2], establishes new requirements for vehicle type approval concerning emissions and battery durability. The new regulatory framework aims at ensuring low and stable emission levels throughout the entire vehicle lifetime by introducing more stringent requirements for emissions monitoring, system durability, and the regulation of a broader range of pollutants compared with previous emission standards.

At the same time, the ambitious decarbonization targets set by the European Union have accelerated the development of low-emission powertrain technologies. In this scenario, Hybrid Electric Vehicles (HEVs) and Plug-in Hybrid Electric Vehicles (PHEVs) represent one of the most effective transitional solutions toward the progressive electrification of the vehicle fleet.

The PHOENICE (PHev towards zerO EmissioNs & ultimate ICE efficiency) project fits within this framework. Its objective is to develop a C-SUV class Plug-in Hybrid Electric Vehicle demonstrator capable of minimizing both energy consumption and pollutant emissions under real-world driving conditions, with particular emphasis on charge-sustaining operation. At the same time, the project aims at ensuring high vehicle performance and drivability by integrating innovative solutions for internal combustion engine optimization, hybrid energy management, and advanced emission control strategies.

1.2 European Commission Proposals

The European Union has progressively strengthened its environmental policies to reduce both greenhouse gas and air pollutant emissions from the road transport sector. This strategy combines ambitious decarbonization targets with increasingly stringent emission standards for new vehicles, encouraging the development of more sustainable propulsion technologies.

As part of the *Fit-for-55* legislative package [3], Regulation (EU) 2023/851 [4] establishes progressively stricter CO_2 emission targets for new passenger cars over a Worldwide Harmonized

Light Vehicles Test Procedure (WLTP). Specifically, manufacturers are required to achieve a 55% reduction in average fleet CO_2 emissions by 2030 compared with the 2021 baseline, while all new passenger cars registered from 2035 onward must achieve a 100% reduction in tailpipe CO_2 emissions. Rather than imposing a single emission limit for all vehicles, the regulation defines manufacturer-specific fleet targets based on the average mass of the registered vehicles [4].

Alongside greenhouse gas reduction policies, the European Commission has introduced the new Euro 7 regulation [2], which extends and strengthens the existing legislative framework governing pollutant emissions. Compared with the previous standards, Euro 7:

- introduces lower emission limits for nitrogen oxides (NO_x), carbon monoxide (CO), total hydrocarbons (THC) and particle emissions;
- extends the particle number (PN) measurement down to 10 nm compared to the previous value of 23 nm;
- establishes emission limits for additional pollutants such as ammonia (NH_3) and methane (CH_4);
- strengthens durability requirements for emission control systems;
- introduces continuous on-board emissions monitoring;
- expands the scope of regulated emissions to include non-exhaust sources such as brake wear particles [5].

		Mass in running order (MRO) (kg)	Mass of carbon monoxide (CO)		Mass of total hydrocarbons (THC)		Mass of nonmethane hydrocarbons (NMHC)		Mass of oxides of nitrogen (NO_x)		Combined mass of total hydrocarbons and oxides of nitrogen (THC + NO_x)		Mass of particulate matter (PM)		Number of particles (PN_{10})	
			L_1 (mg/km)		L_2 (mg/km)		L_3 (mg/km)		L_4 (mg/km)		$L_2 + L_4$ (mg/km)		L_5 (mg/km)		L_6 (#/km)	
Category	Class		PI	CI	PI	CI	PI	CI	PI	CI	PI	CI	PI	CI	PI	CI
M_1	—		1 000	500	100	—	68	—	60	80	—	170	4,5	4,5	$6x10^{11}$	$6x10^{11}$
N_1	I	MRO ≤ 1 280	1 000	500	100	—	68	—	60	80	—	170	4,5	4,5	$6x10^{11}$	$6x10^{11}$
	II	1 280 < MRO ≤ 1735	1 810	630	130	—	90	—	75	105	—	195	4,5	4,5	$6x10^{11}$	$6x10^{11}$
	III	1 735 < MRO	2 270	740	160	—	108	—	82	125	—	215	4,5	4,5	$6x10^{11}$	$6x10^{11}$
Note:			PI = positive ignition. CI = compression ignition.													

Figure 1: Euro 7 exhaust emission limits for Passenger Cars of Category M1 and Light-Duty Vans of Category N1 [2]

A key objective of the Euro 7 regulation is to reduce the gap between laboratory certification tests and real world vehicle operation. To this end, the legislation extends the durability period of emission control systems, ensuring that their performance is maintained throughout the vehicle lifetime, as highlighted by Dornoff and Rodriguez [5]. These requirements demand more robust exhaust after-treatment systems capable of maintaining high conversion efficiencies with different performance targets set after 8 years or 160000 km and after 10 years or 200000 km [5].

Meeting the ambitious European targets for both greenhouse gas and pollutant emissions represents a significant challenge for conventional internal combustion engine vehicles. In this context, Hybrid Electric Vehicles and Plug-in Hybrid Electric Vehicles are widely recognized as effective transitional technologies toward road transport sector electrification. By combining an internal combustion engine with one or more electric machines, PHEVs can substantially reduce fuel consumption and emissions while preserving vehicle range and operational flexibility.

Nevertheless, several experimental studies have highlighted that the environmental benefits of PHEVs strongly depend on their real-world operating conditions. As indicated by Trentadue et al. [6] and by Plötz et al. [7], their actual emissions are influenced by driving patterns, charging frequency, and energy management strategies, which determine the proportion of vehicle operation in electric mode and charge-sustaining mode. Consequently, optimizing the control strategy and the energy management plays a key role in reducing fuel consumption and pollutant emissions while maintaining the battery state of charge within the desired operating window, as shown by Serrao et al. [8].

Within this regulatory framework, the PHOENICE project aims to develop a PHEV demonstrator capable of complying with future emission regulations while simultaneously minimizing fuel consumption and pollutant emissions under real driving conditions.

1.3 The Role of the Research

To comply with the increasingly stringent emission regulations introduced by the European Union, research and development activities have played a fundamental role in the advancement of innovative powertrain technologies. While vehicle electrification represents the cornerstone of the European decarbonization strategy, considerable research efforts continue to focus on improving efficiency and reducing the environmental impact of internal combustion engines (ICEs). Owing to their high energy density, technological maturity, and compatibility with hybrid powertrains, ICEs are expected to remain an essential component of future electrified vehicles.

Among the most effective approaches to improving engine efficiency are downsizing and turbocharging. Downsizing consists of reducing engine displacement while maintaining comparable power output, allowing the engine to operate at higher average loads where fuel conversion efficiency is generally improved, as indicated by Heywood [9]. Turbocharging compensates for the reduced displacement by increasing the intake air density, thereby preserving engine performance and torque characteristics. This combination has proven particularly effective in reducing fuel consumption while maintaining vehicle performance, as proved by Hu et al. [10], and is also suitable for hybrid architectures.

Teodosio et al. [11] indicated that further improvements can be achieved through the adoption of low-pressure exhaust gas recirculation (LP-EGR). By recirculating cooled exhaust gases upstream of the compressor, LP-EGR lowers combustion temperatures, mitigates knock propensity in turbocharged spark-ignition engines, and enables operation at more efficient spark timings. As a result, both fuel consumption and pollutant emissions can be reduced without compromising engine performance.

Another promising technology is cylinder deactivation, which temporarily deactivates one or more cylinders during low-load operation. By increasing the load on the remaining active cylinders, pumping losses are reduced and the engine operates closer to its optimum efficiency region. Consequently, significant improvements in part-load fuel economy can be achieved, as proved by Leone and Pozar [12]. Fridrichová et al. [13] highlight that the integration of cylinder deactivation with hybrid electric powertrains further enhances its effectiveness by allowing the internal combustion engine to operate more frequently under favourable load conditions, especially for low battery recharging targets.

Advanced combustion concepts have also attracted considerable attention as a means of simultaneously improving efficiency and reducing emissions. Among these, Homogeneous Charge Compression Ignition (HCCI), also referred to as Controlled Auto-Ignition (CAI), combines the high efficiency of compression ignition with the low particulate emissions typical of premixed combustion. By promoting low-temperature combustion of highly diluted homogeneous mixtures, HCCI significantly reduces nitrogen oxide and soot formation while improving thermal efficiency, as shown by Stanglmaier and Roberts [14] and by Epping et al. [15]. Although practical implementation remains challenging due to combustion control limitations, several advanced concepts have been proposed. A notable example is Mazda's Spark Controlled Compression Ignition (SPCCI) technology, implemented in the Skyactiv-X engine, where spark ignition is used to initiate and stabilize the compression ignition process over a wide range of operating conditions [16].

Within this technological scenario, the PHOENICE project aims to demonstrate the potential of an advanced, high-efficiency internal combustion engine integrated into a Plug-in Hybrid Electric Vehicle. By combining state-of-the-art engine technologies with electrification and advanced energy management strategies, the project seeks to achieve substantial reductions in both greenhouse gas and regulated pollutant emissions while maintaining high vehicle performance and drivability.

1.4 The PHOENICE Project

Within the European framework of decarbonization strategy for the transport sector, the PHOENICE (PHev towards zerO EmissioNs & ultimate ICE efficiency) project aims to demonstrate the potential of a high-efficiency internal combustion engine integrated into a C-SUV Plug-in Hybrid Electric Vehicle (PHEV). Funded under the European Union's Horizon 2020 research and innovation programme, the project focuses on the development of a PHEV demonstrator capable of simultaneously reducing fuel consumption and pollutant emissions under real driving conditions while maintaining good performance and drivability.

To achieve these objectives, the proposed propulsion system integrates different innovative solutions, such as a highly diluted combustion, an increased compression ratio, the Miller cycle, and electrified boosting technologies to maximize engine thermal efficiency while ensuring compliance with future Euro 7 emission requirements [17]. The project targets a fuel consumption reduction of approximately 10% with respect to the reference vehicle operating in charge-sustaining mode, while achieving a peak gross indicated efficiency of 47% [18].

Fuel Consumption	-10% vs Baseline Vehicle on a CS WLTC test
ICE Efficiency	47% Peak Gross Indicated Thermal Efficiency

Table 1: PHOENICE Project targets

A key feature of the PHOENICE engine is the adoption of a dual-charge dilution strategy, obtained through the combined use of lean combustion and cooled exhaust gas recirculation (EGR). Together with an optimized in-cylinder flow field and electrically assisted boosting systems, these technologies improve combustion efficiency, reduce engine-out emissions, and extend the operating range of highly diluted combustion. The resulting engine architecture is specifically designed to exploit the synergies between advanced combustion concepts and hybrid powertrain operation, thereby maximizing overall vehicle efficiency under real-world driving conditions [17].

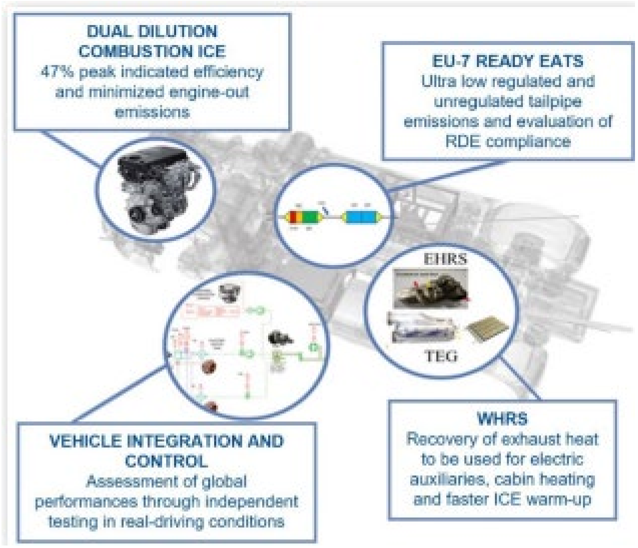

Figure 2: PHOENICE Project innovation areas [17]

The engine architecture and the technologies developed within the PHOENICE project are presented in detail in *Chapter 2*. Particular attention is devoted to the combustion system and the engineering solutions adopted to achieve the project's efficiency and emission targets.

1.5 The scope of the thesis

This thesis was carried out within the framework of the PHOENICE project and primarily aimed at developing a virtual test rig of the vehicle under investigation to optimize its operating strategy with the objective of reducing fuel consumption and emissions.

The research was conducted primarily using the GT-SUITE simulation platform, based on the datasets provided by IFPEN and the Politecnico di Torino. In the first phase, the engine Digital Twin was optimized over a wide range of operating conditions, by calibrating a Three Pressure Analysis model to accurately reproduce the evolution of in-cylinder turbulence. In addition, three-dimensional CFD simulations were performed in the CONVERGE environment to evaluate the intake valves discharge coefficients and characterize the backflow phenomenon associated with the Miller cycle. Subsequently, a physics-based vehicle model was developed to simulate the vehicle behaviour over the regulatory driving cycles**.** The implementation of an Equivalent Consumption Minimization Strategy determined a local optimum for energy management at each timestep of the driving cycle, thereby reducing fuel consumption and pollutant emissions, in compliance with increasingly stringent regulations.

2 The PHOENICE Project

2.1 Introduction

The PHOENICE project aims to develop a C-SUV Plug-in Hybrid Electric Vehicle capable of reducing both fuel consumption and pollutant emissions under real driving conditions while maintaining the performance and drivability expected from modern production vehicles. The project targets a peak indicated thermal efficiency of 47% together with an approximately 10% reduction in fuel consumption with respect to the baseline vehicle operating in charge sustaining mode, while ensuring compliance with the Euro 7 emission requirements.

The engine developed within the PHOENICE project is based on a 1.3 L four-cylinder turbocharged spark-ignition engine, which serves as the reference architecture for the implementation of the advanced combustion and control technologies developed throughout the project. Compared with the baseline engine, the powertrain has been extensively redesigned to enable stable operation under highly diluted combustion conditions while adopting aggressive Miller strategies.

The proposed engine concept combines several complementary technologies, including highly diluted combustion through lean operation and cooled exhaust gas recirculation (cooled EGR), an increased compression ratio, an aggressive Miller cycle, and an electrified boosting system. Furthermore, the implementation of an advanced exhaust after-treatment system, made of both a close-coupled section and an underfloor section, together with the synergistic interaction of these solutions enhances fuel conversion efficiency and reduces emissions, making the engine particularly suitable for integration into a hybrid powertrain [17].

This chapter presents the PHOENICE engine architecture in detail, describing the main technologies adopted to achieve the project's efficiency and emission targets.

2.2 The Engine Technical Specifications

The PHOENICE prototype engine is derived from a state-of-the-art 1.3 L four-cylinder turbocharged gasoline direct injection (GDI) spark-ignition engine, which was extensively redesigned to implement the advanced combustion technologies developed within the project. The main specifications of the engine are summarized in Table 2.

Engine Specifications	
Cylinders	*4 in line*
Displacement	*1332 cm^3*
Bore x Stroke	*70 mm x 86.5 mm*

Compression Ratio	*13.6:1*
Number of valves	*16*
VVA system	*MultiAir III (intake only)*
Turbocharging	*48 V VNT E-Turbo*
Fuel Injection System	*GDI*
Maximum Injection Pressure	*350 bar*
EGR System	*Cooled Low Pressure (LP)*
Rated Power (target)	*100 kW @ 4500 rpm*
Rated Torque (target)	*218 Nm @ 3500 rpm*

Table 2: PHOENICE Engine Technical Specifications

The engine architecture was optimized to operate under highly diluted combustion conditions while maximizing thermal efficiency. As described by Tahtouh et al. [19], the resulting engine concept integrates several complementary technologies, including a Dual Dilution Combustion Approach (DDCA), an increased compression ratio, an aggressive Miller cycle, electrified boosting, and an upgraded gasoline direct injection system capable of operating at injection pressures up to 350 bar. Together, these solutions enable a target indicated thermal efficiency of approximately 47% while contributing to a fuel consumption reduction of around 10% with respect to the reference vehicle operating in charge-sustaining mode.

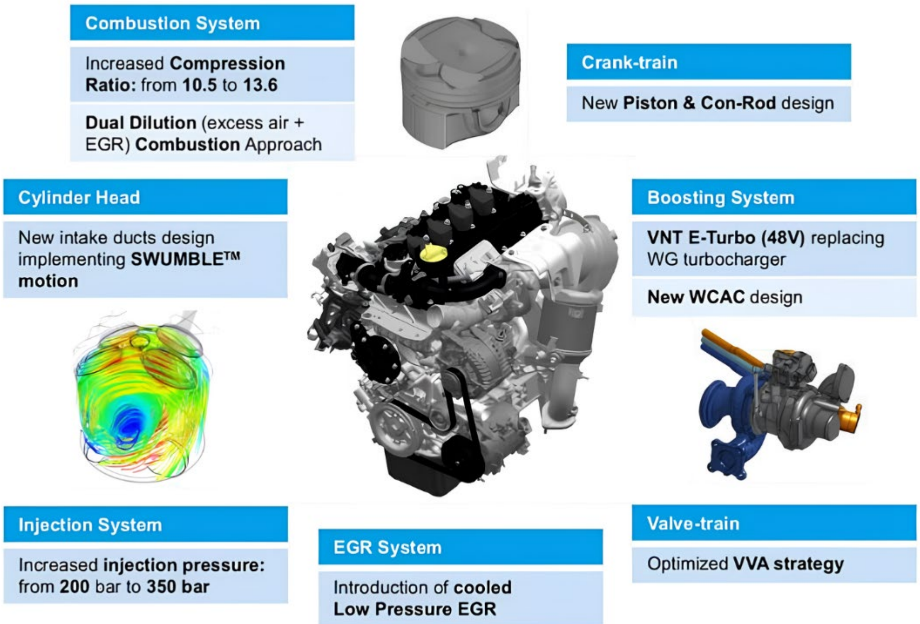

Figure 3: Main PHOENICE engine technologies [17]

The cornerstone of the combustion system is the Dual Dilution Combustion Approach, which combines homogeneous lean combustion with cooled low-pressure exhaust gas recirculation (LP-EGR). This strategy increases the thermal capacity of the in-cylinder mixture, reducing combustion temperatures and improving both thermal efficiency and engine-out emissions. However, the higher dilution levels also reduce flame propagation speed and increase combustion instability [17].

To compensate for these effects, the intake ports and piston geometry were specifically redesigned to generate an innovative in-cylinder charge motion known as Swumble™, which combines the features of both swirl and tumble motions. As described by Tahtouh et al. [17], this solution enhances turbulence levels around the spark timing, promoting faster flame propagation and improving combustion stability under highly diluted operating conditions.

A further key feature of the PHOENICE engine is the adoption of an aggressive Miller cycle enabled by the MultiAir III variable valve actuation (VVA) system. By delaying the intake valve closing after Bottom Dead Centre (BDC), the effective compression ratio is reduced while preserving the benefits of a high geometric expansion ratio. Tahtouh et al. [20] prove that, in addition to limiting the mixture temperature during compression, this strategy reduces pumping losses during part-load operation by allowing the engine to operate with a more open throttle, thereby improving overall fuel conversion efficiency.

The engine is complemented by a 48 V electrified variable-nozzle turbocharger (VNT), specifically designed to satisfy the requirements associated with highly diluted combustion and Miller cycle operation. The integrated electric machine assists the turbocharger during transient operating conditions, improving boost response and reducing turbo lag. Under suitable operating conditions, it can also operate as a generator, recovering part of the exhaust gas energy and contributing to the overall efficiency of the hybrid powertrain [17] [19].

Finally, the PHOENICE prototype is equipped with an advanced exhaust after-treatment system (EATS) designed to comply with the Euro 7 emission requirements. The close-coupled section comprises an Electrically Heated Catalyst (EHC), a Three-Way Catalyst (TWC), and a Gasoline Particulate Filter (GPF), ensuring rapid catalyst light-off and efficient control of gaseous and particulate emissions. The underfloor section incorporates a Selective Catalytic Reduction (SCR) system, preceded by a NOx oxidation catalyst and followed by an Ammonia Slip Catalyst (ASC), enabling effective NOx reduction during lean engine operation while minimizing ammonia emissions [19].

The combination of these technologies results in a highly efficient spark-ignition engine suitable for plug-in hybrid applications, where advanced combustion strategies and electrified powertrain operations can be effectively integrated into the demonstrator vehicle to achieve the ambitious efficiency and emission targets of the PHOENICE project. As described by Zagun [21], the implementation of an optimal control strategy in such powertrains could further enhance the fuel economy potential of electrified vehicles, thereby playing a key role in reducing the environmental impact of both HEVs and PHEVs.

In this context, the ability to predict vehicle behaviour through a virtual test rig is essential to extend the scope of the PHOENICE project, providing the basis for the development and the implementation of advanced energy management control strategies, which are presented in the following chapters.

3 Methodology

3.1 Introduction

This chapter presents the methodology adopted in the research activity to extend the existing simulation platform with the aim of maximizing both engine and vehicle performance. In addition to refining the engine Digital Twin to accurately predict the engine behaviour under different operating conditions, this work also focuses on developing a vehicle model capable of simulating the vehicle response over an entire driving cycle.

To achieve these objectives, the development of the simulation platform was divided into the following main stages:

- Engine Model Refinement: initially, a Three Pressure Analysis (TPA) model was calibrated and validated within the GT-SUITE environment to accurately predict the in-cylinder turbulence evolution. Subsequently, three-dimensional CFD simulations were performed in CONVERGE Studio to determine the valve discharge coefficients, enabling a more accurate estimation of the air mass trapped inside the cylinder. The integration of these analyses significantly improved the predictive capability of the engine Digital Twin over a wide range of operating conditions.

- Development of a Vehicle Virtual Test Rig: based on the available engine data and the prototype vehicle specifications, a 0D and 1D map-based vehicle model was developed. The resulting virtual test rig is capable of autonomously simulating vehicle operation and optimizing energy management according to the selected driving cycle.

3.2 Data

The engine model correlation and validation activities were carried out using the data obtained by the Politecnico di Torino through three-dimensional CFD simulations. The available dataset includes several operating points, characterized by different combinations of the main operating parameters, namely engine speed, load, and the possible presence of the fuel injection event.

The vehicle model, on the other hand, was developed using the dataset provided by IFPEN for the prototype vehicle employed in the roller bench simulations. In addition to the vehicle specifications, the IFPEN dataset includes the experimental data collected during the testing campaign. Specifically, it provides the speed profiles of the driving cycles together with the signals acquired from the Engine Control Unit (ECU), which were used for the validation of the vehicle virtual test rig.

3.2.1 Politecnico di Torino Dataset

The dataset provided by Politecnico di Torino was used for the correlation of the TPA model. For each operating case, the following information was available:

- engine speed and load;
- presence of the fuel injection event and, if necessary, spark advance (SA), fuel mass flow rate, injection pressure, and Start of Injection (SOI);
- Exhaust Gas Recirculation (EGR) rate;
- intake and exhaust air mass flow rates;
- intake and exhaust pressure and temperature;
- valve lift profiles;
- Turbulent Kinetic Energy (TKE) and Length Scale (LS) profiles over the entire engine cycle;
- in-cylinder pressure, temperature, and mass traces.

The availability of cases with and without fuel injection under the same operating conditions is essential for assessing the effect of injection on the evolution of the in-cylinder turbulence. In particular, the injection event directly affects the TKE profile, thereby influencing the air-fuel mixing process.

Overall, the dataset comprises five cases corresponding to three different engine operating points. The main characteristics of each operating condition are summarized in Table 3.

Case Number	Engine Speed [rpm]	BMEP [bar]	Injection	λ [-]	EGR [%]	SA [°CA aTDCf]
1	*4500*	*16*	✗	-	*5.03*	-
2	*4500*	*16*	☒	*1*	*5.03*	*-5*
3	*2500*	*10*	✗	-	*10.76*	-
4	*2500*	*10*	☒	*1.16*	*10.76*	*-16*
5	*2000*	*6*	☒	*1.14*	*10.95*	*-23*

Table 3: Engine operating points provided by Politecnico di Torino

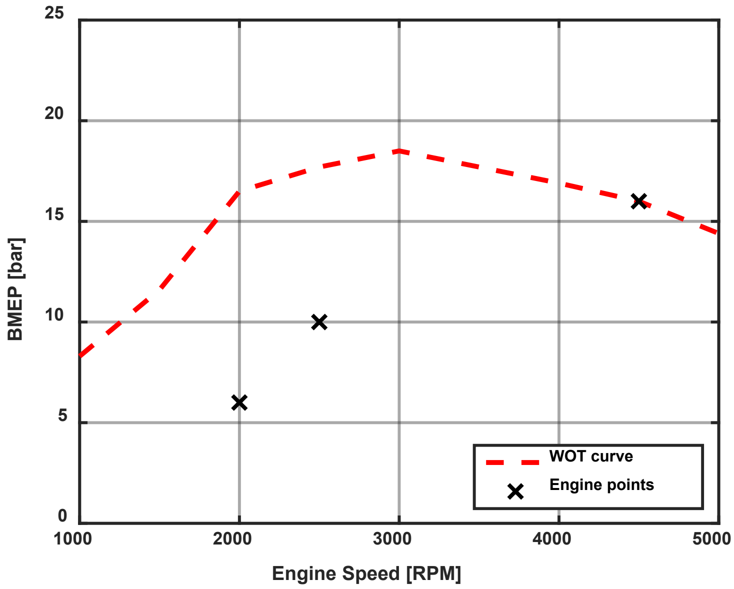

Figure 4: Engine operating points

Although the dataset comprises a relatively limited number of operating points, it provides a representative coverage of the entire engine operating map, spanning conditions from low engine speeds and low loads to high speeds and elevated Brake Mean Effective Pressure (BMEP) values. As shown in Figure 4, the dataset also includes an operating point located on the Wide Open Throttle (WOT) curve, ensuring that full-load engine operation is represented. This range of operating conditions enabled the calibration of the TPA model, thereby improving the predictive capability of the engine model, particularly in the estimation of the in-cylinder turbulence evolution.

3.2.2 IFPEN Dataset

The development of the vehicle model was based on the dataset provided by IFPEN, which includes the technical specifications of the main drivetrain components, namely:

- Internal Combustion Engine (ICE): in addition to the main geometric parameters, such as compression ratio, displacement, and bore, the dataset provides key performance parameters, including Brake Mean Effective Pressure (BMEP), Friction Mean Effective Pressure (FMEP), and Brake Specific Fuel Consumption (BSFC);
- Electric Machines (P0 and P4): torque-speed characteristic curves and electromechanical conversion power loss maps are available;
- Battery Pack: the dataset includes the number of cells, their main properties (such as capacity and nominal voltage), and the operating limits of the State of Charge (SOC);
- Transmission: gear ratios and their corresponding efficiencies are provided for each gear;

- Vehicle: the vehicle mass and coast-down coefficients are available, allowing the calculation of the external road loads acting on the vehicle as a function of vehicle speed.

In addition to the technical specifications, IFPEN also provided the experimental data acquired during the roller bench tests, performed over two regulatory driving cycles: the Worldwide Harmonized Light Vehicles Test Cycle (WLTC) and the Real Driving Emissions (RDE). In particular, the dataset includes:

- the target vehicle speed profiles for the considered driving cycle;
- the average CO_2 emissions and fuel consumption over the entire driving cycle;
- the signals acquired from the Engine Control Unit (ECU), which were used during the calibration and validation phases of the vehicle virtual test rig.

3.3 Engine Digital Twin Refinement

The research activity began with two complementary investigations focused on the cold-flow process within the cylinder, with the aim of enhancing the 1D simulation platform. In the first stage, the TPA model was calibrated to reproduce the in-cylinder turbulence evolution provided by the Politecnico di Torino. Subsequently, 3D CFD simulations were performed to determine the valve discharge coefficients. Together, these analyses improved the predictive capability of the engine Digital Twin, particularly during the intake and compression strokes.

3.3.1 TPA Model

The TPA model enables the evaluation of the thermodynamic evolution of the in-cylinder mixture based on three pressure signals: the intake port pressure, the in-cylinder pressure, and the exhaust port pressure. The intake port pressure is imposed as a boundary condition downstream of the intake manifold and defines the thermodynamic conditions of the intake flow, while also determining the air mass trapped inside the cylinder. The exhaust port pressure represents the turbine inlet conditions and influences both the residual gas fraction and the trapping ratio. The in-cylinder pressure is the primary input to the TPA model, as it is used both to reconstruct the combustion process through the calculation of the burn rates and to determine the thermodynamic state evolution of the mixture from Intake Valve Closing (IVC) to Exhaust Valve Opening (EVO).

The TPA model therefore consists of a single cylinder with the corresponding intake and exhaust ports. Although it represents a simplified engine model, it enables the calibration of the main turbulence parameters with a relatively low computational cost, making it an effective tool for improving the predictive capability of the engine Digital Twin. Given the innovative in-cylinder charge motion concept, combined with the adoption of aggressive Miller valve timing strategies, the accurate prediction of in-cylinder turbulence is essential, as it has a significant impact on the subsequent combustion process.

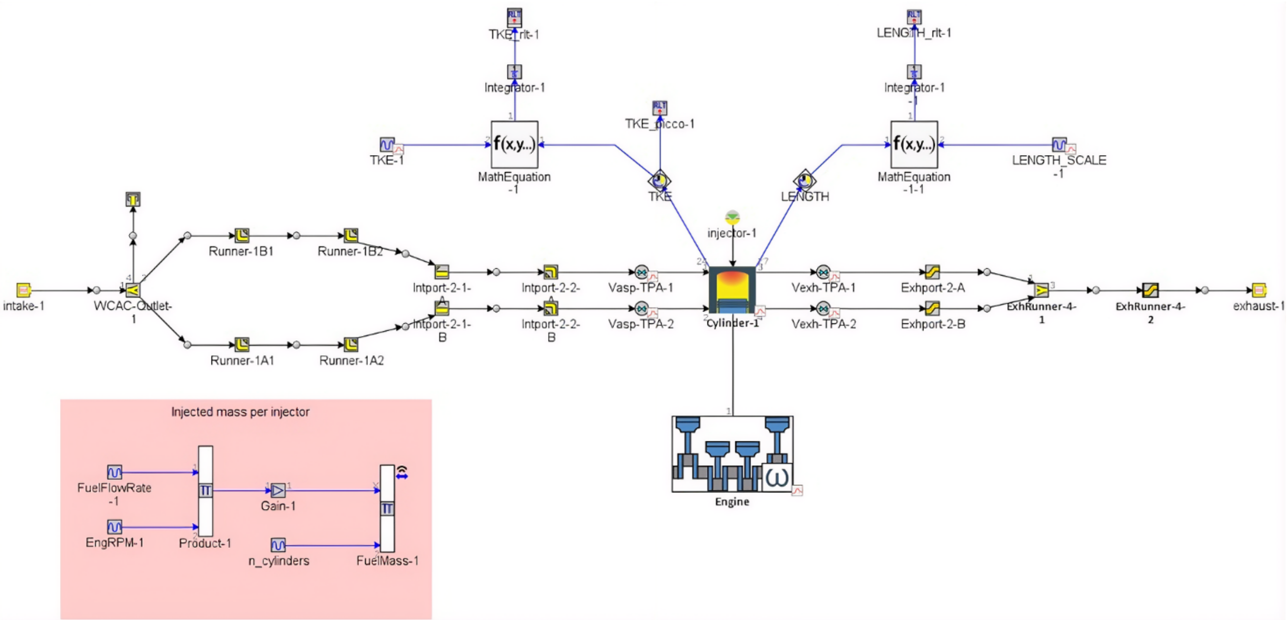

Figure 5: TPA model on GT-SUITE simulation platform

The main inputs to the model are:

- intake and exhaust thermodynamic conditions: since the engine is turbocharged, pressure and temperature are specified at the intake manifold downstream of the compressor and engine out at the turbine inlet. To improve numerical stability, both the mean values and the crank-angle-resolved profiles are provided;
- combustion chamber wall temperatures: separate temperatures are prescribed for the cylinder head, liner and piston;
- cranktrain geometrical features: bore, stroke, and connecting rod length;
- combustion parameters, when fuel injection is present: fuel mass flow rate, injected fuel mass, injection pressure, Start of Injection, spark advance, and EGR rate;
- valve lift profiles;
- in-cylinder pressure, Turbulent Kinetic Energy, and Length Scale traces. The profiles obtained from the 3D CFD simulations feature a crank-angle resolution finer than 0.1 Crank Angle Degree (CAD), allowing the thermodynamic cycle to be resolved with a large number of calculation points, thereby improving the accuracy of the simulation results.

Subsequently, to ensure a consistent correlation between the TPA model and the dataset provided by the Politecnico di Torino across all five operating conditions, the following parameters were kept identical to those adopted in the reference 3D CFD model.

TPA Parameters	
Compression Ratio	*13.6*
Heat Transfer Multiplier	*1.5*

Table 4: CR and HTM values in the TPA model

The analysis of the available data shows that, under the same operating conditions, fuel injection leads to a reduction in TKE as the Top Dead Centre firing (TDCf) is approached. Although an attempt was made to reproduce this behaviour using the TPA model, the predicted results do not replicate the same trend, as shown in Figure 6.

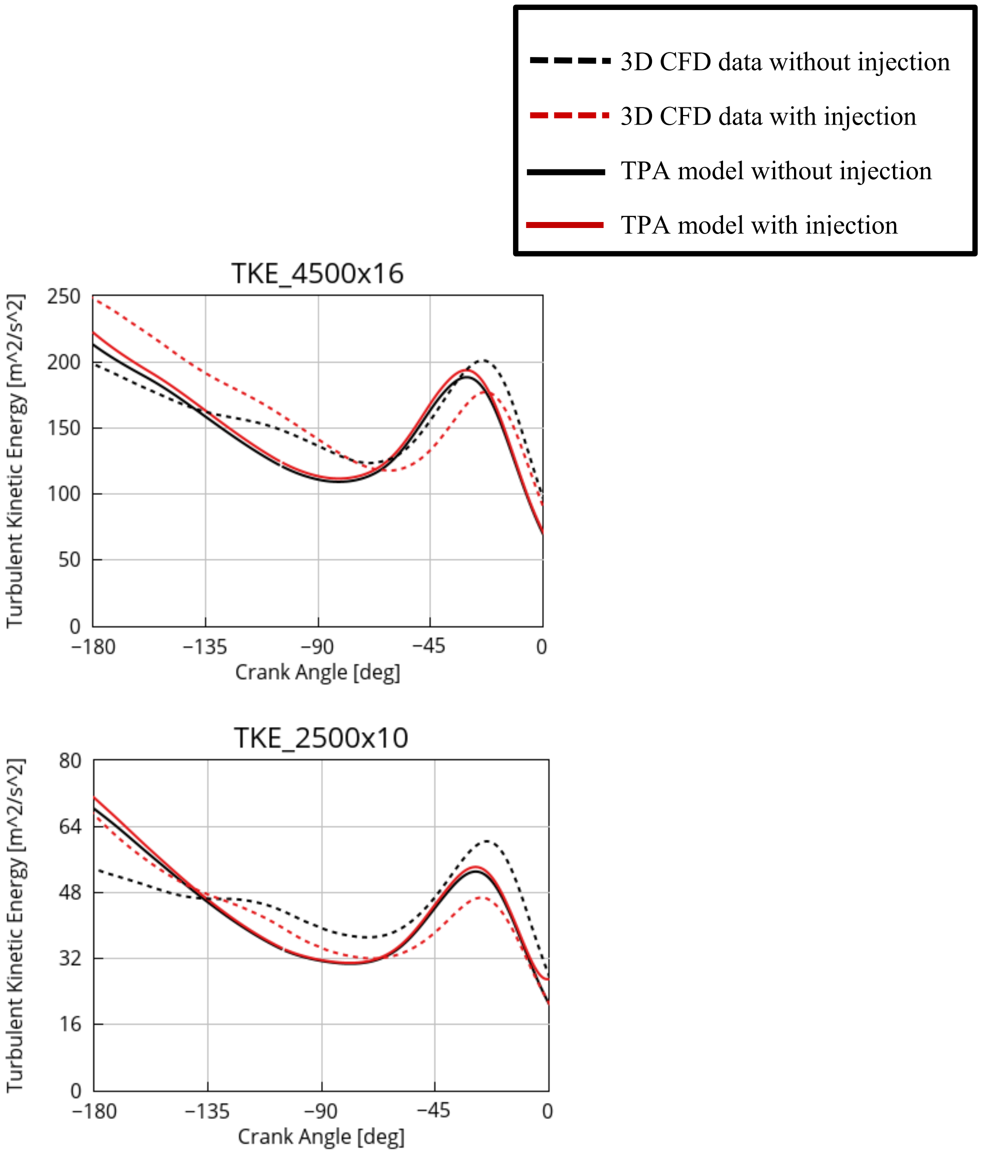

Figure 6: TKE profiles with and without fuel injection

Consequently, only the operating conditions including fuel injection were implemented in the model, and the calibration procedure was carried out based on the cases presented below.

Updated Case Number	Engine Speed [rpm]	BMEP [bar]	Injection	λ [-]	EGR [%]	SA [°CA aTDCf]
1	*4500*	*16*	☒	*1*	*5.03*	*-5*
2	*2500*	*10*	☒	*1.16*	*10.76*	*-16*
3	*2000*	*6*	☒	*1.14*	*10.95*	*-23*

Table 5: Updated engine operating points in the Politecnico di Torino dataset

GT-SUITE provides several parameters for characterizing the in-cylinder flow. The calibration of these coefficients enables a good correlation between the results obtained from the 3D CFD simulations and those predicted by the TPA model, particularly in terms of TKE and LS profiles. This, in turn, improves the prediction of in-cylinder turbulence, thereby enhancing the predictive capability of the engine model.

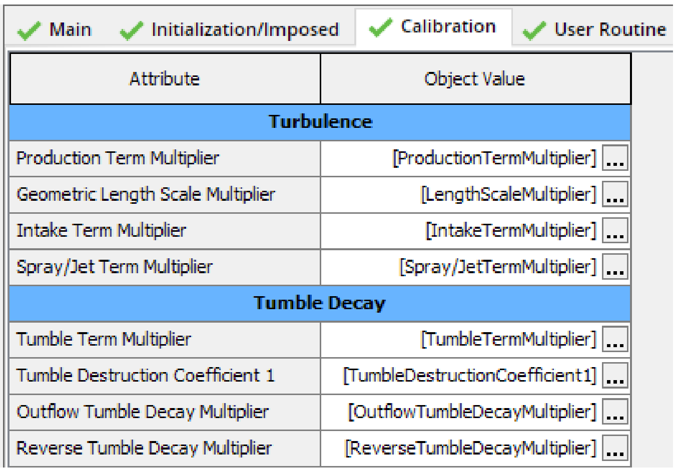

Figure 7: Turbulence calibration parameters available on GT-SUITE

Each parameter influences the evolution of the in-cylinder turbulence in a different way and therefore requires a dedicated calibration procedure. In particular:

- the *Production Term Multiplier* increases the production of TKE from the mean flow;
- the *Geometric Length Scale Multiplier* controls the characteristic length scale at which turbulence dissipation occurs. Consequently, increasing this parameter results in a higher turbulence intensity;
- the *Intake Term Multiplier* and the *Spray/Jet Term Multiplier* represent the contributions of the intake flow and the fuel injection event, respectively, to the mean kinetic energy;

- the *Tumble Term Multiplier* quantifies the turbulence generated by the decay of the tumble motion;
- the *Tumble Destruction Coefficient 1* controls the rate of tumble decay;
- the *Outflow Tumble Decay Multiplier* and the *Reverse Tumble Decay Multiplier* describe the effects of Late Intake Valve Closing (LIVC) and Early Intake Valve Closing (EIVC), respectively, on tumble decay. Given the aggressive Miller valve timing strategies adopted to reduce end-of-compression temperatures, an accurate calibration of the former parameter is essential, whereas the influence of the latter can be considered negligible.

The crank angle (CA) interval selected for the calibration of the TPA model includes only the intake and compression strokes. An accurate prediction of turbulence during these phases is essential to correctly describe the evolution of the in-cylinder mixture prior to ignition. This results in an improved predictive capability of the engine Digital Twin and, consequently, in a more accurate simulation of the combustion process.

As a first step, a sensitivity analysis was carried out to evaluate the influence of each calibration parameter on the TKE and LS profiles independently. Thanks to the low computational cost of the TPA model, an initial manual fine-tuning of the turbulence parameters was performed to assess their effect on the main quantities of interest. Among the parameters investigated, the Spray/Jet Term Multiplier exhibited the most significant influence on the evolution of TKE across all the operating conditions considered. Therefore, its value was selected by identifying an optimal compromise that ensured a satisfactory correlation with the CFD results over the entire dataset.

Turbulence Calibration Parameters	**Initial Value**	**Updated Value**
Spray/Jet Term Multiplier	*0.10*	*0.24*

Table 6: Spray/Jet Term Multiplier optimal value

A higher value of the Spray/Jet Term Multiplier increases the contribution of TKE associated with the fuel injection event, thereby promoting more intense turbulence generation. As a result, the air-fuel mixing process is enhanced, and the TKE levels predicted by the TPA model become more consistent with those obtained from the 3D CFD simulations.

Once this parameter had been fixed, the remaining calibration parameters were optimized using the Design Optimizer implemented in GT-SUITE, with the aim of identifying the combination of values that most accurately reproduces the TKE and LS profiles over the crank-angle interval of interest. To this end, a multi-objective optimization approach was adopted, combining a genetic algorithm with the Pareto optimality criterion. This procedure identifies the design configurations that minimize the Root Squared Error (RSE) between the TPA model predictions and the 3D CFD results, evaluated over a prescribed integration window.

Integration Window	[CA aTDCf]
Start	*-180*
End	*0*

Table 7: Integration window used in the optimization process

$$RSE = \frac{\left|\sqrt{(x-y)^2}\right|}{x} \quad (1)$$

$$where \begin{cases} RSE\ is\ the\ root\ squared\ error \\ x\ is\ the\ TKE\ (or\ LS)\ value\ provided\ by\ the\ 3D\ model\ for\ the\ i-th\ crank\ angle \\ y\ is\ the\ TKE\ (or\ LS)\ value\ simulated\ by\ the\ TPA\ model\ for\ the\ i-th\ crank\ angle \end{cases}$$

In addition, a constraint was imposed to ensure that the peak TKE remained within a ±10% tolerance of the corresponding reference maximum value.

The calibration parameters included in the optimization, together with their corresponding limits, as defined based on the results of the sensitivity analysis, are summarized in the table below.

Turbulence Calibration Parameters	*Lower Limit*	*Upper Limit*
Production Term Multiplier	*0.10*	*4.00*
Geometric Length Scale Multiplier	*0.50*	*1.30*
Intake Term Multiplier	*0.10*	*4.00*
Tumble Term Multiplier	*0.10*	*5.00*
Tumble Destruction Coefficient 1	*0.01*	*0.15*
Outflow Tumble Decay Multiplier	*0.25*	*1.40*

Table 8: Parameters introduced into the Design Optimizer

The optimization was carried out using the operating points located at the boundaries of the engine operating map in order to account for significantly different operating conditions, spanning a wide range of engine speeds and loads.

The resulting optimized calibration parameters are reported in Table 9.

Turbulence Calibration Parameters	***Initial Value***	***Optimized Value***
Production Term Multiplier	*0.71*	*0.97*
Geometric Length Scale Multiplier	*0.80*	*1.91*
Intake Term Multiplier	*2.40*	*2.31*
Tumble Term Multiplier	*1.97*	*1.62*
Tumble Destruction Coefficient 1	*0.11*	*0.09*
Outflow Tumble Decay Multiplier	*0.26*	*0.25*

Table 9: Turbulence calibration parameters optimized values

Subsequently, the TPA model was validated by applying the optimized calibration parameters to the remaining operating case included in the dataset. This validation procedure made it possible to assess both the effectiveness of the turbulence calibration and the reliability of the model's predictive capability.

3.3.2 Intake Ports Flow Analysis

Following the calibration of the turbulence model, the refinement of the engine Digital Twin continued with the investigation of the cold-flow process in the intake ports and the subsequent flow of the fresh charge into the cylinder through the intake valves. The objective of this analysis was to determine the discharge coefficients (CD), initially under forward-flow conditions.

Given the adoption of Miller strategies enabled by the variable valve actuation system, which allows the intake valve closing timing to be adjusted according to the operating conditions, it is essential to characterize the backflow phenomenon, namely the tendency of the fresh charge to flow back from the cylinder into the intake ports due to the pressure rise occurring inside the cylinder when the intake valves remain open beyond Bottom Dead Centre. To accurately describe this phenomenon, the same model, suitably modified, was also employed to determine the discharge coefficients under reverse-flow conditions.

The valve flow analysis was based on a three-dimensional single-cylinder model, including the corresponding intake and exhaust ports, provided by the Politecnico di Torino.

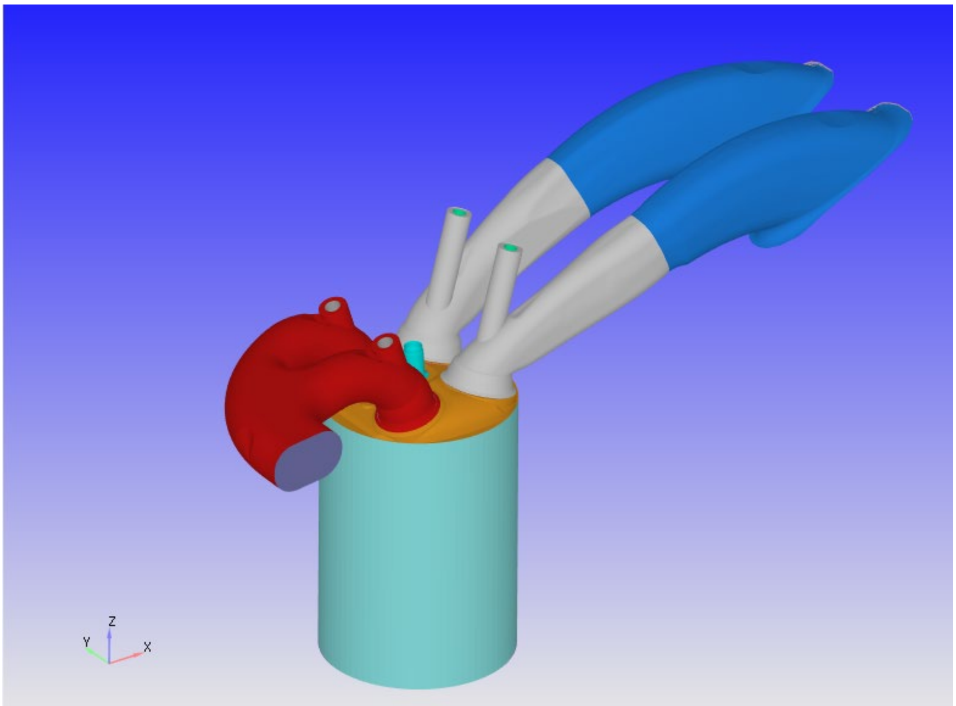

Figure 8: Baseline single-cylinder 3D model provided by Politecnico di Torino

Subsequently, the original model was simplified through a series of geometric modifications aimed at reducing the computational cost while preserving the fluid dynamic characteristics of the system. In particular, the following changes were introduced:

- the exhaust ports and valves were removed, as they were considered to have a negligible influence on the objectives of the study;
- an intake manifold was added, modelled as a hemispherical plenum with a diameter equal to three times the cylinder bore;
- the cylinder liner length was increased to twice the bore;
- a measurement region was introduced at 1.5 times the bore from the cylinder head;
- the spark plug and piston were removed to further simplify the computational domain;
- the lower end of the cylinder liner was closed with a flat surface.

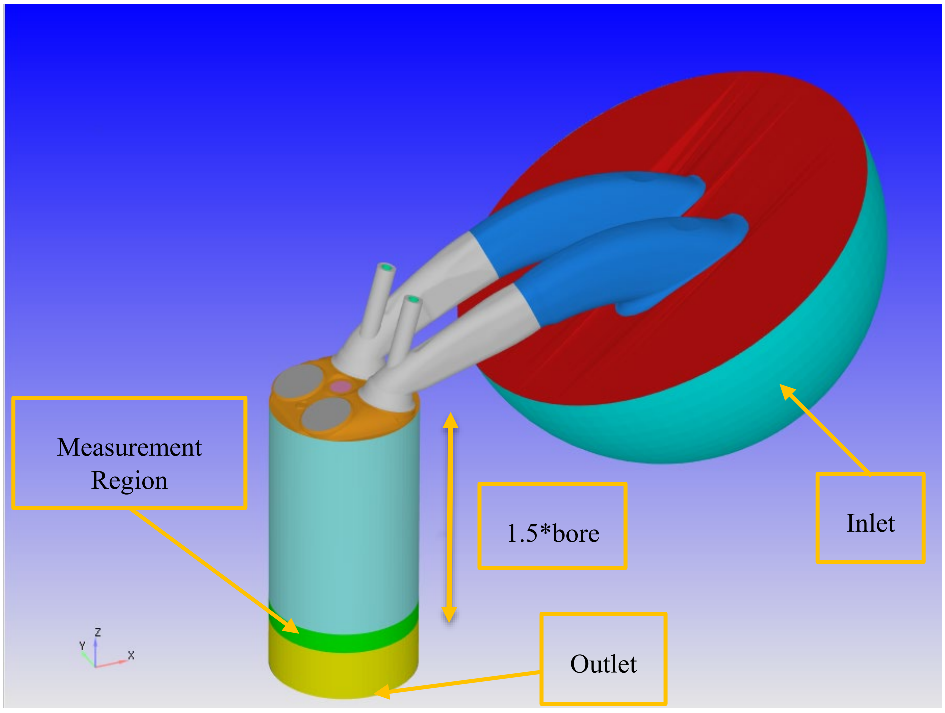

Figure 9: Simplified model with the appropriate geometric modifications

The simulations were carried out using the following boundary conditions:

- a total pressure of 100 kPa was imposed at the inlet, while a static pressure of 95 kPa was prescribed at the outlet, resulting in a pressure drop of 5000 Pa;
- the initial temperatures of both the fluid and the walls were set to 300 K;
- the walls were assumed to be adiabatic by imposing Neumann boundary conditions, thus preventing heat transfer between the fluid and the solid surfaces;
- steady-state flow conditions were assumed.

The discharge coefficients were subsequently determined by evaluating the air mass flow rate through the measurement region for different valve lift values.

Lift Values [mm]	
Low Lift	*0.2 – 0.5 – 1*
Medium to High Lift	*2 – 3 – 4 – 6 – 8 – 10 – 11*

Table 10: Valve Lift values adopted in the analysis

Regarding the domain discretization, a base grid composed of cubic cells with an edge length of 2 mm was adopted. To improve the accuracy of the solution in regions characterized by high velocity gradients, a first level of local mesh refinement was introduced in proximity of the cylinder inlet section, reducing the cell size to 0.25 mm in all three spatial directions.

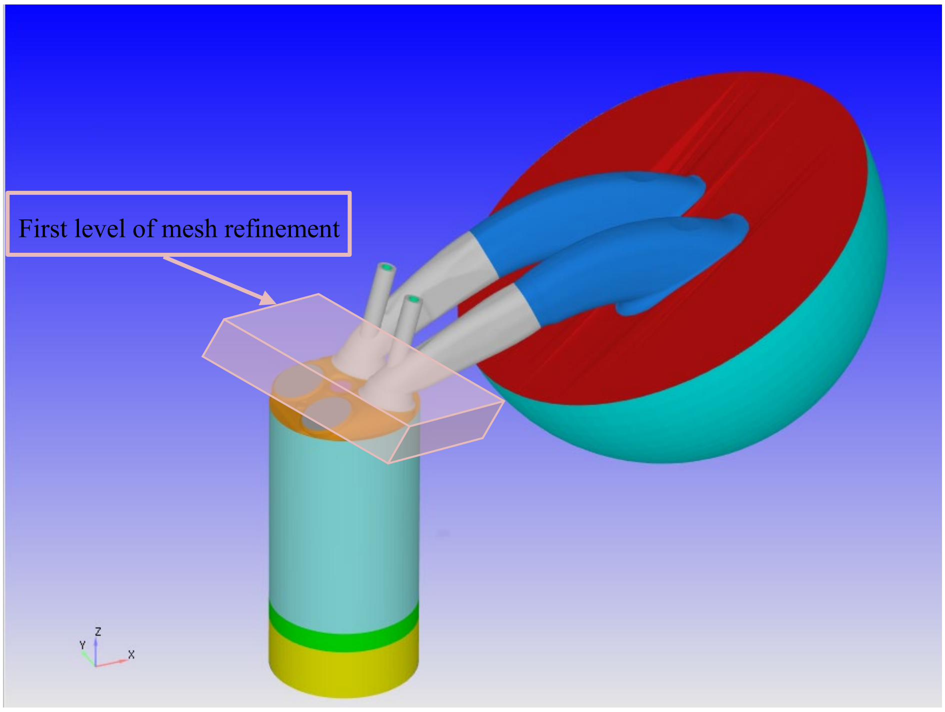

Figure 10: Location of the first level of mesh refinement

This configuration was designated as V01 and was adopted for medium-to-high valve lifts, equal to or greater than 2 mm. For valve lifts values below 2 mm, a further mesh refinement was required to preserve the reliability of the simulations. However, to maintain an appropriate trade-off between the number of cells (and consequently the computational cost) and the accuracy of the results, the additional refinement was restricted to the intake valve throat region only. Based on these considerations, a second configuration, designated as V02, was developed. This configuration retains all the features of V01 while introducing an additional level of local mesh refinement through a fixed embedding applied to the *Intake Valve Throat* boundary.

Fixed Embedding Characteristics	
Scale	*5*
Embed Layers	*3*
Cells Size	*62.5 μm*

Table 11: Main properties for the second level of mesh refinement

Overall, the V02 configuration consists of a mesh comprising approximately 8.5 million cells, compared to about 6 million cells for V01. For simulations involving low valve lift values, such discretization provided the best compromise between simulation time, computational cost, and solution convergence.

The valve lift values and the corresponding grid configurations adopted for the 3D CFD simulations are summarized in Table 12:

Lift	Range	Version
Low Lift	*from 0.1 mm up to 1 mm*	*V02*
Medium to High Lift	*from 2 mm up to 11 mm*	*V01*

Table 12: Valve lifts and the corresponding model configurations

The discharge coefficients were then calculated from the air mass flow rate measured at the measurement region using the following expressions.

$$CD = \frac{\dot{m}}{A_R * \rho_{is} * U_{is}} \quad (2)$$

$$A_R = \frac{\pi * D_{REF}^2}{4} \quad (3)$$

$$where \begin{cases} CD \text{ is the discharge coefficient for the imposed lift} \\ \dot{m} \text{ is the mass flow rate through the measurement region, from 3D simulations} \\ A_R \text{ is the reference flow area} \\ D_{REF} \text{ is the reference valve diameter equal to } 24.786 \text{ mm} \\ \rho_{is} \text{ is the isoentropic density at the throat} \\ U_{is} \text{ is the isoentropic velocity at the throat} \end{cases}$$

Finally, the forward discharge coefficients were compared with the experimental data provided by IFPEN, reported below as a function of the ratio between the valve lift (L) and the reference valve diameter (D).

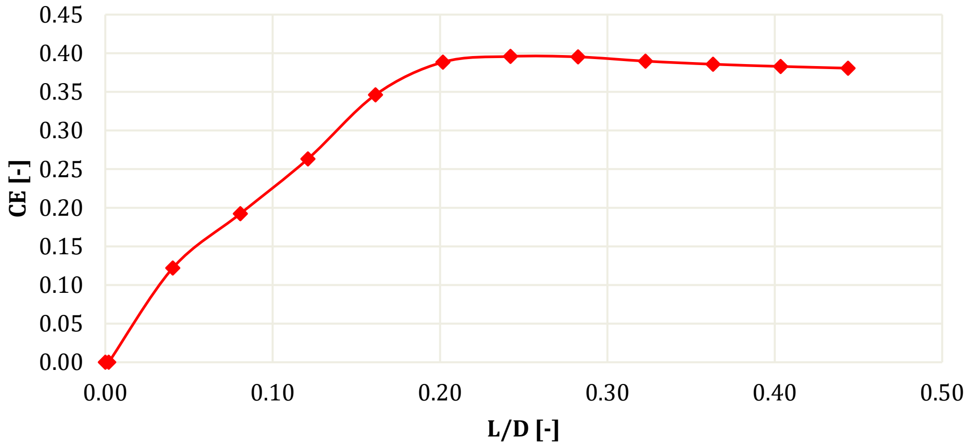

Figure 11: Discharge Coefficient values provided by IFPEN

To determine the discharge coefficients under reverse-flow conditions, required to characterize the effects of backflow on the volumetric efficiency and the trapped air mass inside the cylinder, a similar procedure to that described above was followed. The imposed pressure drop, the valve lift values considered, and the mesh configurations (V01 and V02) remained unchanged. The only modifications concerned the model geometry, specifically:

- the inlet and outlet regions were reversed, together with their corresponding pressure boundary conditions;
- the outlet region was restricted to the lower portion of the hemispherical intake plenum;
- a second measurement region was introduced in the upper part of the plenum to monitor the air mass flow rate during backflow events.

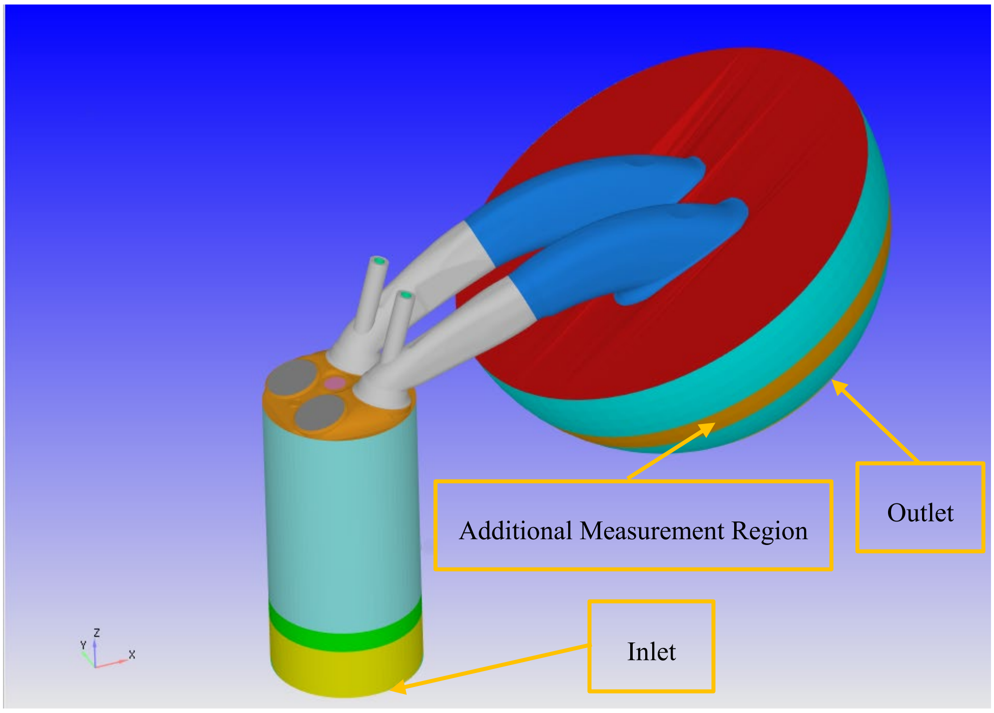

Figure 12: Model changes for the reverse discharge coefficient simulations

Starting from the simplified three-dimensional single-cylinder model, a valve flow analysis was carried out to characterize the flow through the intake ports. The air mass flow rates through the intake valves obtained from the CFD simulations were used to calculate the discharge coefficients under both forward and reverse-flow conditions. The resulting coefficients were then incorporated into the 1D engine model, improving its predictive capability, particularly in the estimation of the trapped air mass. Furthermore, the combination of the updated discharge coefficients with the turbulence parameters previously calibrated enabled a further refinement of the combustion process simulation, thereby enhancing the overall reliability of the engine Digital Twin.

3.4 Vehicle Virtual Test Rig

The development of the vehicle virtual test rig represented the core of the present research activity, serving as a key element in the extension of the existing simulation platform.

Figure 13: C-SUV class PHEV considered

The vehicle considered in this study is a C-SUV class Plug-in Hybrid Electric Vehicle. Its hybrid architecture combines a high-efficiency spark-ignition engine, whose Digital Twin was refined through the analyses described in the previous sections, with two electric machines placed in P0 and P4 positions, respectively. The internal combustion engine provides torque to the front axle through a six-speed automatic transmission, while the P0 electric machine operates as a starter. The e-motor in P4 position acts as prime mover when the Electric Vehicle (EV) mode is selected; under hybrid operating conditions, it delivers additional torque to the rear axle, enabling the electric All-Wheel Drive (e-AWD). Both electric machines are also capable of energy harvesting during regenerative braking phases.

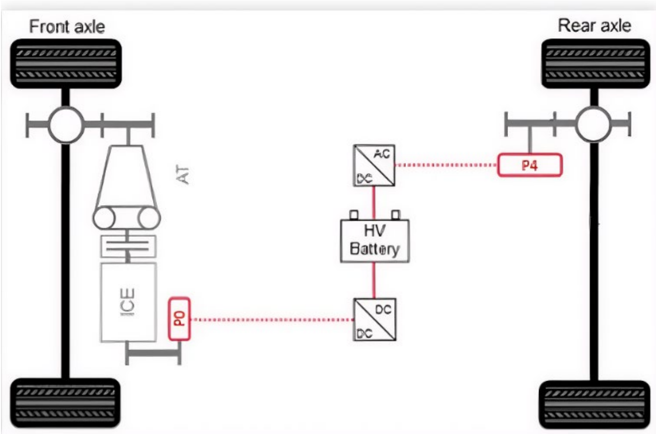

Figure 14: P0 P4 hybrid architecture

The virtual test rig was developed with the aim of accurately reproducing the vehicle dynamic behaviour while enabling the optimization of its operating strategy. To this end, the Equivalent Consumption Minimization Strategy (ECMS) was implemented using the dedicated controller available in GT-SUITE. This control strategy defines a local optimum for energy management in each instant of the driving cycle, thereby contributing to reduced fuel consumption and emissions.

The following sections describe the methodology adopted for the development of the virtual test rig, from the modelling of the main system components to the implementation of the control strategy.

3.4.1 Hybrid Drivetrain Implementation in GT-SUITE

The data provided by IFPEN were initially used to develop a physics-based vehicle model. This approach enabled the main powertrain subsystems to be represented using 0D and 1D map-based models.

In compliance with the vehicle hybrid architecture, the P4 electric machine was connected to the rear axle through a differential while the front axle was modelled by considering, in sequence:

- the P0 electric machine and the corresponding gear connection to the internal combustion engine;
- the spark-ignition engine, including the fuel rate, total air flow and emissions maps;
- the transmission system, consisting of a clutch, a torque converter, and a six-speed automatic transmission;
- the driveshaft and the front differential.

Finally, the vehicle model was defined using the vehicle mass and the coast-down coefficients provided by IFPEN.

Vehicle Characteristics	
Mass [kg]	*2014*
Coast Down Coefficient A [N]	*170.2*
Coast Down Coefficient B [N/(km/h)]	*0.4087*
Coas Down Coefficient C [N/(km/h)²]	*0.04601*

Table 13: Vehicle Parameters

The three coast-down coefficients were used to model the external resistive forces acting on the vehicle. Specifically, they were employed to represent the contributions of aerodynamic drag and rolling resistance loads through the following polynomial expression.

$$F = A + B * V + C * V^2 \quad (4)$$

$$where \begin{cases} F\ represents\ the\ external\ loads\ on\ the\ vehicle \\ A, B\ and\ C\ are\ the\ three\ coastdown\ coefficients \\ V\ is\ the\ vehicle\ speed \end{cases}$$

When the vehicle is stationary, the resistive force is therefore determined solely by the coefficient A. As the vehicle speed increases, the contributions of the first and second-order terms become progressively more significant, with the quadratic term becoming the predominant contribution to external loads at high vehicle speeds.

Subsequently, the Battery Management System (BMS) and the battery pack were implemented. For this purpose, the *NodeElectrical* template available in GT-SUITE was adopted, allowing the physical fidelity of the model to be enhanced by establishing an electrical connection between the battery pack and the P0 and P4 electric machines.

The baseline layout of the vehicle virtual test rig is shown in Figure 15.

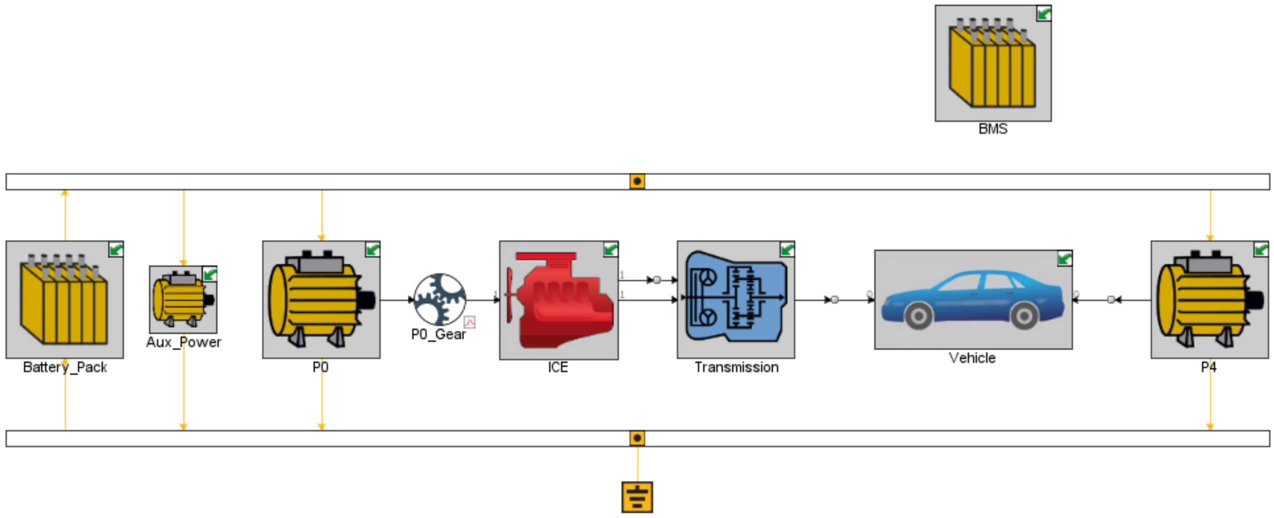

Figure 15: Virtual Test Rig Baseline Layout

Next, the driver model was introduced using the *VehDriverAdvanced* template, which controls the gear number and the accelerator, brake and clutch pedal positions based on the target vehicle speed.

The performance of Plug-in Hybrid Electric Vehicles is commonly assessed by means of the Worldwide Harmonized Light-Duty Vehicles Test Procedure (WLTP), whose reference speed profile, provided by IFPEN, is shown in Figure 16.

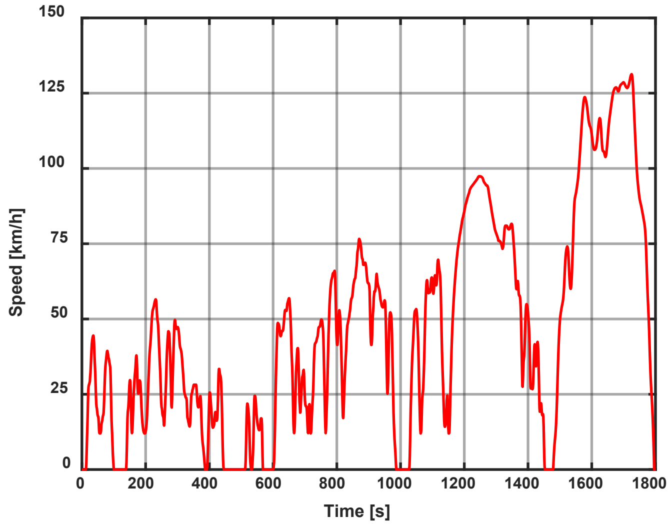

Figure 16: WLTC speed profile

The present research focused on the analysis of vehicle behaviour over a Worldwide Harmonized Light Vehicles Test Cycle performed in Charge Sustaining (CS) mode. In this operating mode, the battery State of Charge at the end of the cycle differs only slightly from its initial value as the power demand is shared between the electric motors and the internal combustion engine. This contrasts with Charge Depleting (CD) mode, in which the battery, initially close to full charge, is progressively depleted throughout the driving cycle, with the electric motors serving as the primary source of propulsion.

3.4.2 ECMS Controller Setup

To further extend the scope of the project and provide a virtual test rig capable of optimizing the vehicle operating mode, an Equivalent Consumption Minimization Strategy was implemented. This control strategy, based on static optimization, determines the locally optimal energy management solution at each instant of the driving cycle, thereby contributing to reduced fuel consumption and emissions.

In GT-SUITE, the strategy was implemented using the *ECMSController* template. Its operation relies on a secondary model, referred to as a surrogate model, in which a *Vehicle Kinematic Analysis* (VKA) template was integrated to perform the *Backward State Optimization* procedure. In GT-SUITE environment, the *backward* kinematic solution imposes the target vehicle speed and solves for the power (or torque) demand from the energy sources, namely the ICE and the electric machines. This approach is applicable only to map-based components. Consequently, it cannot capture the mass and heat transfer phenomena occurring within the thermal management system. However, this limitation does not affect the present study, as the thermal management system lies outside its scope. In contrast, the *forward* kinematic solution approach imposes the power (or torque) delivered by the energy sources and computes the resulting vehicle response through the drivetrain to the wheels. Owing to its formulation, the backward kinematic approach provides the basis for the development of optimal control strategies, such as the ECMS.

At each time step defined by the ECMSController, the main model and the surrogate model communicate through a discrete data exchange. Specifically, the ECMSController, implemented in the main model, sends the *Vehicle State Signals* required to perform the backward optimization to the Vehicle Kinematic Analysis (VKA) template in the surrogate model. In turn, the VKA returns the *Optimal Control Signals* generated by the optimization process to the ECMSController. These signals are then used by the main model to solve the vehicle dynamics using a forward solution approach. In this way, a closed-loop data exchange is established between the two models.

The Vehicle State Signals transmitted to the surrogate model as input signals are the following.

Vehicle State Signals	**Output Part in Main Model**	**Input Part in Surrogate Model**
P0 Maximum Discharge Power	*BMS*	*P0*
P0 Maximum Charge Power	*BMS*	*P0*
P4 Maximum Discharge Power	*BMS*	*P4*
P4 Maximum Charge Power	*BMS*	*P4*
Angular Acceleration Target	*Vehicle Driver Advanced*	*VKA*
Wheel Torque Request	*Vehicle Driver Advanced*	*Shaft*

Table 14: Vehicle State Signals

For the sake of simplicity, the surrogate model does not include:

- the vehicle part, which is replaced by a single shaft on which the wheel torque request is applied;
- the electrical nodes. Their physical behaviour is replicated by imposing a battery load equal to the sum of the power demands of the two electric machines;
- the torque converter, whose inclusion resulted in inaccurate simulations. Since the surrogate model operates with an imposed vehicle speed, the absence of the torque converter does not affect the calculation of the backward optimization.

At each communication interval, the surrogate model returns the Optimal Control Signals to the main model, where they are used as input signals. These signals are presented in Table 15.

Optimal State Signals	Output Part in Surrogate Model	Input Part in Main Model
Gear Number	*Transmission*	*Transmission*
P0 Torque	*P0*	*ECU*
P4 Torque	*P4*	*ECU*
ICE Torque	*ICE*	*ECU*
VKA_Source	*VKA*	*ECU*

Table 15: Optimal State Signals

The *VKA_Source* signal identifies the vehicle operating mode: a value of 3 corresponds to the hybrid mode, whereas a value of 2 indicates full-electric operation.

The Optimal Control Signals are then processed according to their respective functions. The transmission directly receives the gear number, whereas the remaining signals are handled by the engine control unit (ECU), which is modelled with the following components:

- an *ICEControllerAdv* template, which receives the engine speed and the engine torque, provided by the ECMSController, as inputs and generates as outputs the corresponding torque command based on the engine idle speed, starter speed, and fuel cut-off parameters;
- an *EventManager* part, which receives as inputs the vehicle operating mode (VKA_Source) together with the optimal torque demands for the P0 and P4 electric machines, denoted as *P0TrqOpt* and *P4TrqOpt* respectively, and operates according to the following logic.

Event No.	Mode	Event Exit Criterion	Next Event No.	ICE State	Clutch Actuator Position	P0 Torque	P4 Torque	Starter Torque [Nm]
1	*E-Drive*	*VKA_Source = 2*	*2*	*0 (Off)*	*100% (open)*	*0*	*P4TrqOpt*	*0*
2	*ICE Start*	*ICESpeed<900rpm*	*3*	*1 (On)*	*100%*	*0*	*P4TrqOpt*	*30*
3	*Hybrid*	*VKA_Source = 3*	*1*	*1*	*0% (closed)*	*P0TrqOpt*	*P4TrqOpt*	*0*

Table 16: Event Manager Setup

To overcome the *Starter State* conditions of the ICE, corresponding to engine speeds below 900 rpm, a fixed torque of 30 Nm was applied using a *Torque* template. This solution prevented abrupt variations in the torque delivered by the P0 e-motor during the engine start-up phase.

The main model and its corresponding surrogate model are therefore structured as shown in Figures 17 and 18.

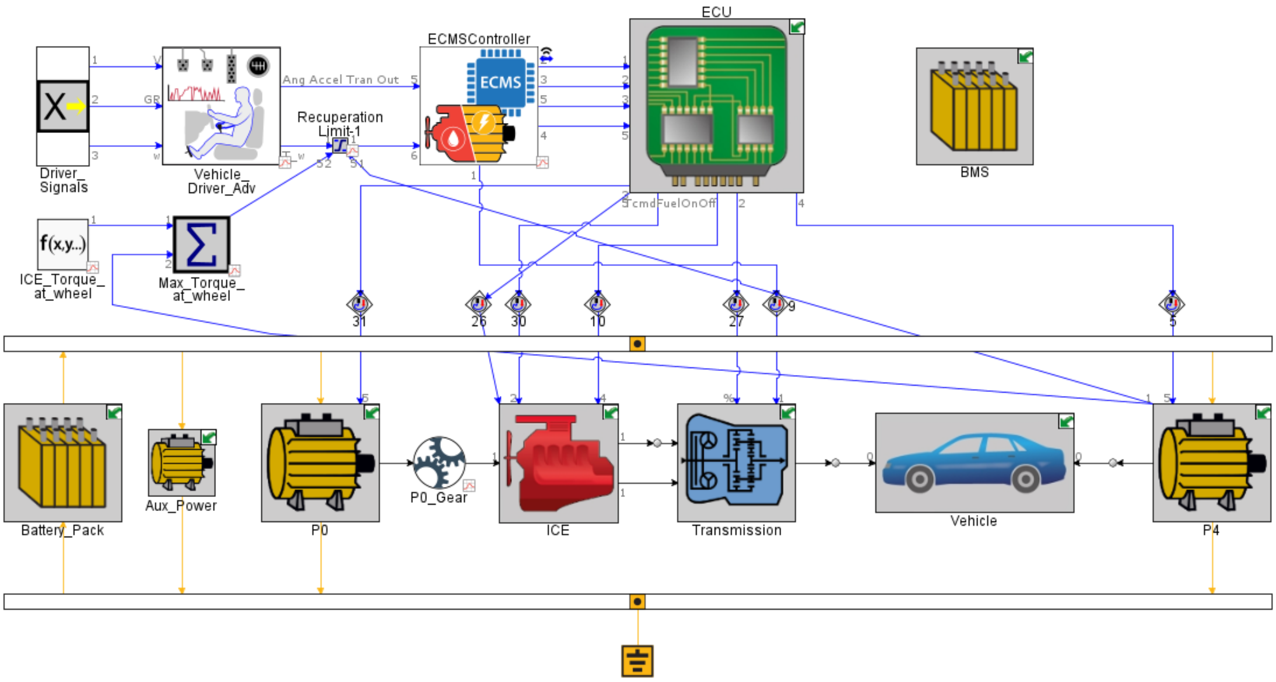

Figure 17: Vehicle Main Model

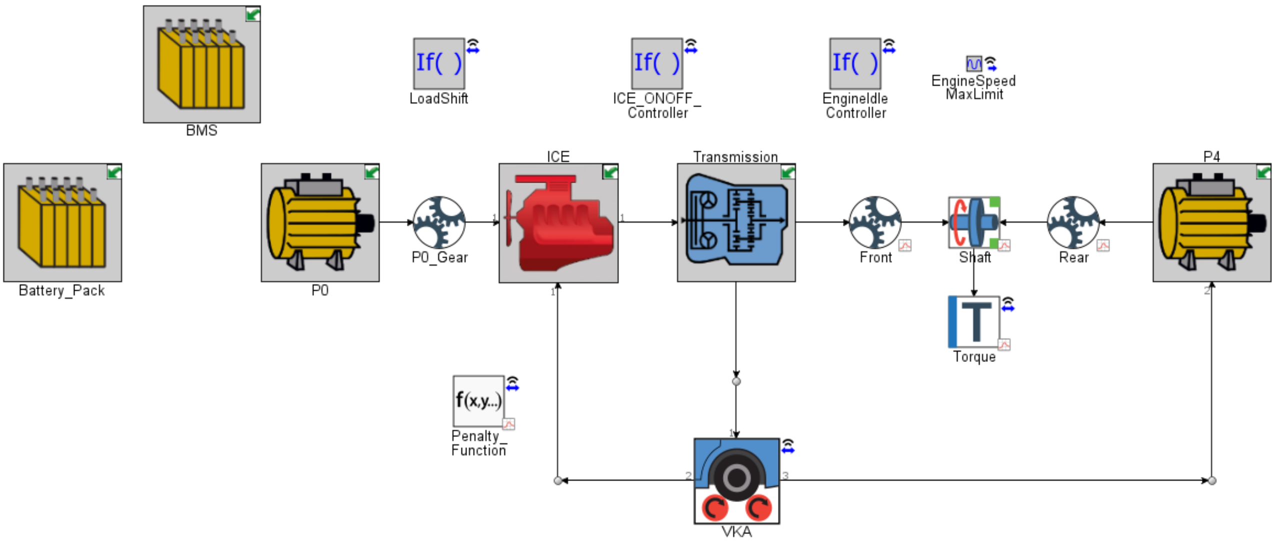

Figure 18: Vehicle Surrogate Model

The main model includes both lower and upper limits to the wheel torque request. The lower limit is determined by the Minimum Motor Torque of the P4 electric machine at the wheels, computed through the rear differential final drive ratio and the corresponding transmission efficiencies, thereby ensuring compliance with the battery charging limits. The upper limit, on the other hand, is defined by the sum of the Maximum Motor Torque of the P4 machine and the Maximum Torque at Current Speed of the internal combustion engine, both at the wheels.

In the surrogate model, the following operating conditions were specified to ensure the correct operation of the vehicle. In particular:

- when the vehicle operates in all-electric mode, the clutch actuator position is set to 100, the torque demand of the P0 motor is set to zero, and the internal combustion engine is kept switched off with the idle speed equal to zero;
- when the vehicle operates in hybrid mode, the clutch actuator position is set to 0, the internal combustion engine is switched on, and its idle speed is fixed at 850 rpm;
- when the internal combustion engine delivers torque to the wheels, the P4 electric machine is not allowed to operate in regenerative mode.

In the surrogate model, the VKA template, together with the vehicle topology and its operating modes, made it possible to define a set of four control variables relevant to the backward solution approach. These variables are listed in Table 17.

Control Input	Part	Variable Name	Minimum Limit	Maximum Limit	Minimum Resolution	Unit
Active Solution Power Source Port Number	*VKA*	*VKA*	*2*	*3*	*Integers only*	*-*
Requested Brake Torque	*P4*	*P4 Torque*	*-260*	*260*	*5%*	*Nm*
Requested Brake Torque	*P0*	*P0 Torque*	*-60*	*60*	*5%*	*Nm*
Requested Gear Number	*Transmission*	*Gear*	*1*	*6*	*Integers only*	*-*

Table 17: Backward State Optimization Control Inputs

An unconstrained optimization of the control variables may result in undesirable operating conditions due to excessively frequent or abrupt changes in their values. Therefore, the following time delays and change rate were introduced.

Control Input	Negative Time Delay	Positive Time Delay	Purpose
Active Solution Power Source Port Number	*-10 s*	*+10 s*	*Prevent too frequent changes in vehicle operating modes*
Requested Gear Number	*-5 s*	*+1 s*	*Prevent too frequent downshifting which may lead to spikes in wheel torque request*

Table 18: Time Delays for the Backward State Optimization

Control Input	Minimum Change Rate	Maximum Change Rate	Purpose
Requested Gear Number	*-10 s^{-1}*	*+10 s^{-1}*	*Imposing one gear per shift*

Table 19: Change Rate for the Backward State Optimization

In addition, the constraints shown in Table 20 were defined to avoid physically unrealistic operating conditions.

Dependent Variable	Minimum Limit	Maximum Limit
Battery State of Charge	*0.11*	*0.97*
P4 Brake Torque	*Minimum Motor Torque*	*Maximum Motor Torque*
P0 Brake Torque	*Minimum Motor Torque*	*Maximum Motor Torque*
ICE Brake Torque	*Minimum Torque at current speed*	*Maximum Torque at current speed*
ICE Speed	*Idle Speed*	*5000 rpm*
Battery Terminal Power	*Maximum Charge Power*	*Maximum Discharge Power*

Table 20: Dependent Variables Limits for the Backward State Optimization

The idle speed varies according to the engine state: it is set to 0 rpm when the ICE is switched off and to 850 rpm when ICE is on. The Maximum Charge Power is imposed as the lower limit for Battery Terminal Power, as GT-SUITE conventionally represents battery charging phases with negative power values.

Finally, the cost function was defined to express the equivalent fuel consumption, computed as the sum of the actual fuel consumption and a virtual fuel consumption associated with the use of electrical energy.

$$\dot{m}_{eqv} = \dot{m}_f + s * \frac{P_{batt}}{Q_{LHV}} * p \quad (5)$$

$$where \begin{cases} \dot{m}_{eqv} \text{ is the equivalent fuel consumption} \\ \dot{m}_f \text{ is the actual fuel consumption} \\ s \text{ is the equivalence factor} \\ P_{batt} \text{ is the battery terminal power} \\ Q_{LHV} \text{ is the fuel lower heating value} \\ p \text{ is the penalty function} \end{cases}$$

The equivalence factor accounts for both the cost associated with battery usage and the average efficiency of future energy conversions. It represents one of the key calibration parameters of the vehicle model, as it is used to tune the final State of Charge value so that it matches the experimental data provided by IFPEN.

The penalty function was introduced to modulate battery usage as a function of the State of Charge. Specifically, it encourages the use of electrical energy at high SOC levels, while progressively penalizing battery usage as the SOC decreases.

The default formulation adopted by the simulation software is given below.

$$p(SOC) = 1 - \left(\frac{SOC(t) - SOC_{tgt}}{\frac{SOC_{max} - SOC_{\min}}{2}} \right)^{\alpha} \quad (6)$$

$$where \begin{cases} p(SOC)\ is\ the\ penalty\ function \\ SOC(t)\ is\ the\ current\ SOC\ value\ calculated\ by\ GT-SUITE \\ SOC_{tgt}\ is\ the\ target\ SOC\ value\ at\ the\ end\ of\ the\ simulation \\ SOC_{max}\ is\ the\ SOC\ upper\ limit\ value \\ SOC_{min}\ is\ the\ SOC\ lower\ limit\ value \\ \alpha\ is\ the\ penalty\ function\ exponent \end{cases}$$

The resulting penalty function profiles is illustrated in Figure 19.

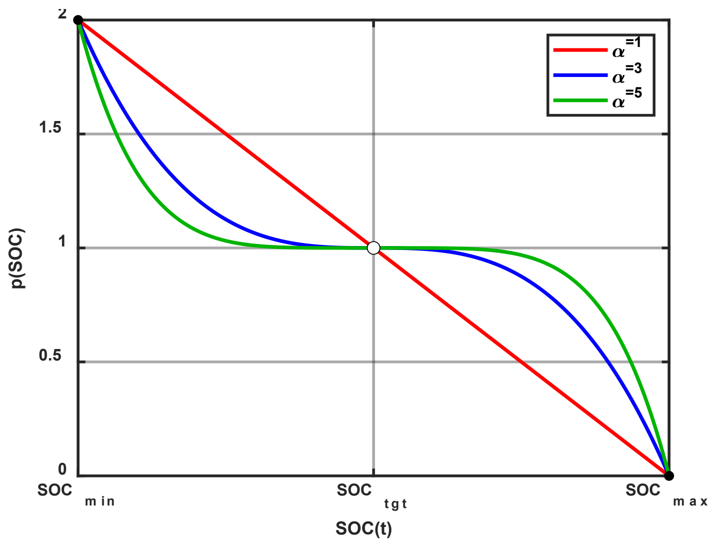

Figure 19: Default Penalty Function

However, when asymmetric SOC limits with respect to the target value are considered, the default penalty function must be modified by introducing two distinct operating ranges, depending on whether the current SOC is above or below the target value.

$$p(SOC) = 1 - \left(\frac{\max(SOC(t) - SOC_{tgt}, 0)}{SOC_{max} - SOC_{tgt}} + \frac{\min(SOC(t) - SOC_{tgt}, 0)}{SOC_{tgt} - SOC_{min}} \right)^{\alpha} \quad (7)$$

IFPEN provided the initial and final SOC values measured during a WLTC performed in Charge Sustaining mode. Accordingly, the target SOC was set equal to the initial SOC value. Using the set of parameters reported in Table 21, the corresponding penalty function was obtained, as shown in Figure 20.

WLTC – CS mode	
Initial SOC	*22.6%*
Final SOC	*19.8%*
Target SOC	*23.0%*
SOC max	*97%*
SOC min	*11%*

Table 21: Asymmetric SOC values

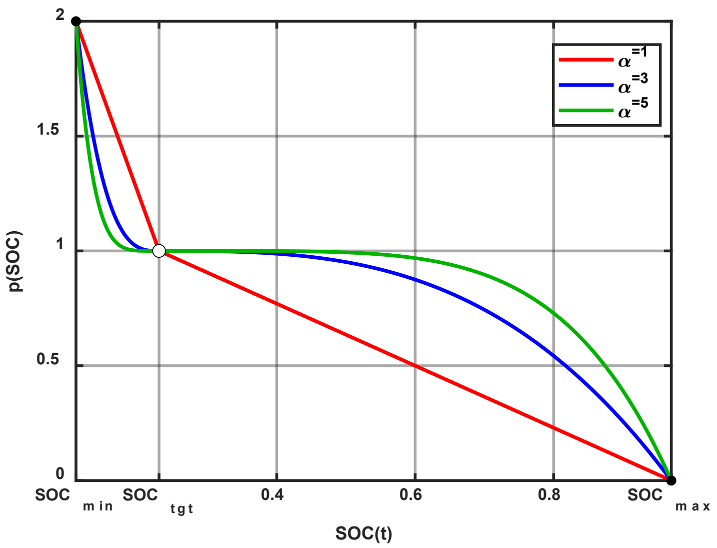

Figure 20: Penalty Function for asymmetric setup

Subsequently, the model was calibrated by tuning the equivalence factor and the penalty function exponent to obtain a final battery State of Charge consistent with the value provided by IFPEN. The model was then validated by comparing the simulation results with the experimental data in terms of average fuel consumption and average CO_2 emissions over the entire WLTC.

3.5 Conclusions

This chapter has presented the methodology adopted for the development of the numerical simulation platform within the PHOENICE project, with the objective of implementing a virtual test rig capable of reproducing the vehicle dynamic behaviour while enhancing the predictive capabilities of the engine Digital Twin.

The research activity began with the calibration of the Three Pressure Analysis model to reproduce the turbulence evolution obtained from the 3D CFD simulations. The optimization of the main turbulence-related parameters and tumble decay coefficients enabled a close agreement between the simulation results and the reference data, thereby improving the predictive capabilities of the model.

Subsequently, a valve flow analysis was carried out to investigate the air flow through the intake ports. The 3D CFD simulations provided the air mass flow rate entering the cylinder, from which both forward and reverse discharge coefficients were computed. This analysis made it possible to characterize the backflow phenomenon, which is particularly relevant when a Late Intake Valve Closing strategy is adopted, leading to a more accurate prediction of the trapped air mass.

The vehicle virtual test rig was then developed using the technical specifications of the prototype provided by IFPEN. Based on this data, a 0D and 1D map-based model was built to reproduce the hybrid vehicle architecture. Finally, an Equivalent Consumption Minimization Strategy was integrated to determine the operating condition that optimizes energy management. The calibration of the equivalence factor, combined with the implementation of an appropriate penalty function, enabled the model to reproduce the vehicle behaviour during a Charge Sustaining WLTC, thus providing results consistent with the experimental measurements acquired by IFPEN during roller bench testing.

Overall, the integration of the TPA turbulence model with the 3D CFD simulations of the intake flow significantly enhanced the predictive capabilities of the engine Digital Twin by refining the prediction of the combustion process. At the same time, the virtual test rig proved to be a reliable tool for analysing vehicle behaviour, particularly in terms of energy management, fuel consumption reduction, and pollutant emissions limitation.

4 Digital Twin Refinement Results

4.1 Introduction

This chapter focuses on the analysis of the results obtained from the numerical simulations carried out on the engine model, through comparison with the dataset provided by the Politecnico di Torino. The main objective of the activities was to optimize the engine Digital Twin in order to enhance its predictive capabilities over a wide range of operating conditions.

The presentation of the results follows the same structure adopted in *Chapter 3*, retracing the main stages of the Digital Twin refinement process. In particular, the chapter is organized as follows:

- presentation of the results obtained with the Three Pressure Analysis (TPA) model, together with the calibration of the turbulence parameters aimed at correlating the one-dimensional model with the reference data;
- comparison between the experimental discharge coefficients and those obtained from the three-dimensional CFD simulations to evaluate the accuracy of the trapped air mass estimation during the intake process.

The analysis of the results made it possible to assess the effectiveness of the adopted methodologies and the contribution of the simulation activities to the progressive refinement of the Digital Twin, highlighting the improvement in its predictive capabilities.

4.2 TPA Model Results

In this section, the results obtained with the Three Pressure Analysis model, calibrated using the dataset provided by Politecnico di Torino, are analysed. The main objective is to assess the model's ability to accurately reproduce the in-cylinder turbulence, which is essential for enhancing the predictive capabilities of the engine Digital Twin.

The working points considered cover a wide range of operating conditions, characterized by significantly different engine speeds, loads, and charge dilution levels. These parameters directly influence not only the combustion process and the engine pumping cycle but also the evolution of in-cylinder turbulence, whose accurate reproduction represents the primary scope of the TPA model.

Charge dilution, achieved through lean-burn operation and exhaust gas recirculation, represents one of the key technologies for attaining the gross indicated thermal efficiency target of 47% established within the project. A higher degree of charge dilution allows a more advanced spark timing, thereby increasing both the peak in-cylinder pressure and the amount of useful work extracted during the expansion stroke. On the other hand, increasing the dilution level significantly reduces the turbulence intensity and the tumble decay, leading to poorer air–fuel mixing and, consequently, a slower combustion process.

Engine speed and load also have a significant influence on the engine operating cycle. In particular, they affect the turbulence evolution, although to a lesser extent than charge dilution, as well as the volumetric efficiency, the intake air mass flow, and the pressure traces.

The analysis of the TPA model results began with the comparison of the simulated in-cylinder pressure and trapped mass profiles against the corresponding reference data. Subsequently, the predicted TKE and LS curves during the intake and compression strokes were compared with the corresponding CFD traces to assess the accuracy of the turbulence reconstruction, thereby improving the simulation of the combustion process under the different operating conditions considered.

As described in the previous chapter, the following steps were carried out to achieve an accurate correlation between the pressure profiles predicted by the model and those provided in the reference dataset:

- imposition of the boundary conditions, consisting of the pressure downstream of the intake manifold and the turbine inlet pressure;
- introduction of the in-cylinder pressure trace provided in the reference dataset;
- consistency of the parameter values reported in Table 22, which were kept unchanged with respect to the reference three-dimensional CFD model.

TPA Parameters	
Compression Ratio	13.6
Heat Transfer Multiplier	1.5

Table 22: Geometric and thermal calibration parameters

During this initial stage, the turbulence parameters previously implemented in the Digital Twin were kept constant. The corresponding values are reported in Table 23.

Turbulence Calibration Parameters	***Initial Value***
Production Term Multiplier	0.71
Geometric Length Scale Multiplier	0.80
Intake Term Multiplier	2.40
Tumble Term Multiplier	1.97
Tumble Destruction Coefficient 1	0.11
Outflow Tumble Decay Multiplier	0.26

Table 23: Turbulence calibration parameters initial values

This resulted in an initial model version, referred to as V01.

The following section presents the results obtained for the three V01 operating points including fuel injection, selected as they are more representative of the actual operating conditions of an internal combustion engine than the corresponding non-injection cases.

Case 1: 4500 rpm x 16 bar BMEP

The first operating point analysed is characterized by high engine speed and high load. Together with a stoichiometric mixture and a low EGR rate, these conditions contribute to high pressure and temperatures levels during the combustion process, thereby limiting the allowable spark advance in order to prevent knock onset, as summarized in Table 24.

Operating Condition 1	
Engine Speed [rpm]	*4500*
BMEP [bar]	*16*
λ [-]	*1*
EGR [%]	*5.03*
Spark advance [CA aTDCf]	*-5*

Table 24: First operating point

Figure 21 shows the results obtained with the TPA model using the CR and HTM values reported in Table 22, while imposing the pressure boundary conditions previously defined.

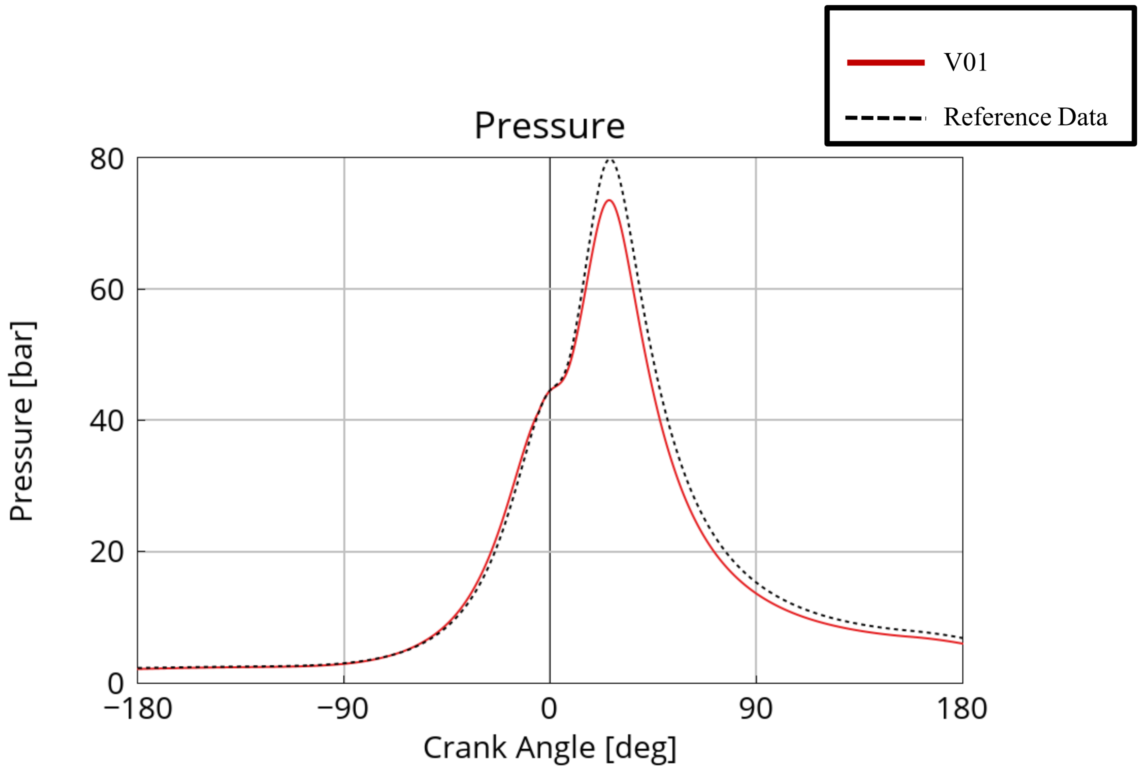

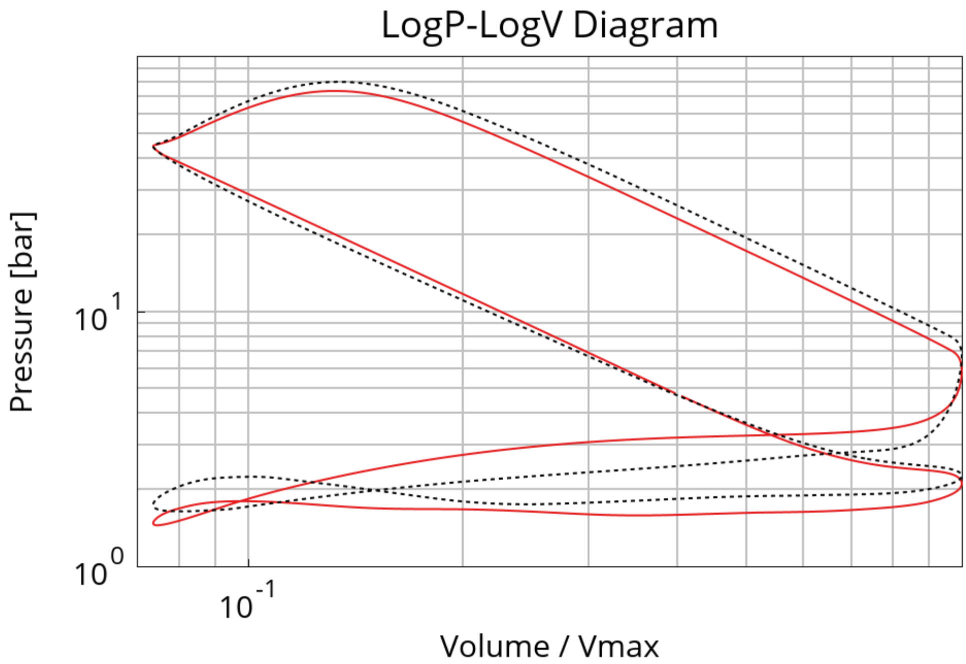

Figure 21: Pressure cycle for 4500 rpm x 16 bar BMEP

The analysis of the results shows that the TPA model is able to accurately reproduce the in-cylinder pressure cycle, particularly during the intake and compression phases, which are of primary interest for the calibration of the turbulence model. The accurate reconstruction of the pressure profile is reflected in a reliable evaluation of the trapped mass after intake valve closing.

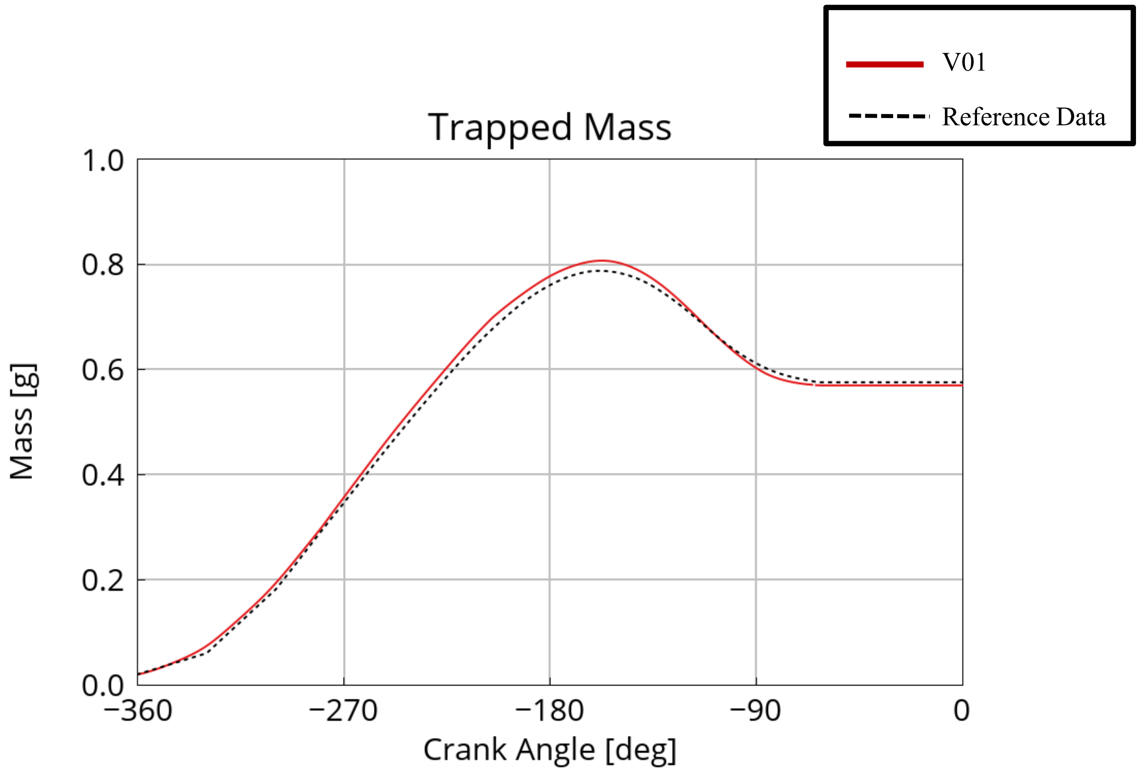

Figure 22: Trapped mass for 4500 rpm x 16 bar BMEP

The results indicate a slight overestimation of the maximum trapped mass value, which is reached shortly after BDC because of the high inertia of the intake air column. The final value at TDC, which is lower than the maximum due to the backflow phenomenon induced by the LIVC strategy, is instead accurately reproduced by the model.

The prediction of the in-cylinder turbulence was assessed by analysing the TKE and Normalized Turbulent Length Scale (LS) profiles obtained with the initial set of turbulence parameter. The corresponding results are presented in Figure 23.

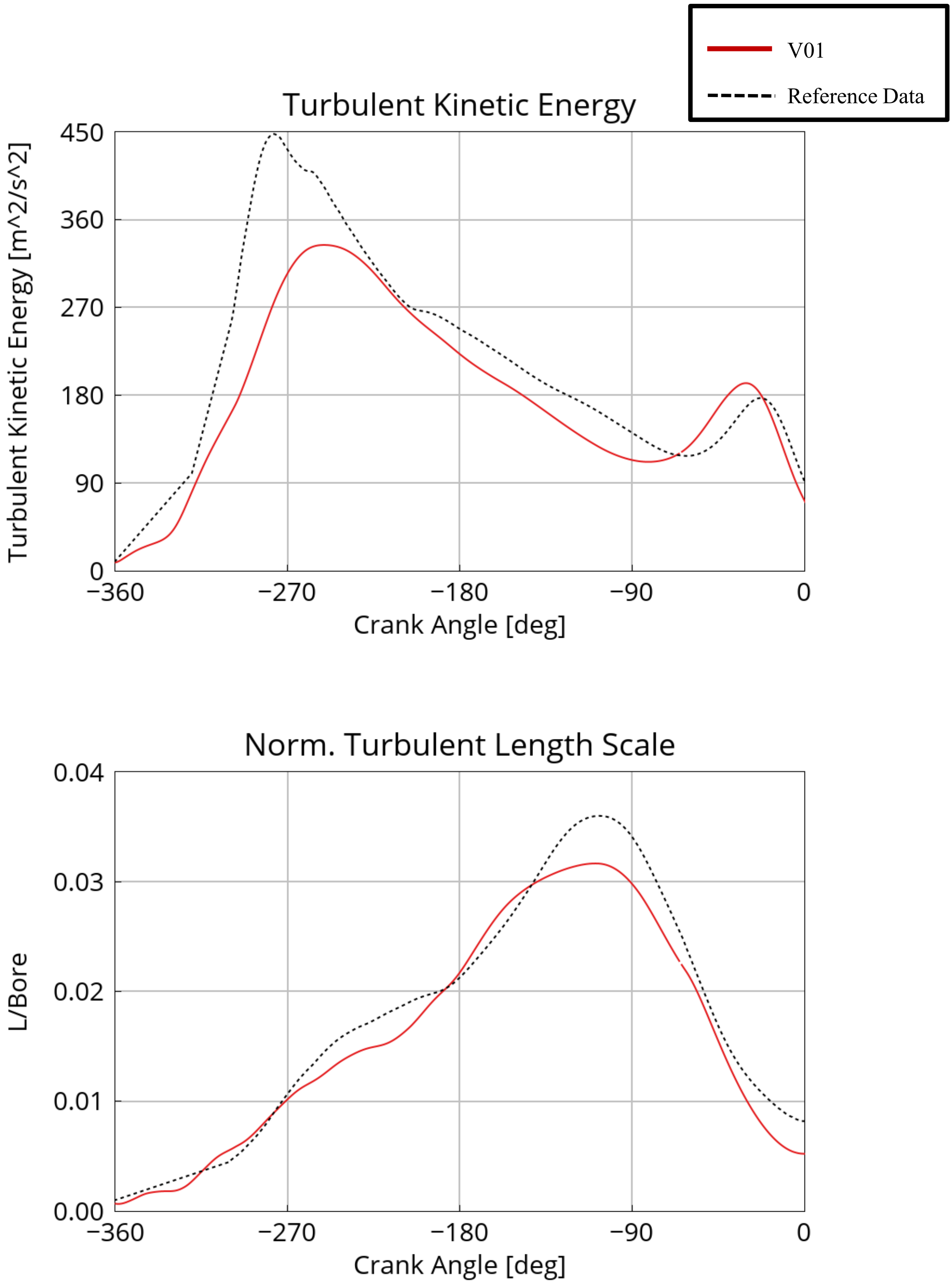

Figure 23: Turbulence profiles for 4500 rpm x 16 bar BMEP

The simulated TKE and LS profiles demonstrate the need for further calibration of the turbulence parameters to improve the reproduction of the reference profiles.

Case 2: 2500 rpm x 10 bar BMEP

The second operating condition is characterized by an intermediate engine speed and a medium load. Compared with the previous case, the increased charge dilution level and the higher EGR rate allow a more advanced spark timing, as summarized in Table 25.

Operating Condition 2	
Engine Speed [rpm]	*2500*
BMEP [bar]	*10*
λ *[-]*	*1.16*
EGR [%]	*10.76*
Spark advance [CA aTDCf]	*-16*

Table 25: Second operating point

The resulting pressure cycle is illustrated below.

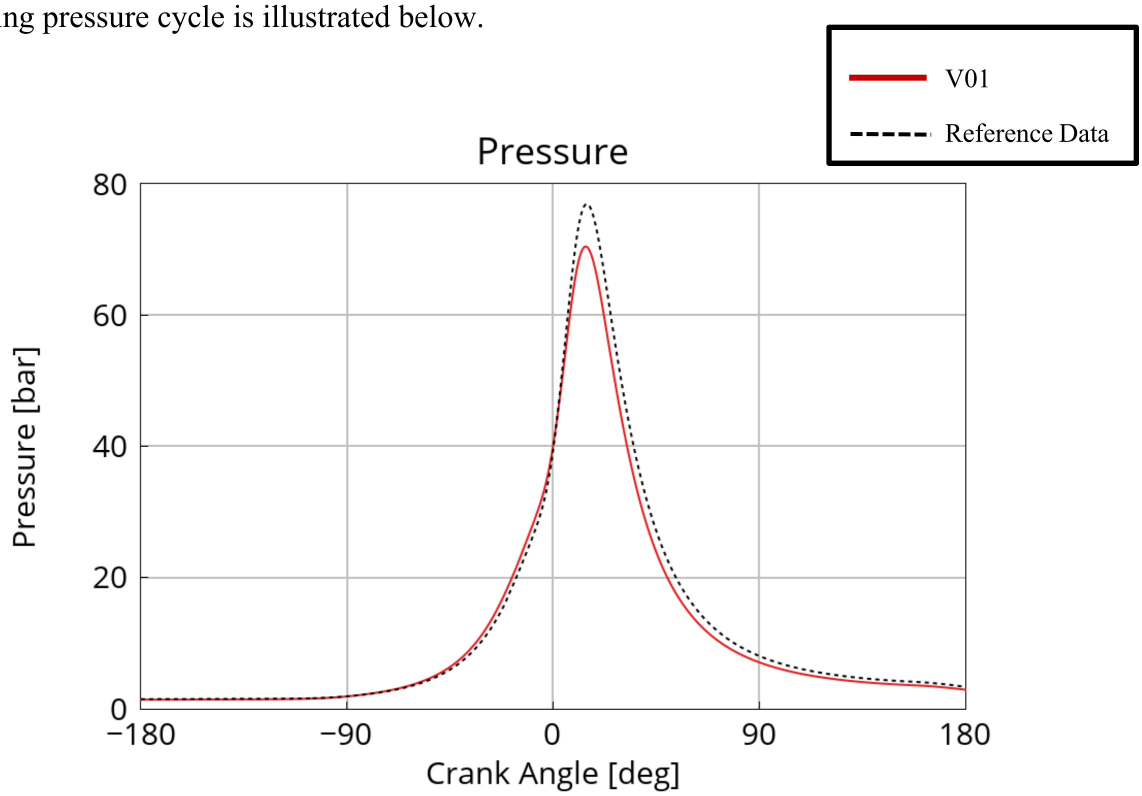

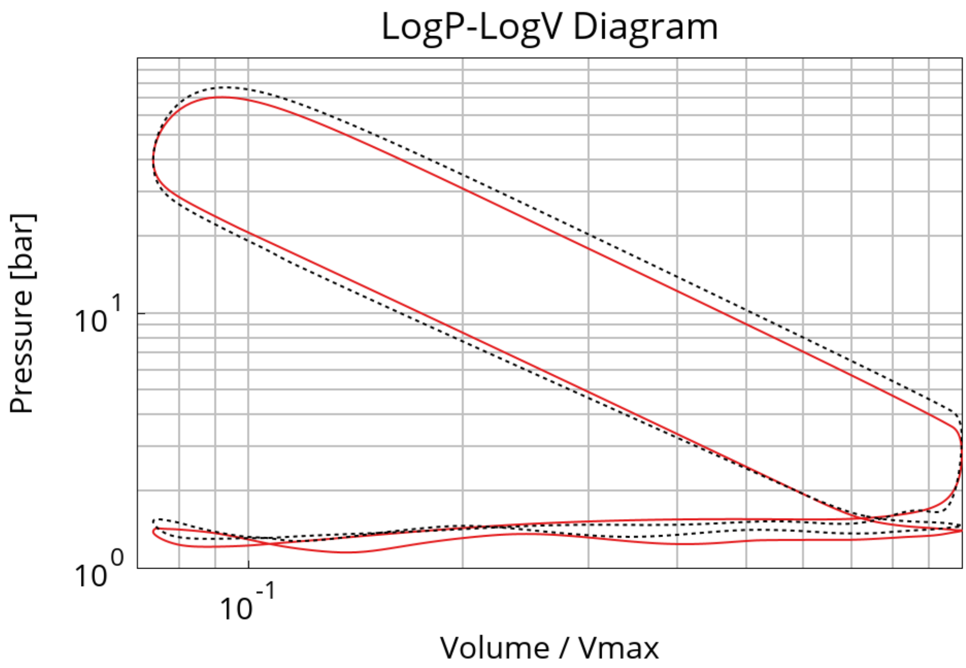

Figure 24: Pressure cycle for 2500 rpm x 10 bar BMEP

The results show good agreement during the intake phase and throughout the entire pumping cycle. Compared with the previously analysed operating condition, a slightly larger discrepancy can be observed during the compression stroke. This deviation results in an overestimation of the trapped mass, although the error at Intake Valve Closing remains below 5%.

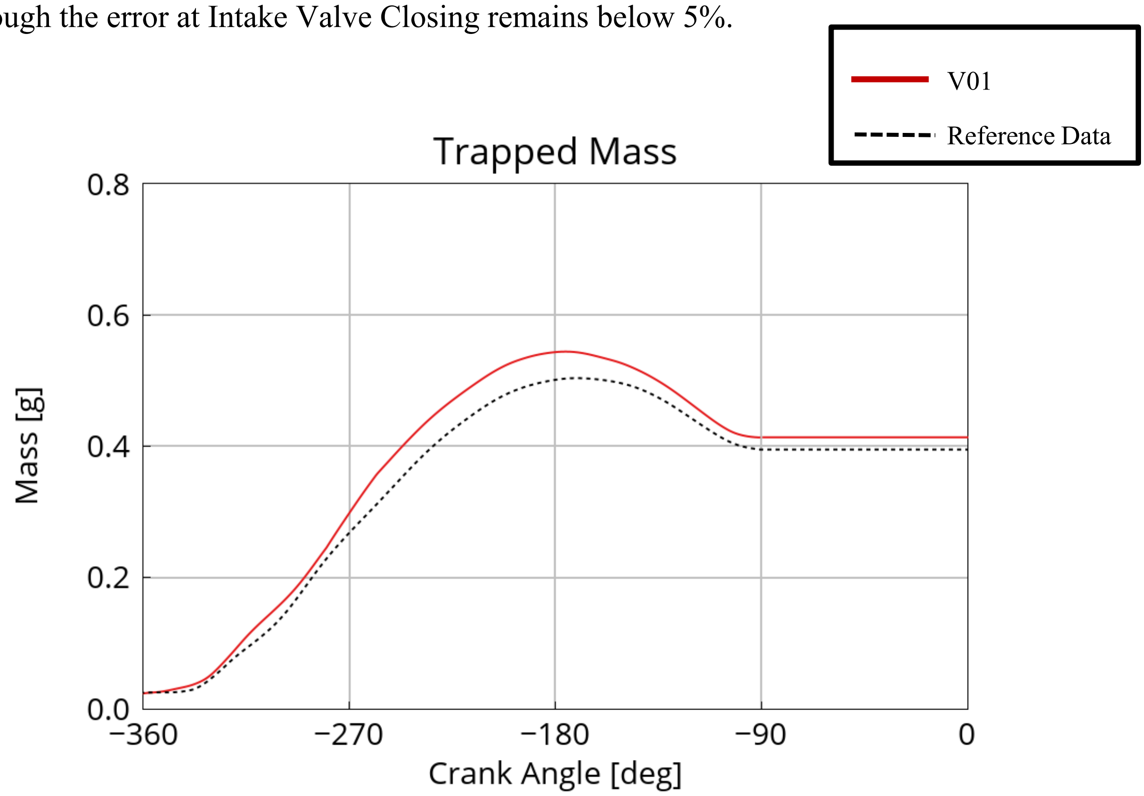

Figure 25: Trapped mass for 2500 rpm x 10 bar BMEP

As in the previous case, the initial turbulence and tumble decay coefficients are not sufficient to accurately reproduce the in-cylinder turbulence evolution, particularly in the crank-angle interval preceding ignition, as shown in Figure 26.

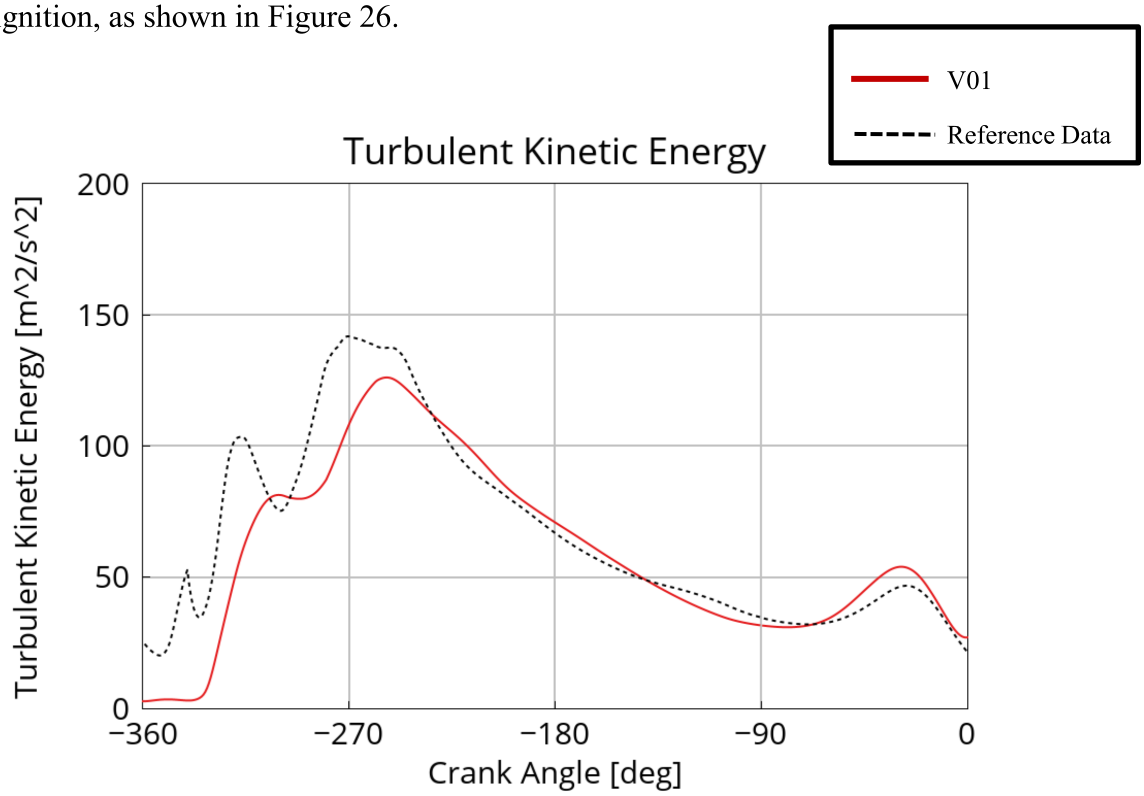

Figure 26: Turbulence profiles for 2500 rpm x 10 bar BMEP

Case 3: 2000 rpm x 6 bar BMEP

The third working point is characterized by a low load and a medium-low engine speed. Together with an EGR rate and a charge dilution level comparable to those of the previous case, these conditions allow a further increase in spark advance, as summarized in Table 26.

Operating Condition 3	
Engine Speed [rpm]	*2000*
BMEP [bar]	*6*
λ *[-]*	*1.14*
EGR [%]	*10.95*
Spark advance [CA aTDCf]	*-23*

Table 26: Third operating point

The resulting pressure cycle is presented in Figure 27.

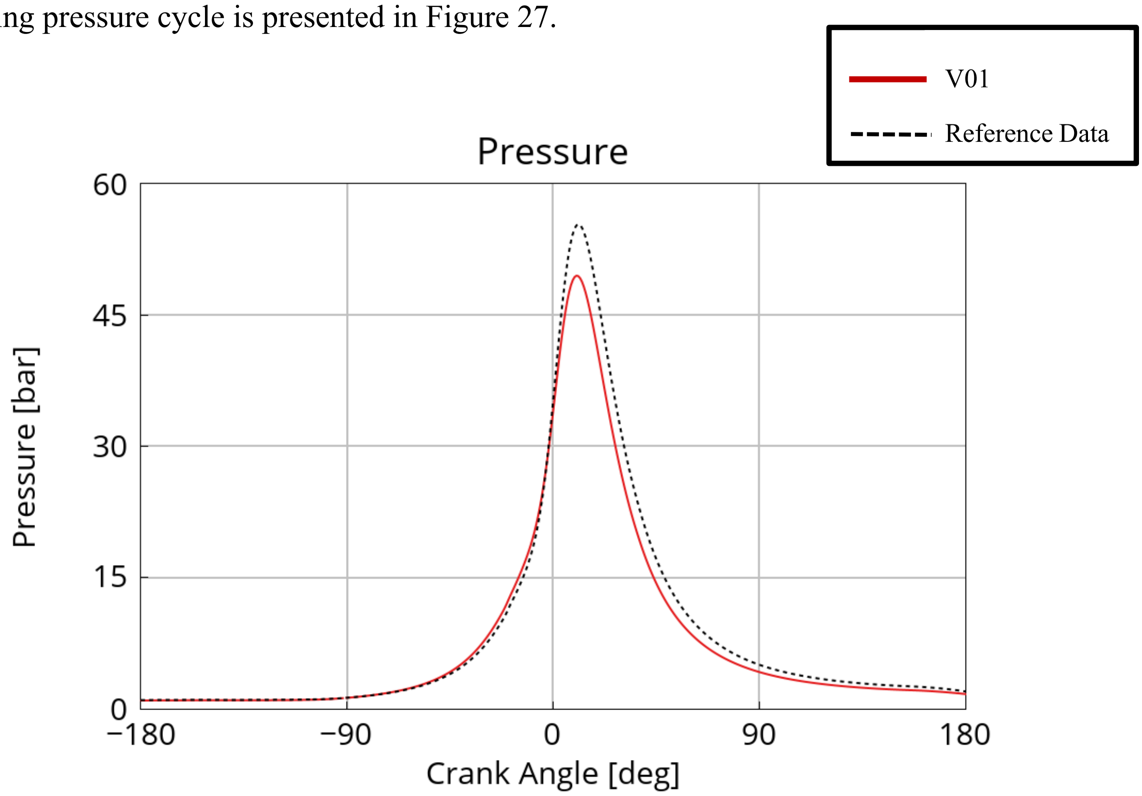

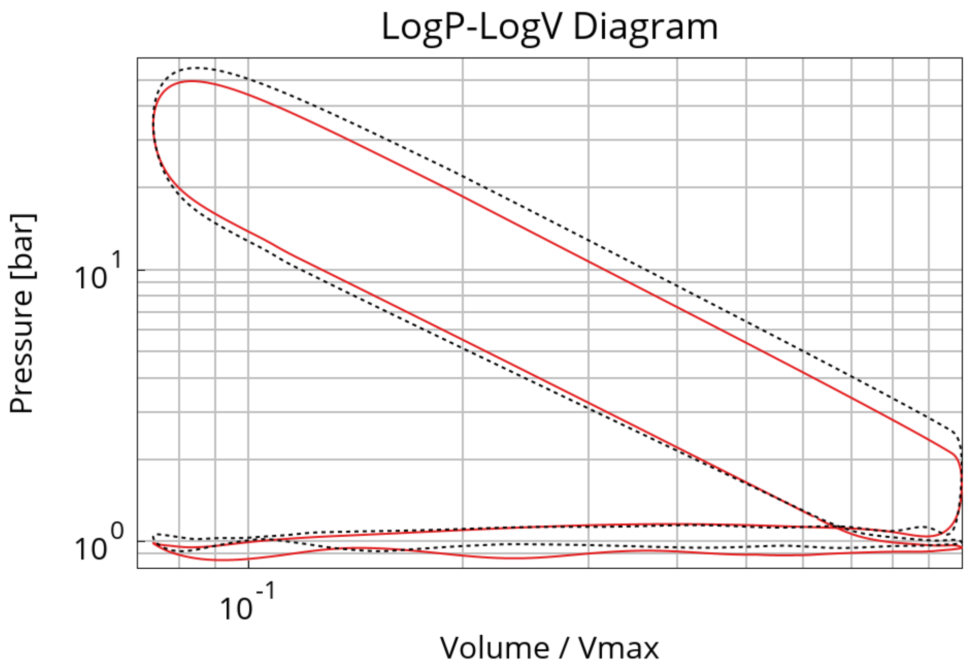

Figure 27: Pressure cycle for 2000 rpm x 6 bar BMEP

In this case, the largest discrepancies are observed during the expansion stroke and are primarily attributed to an overestimated heat transfer coefficient. Conversely, the pumping cycle, as well as the intake and compression phases, is accurately reproduced, resulting in a reliable evaluation of the trapped mass, as illustrated in Figure 28.

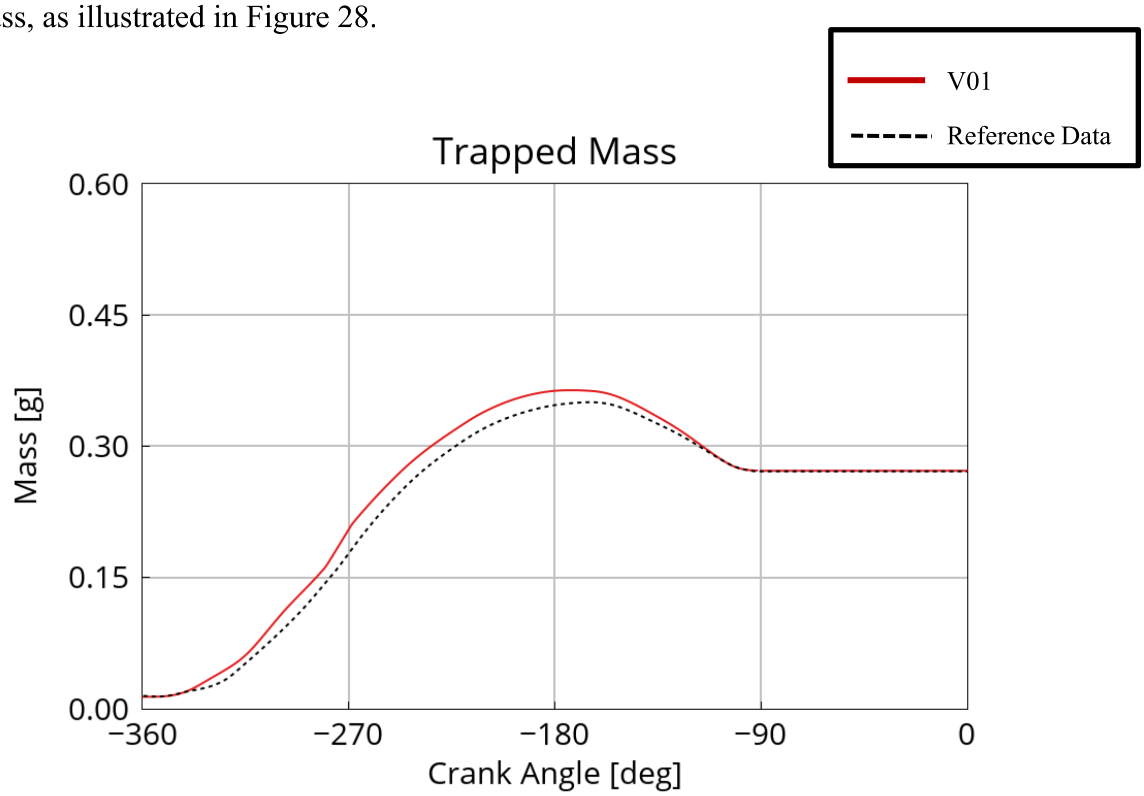

Figure 28: Trapped mass for 2000 rpm x 6 bar BMEP

Similarly, for this operating condition, the model does not accurately reproduce the TKE and LS profiles during the crank-angle interval preceding combustion, as presented in Figure 29.

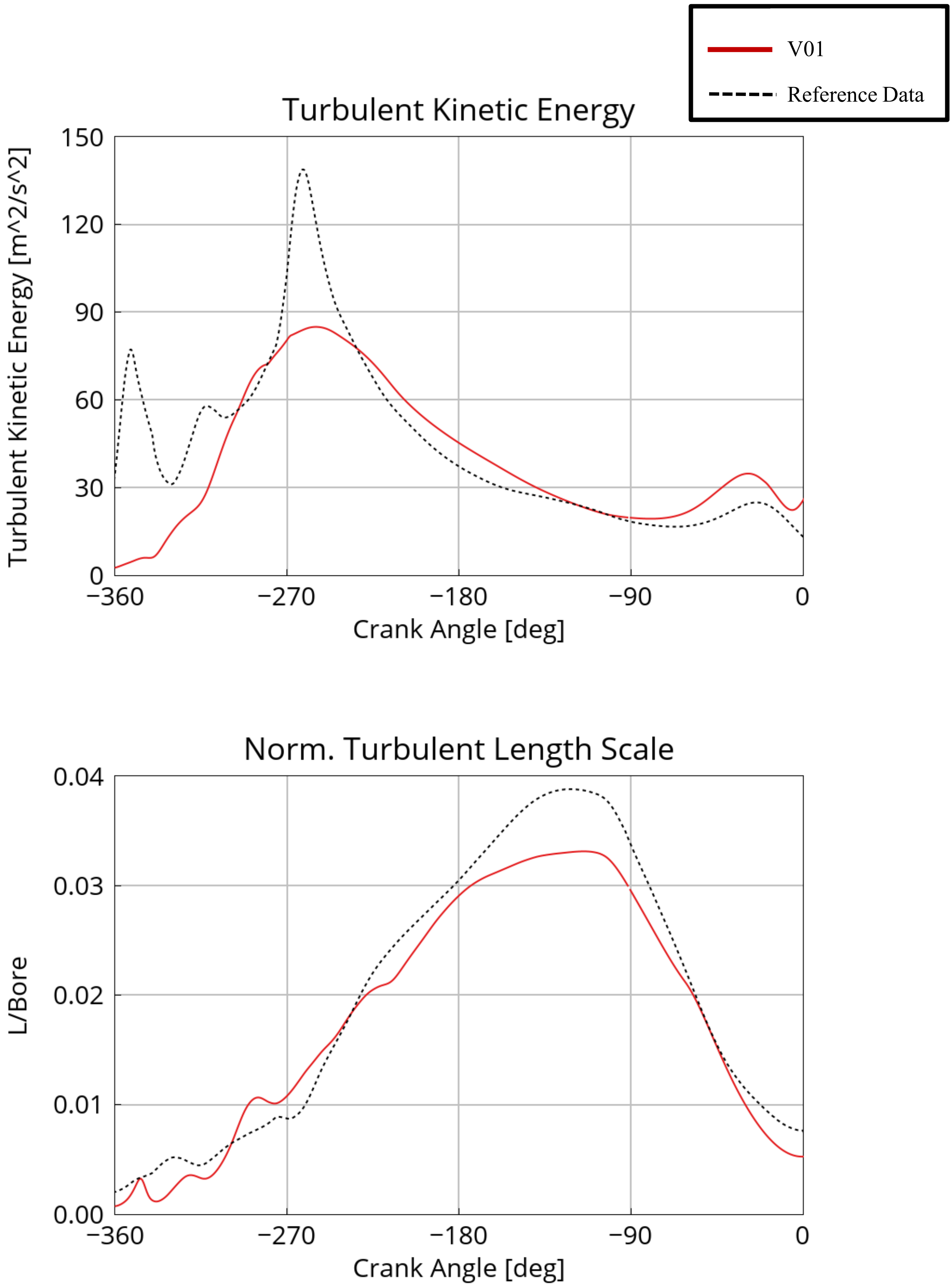

Figure 29: Turbulence profiles for 2000 rpm x 6 bar BMEP

The results obtained with the initial version of the TPA model highlighted the need to calibrate the turbulence and tumble decay parameters, as the simulated TKE and LS profiles exhibited significant deviations from the reference data. The calibration procedure began with a sensitivity analysis aimed at evaluating the influence of each coefficient on the evolution of the in-cylinder turbulence. In particular, the Spray/Jet Term Multiplier, which represents the contribution of fuel injection to mean kinetic energy, proved to be the parameter with the greatest influence on the TKE profile, especially under low-speed and low-load operating conditions, as evidenced in Figure 30.

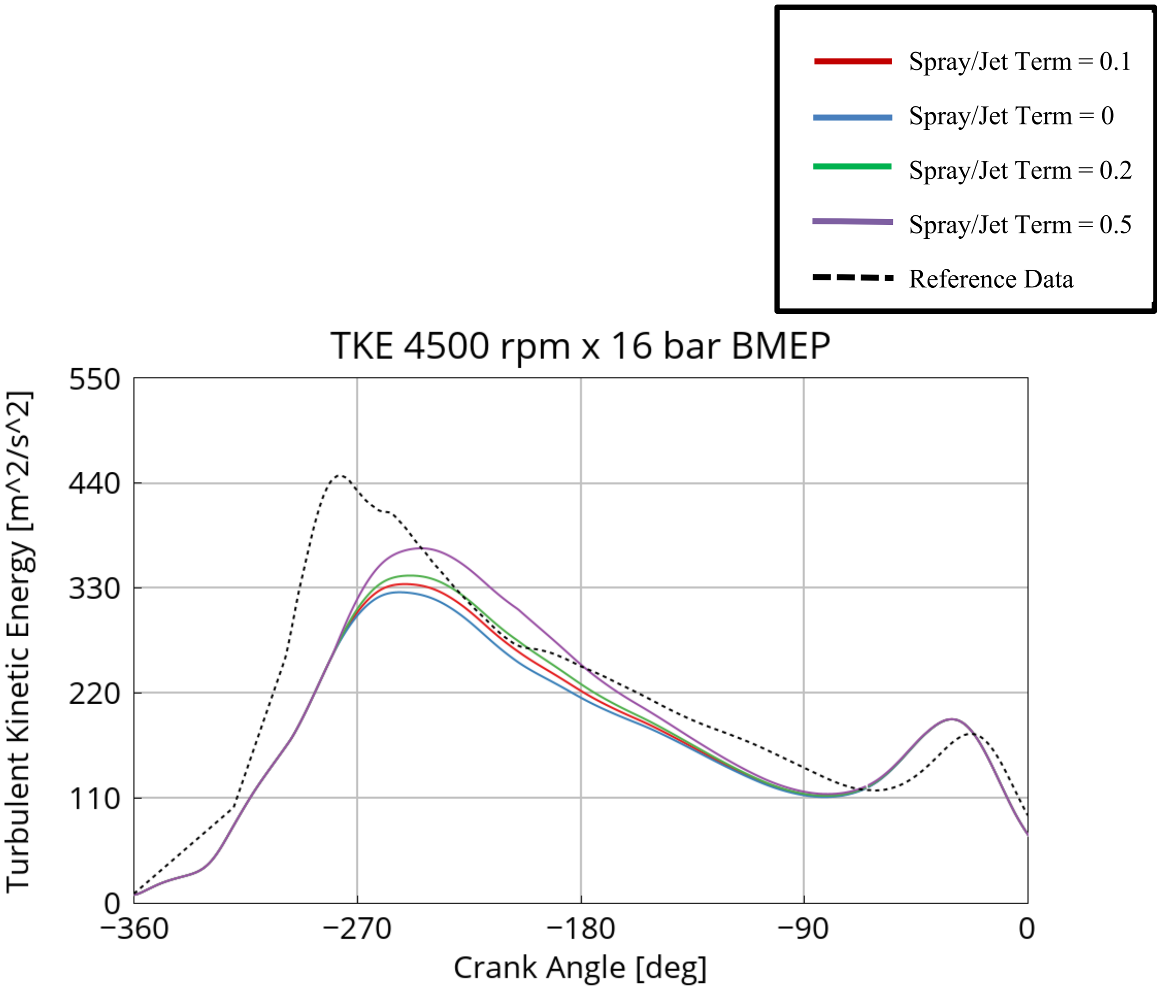

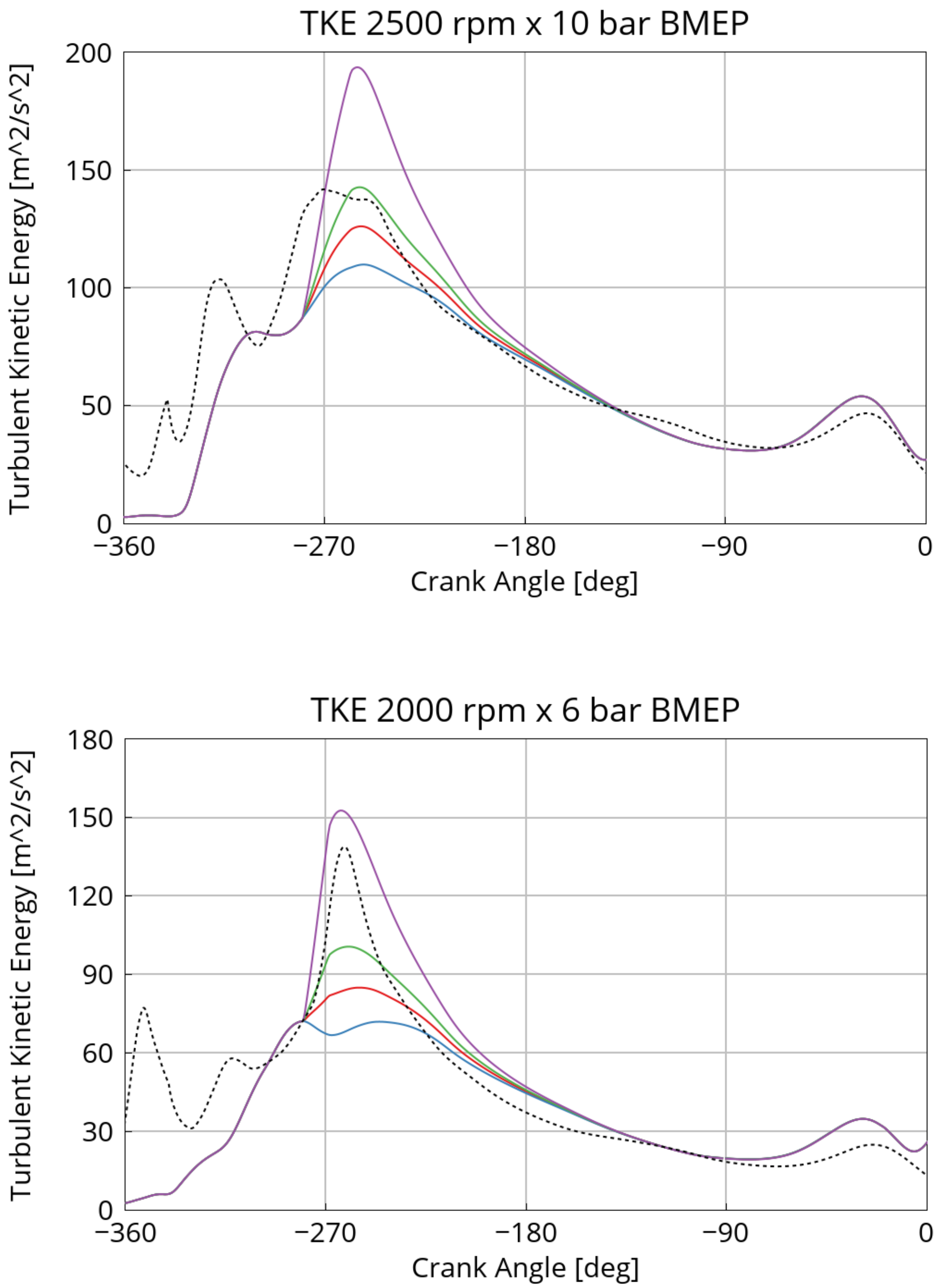

Figure 30: Spray/Jet Term Multiplier influence on TKE profiles

Following the sensitivity analysis, the Spray/Jet Term Multiplier value providing the best overall agreement for all three simulated points was selected:

Sensitivity Analysis Results	Initial Value	Updated Value
Spray/Jet Term Multiplier	*0.10*	*0.24*

Table 27: Spray/Jet Term Multiplier final value

The remaining turbulence parameters were optimized within the GT-SUITE environment to identify the values that minimize the deviation between the simulated and reference TKE and LS profiles during the intake and compression strokes for each operating condition. In contrast, the turbulence evolution during the combustion process and the subsequent exhaust stroke was not considered, since accurately reproducing this phase is particularly challenging and would have a limited impact on the predictive capabilities of the engine Digital Twin.

The following section presents the results obtained with the V02 model, developed using the optimized turbulence parameter values reported in Table 28.

Turbulence Calibration Parameters	*Initial Value*	*Optimized Value*
Production Term Multiplier	0.71	0.97
Geometric Length Scale Multiplier	0.80	1.91
Intake Term Multiplier	2.40	2.31
Tumble Term Multiplier	1.97	1.62
Tumble Destruction Coefficient 1	0.11	0.09
Outflow Tumble Decay Multiplier	0.26	0.25

Table 28: Turbulence parameters optimized values

Case 1: 4500 rpm x 16 bar BMEP

Since the optimization only affected the turbulence parameters, the TPA model results related to the pressure cycle remain unchanged. The corresponding TKE and LS profiles are presented in Figure 31.

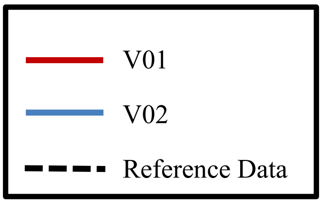

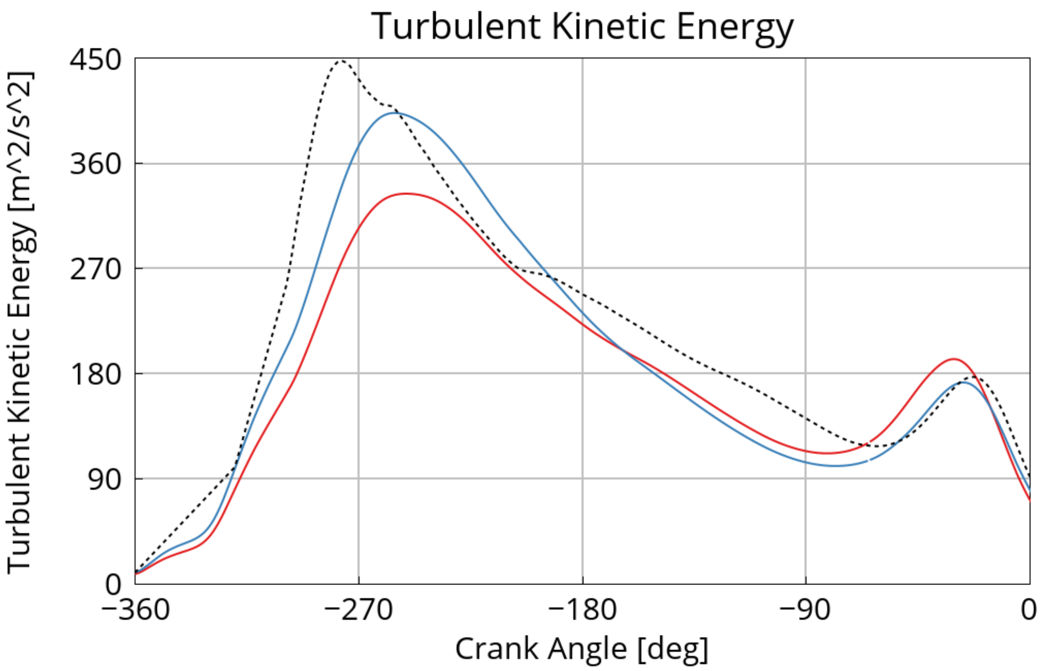

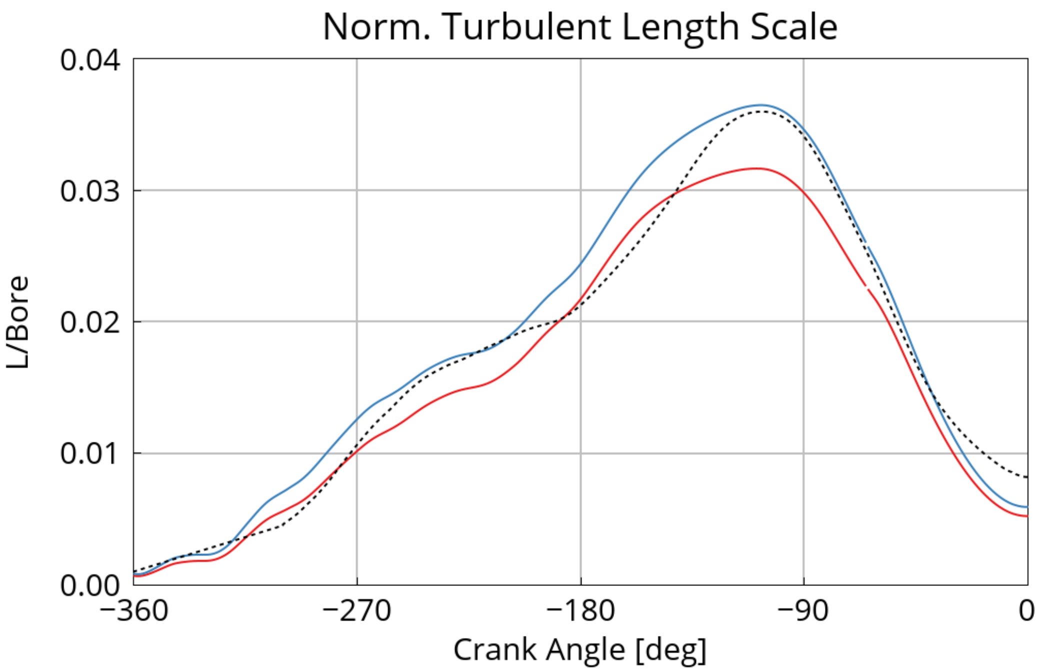

Figure 31: Optimized turbulence profiles for 4500 rpm x 16 bar BMEP

The optimization resulted in improved agreement between the simulated and reference TKE profiles, allowing a more accurate prediction of both the first peak, associated with the turbulence generated by fuel injection, and the second peak, corresponding to the tumble decay following intake valve closing. The LS profile also exhibits a significantly improved correlation.

Case 2: 2500 rpm x 10 bar BMEP

The TKE and LS profiles for the second operating condition are reported in Figure 32.

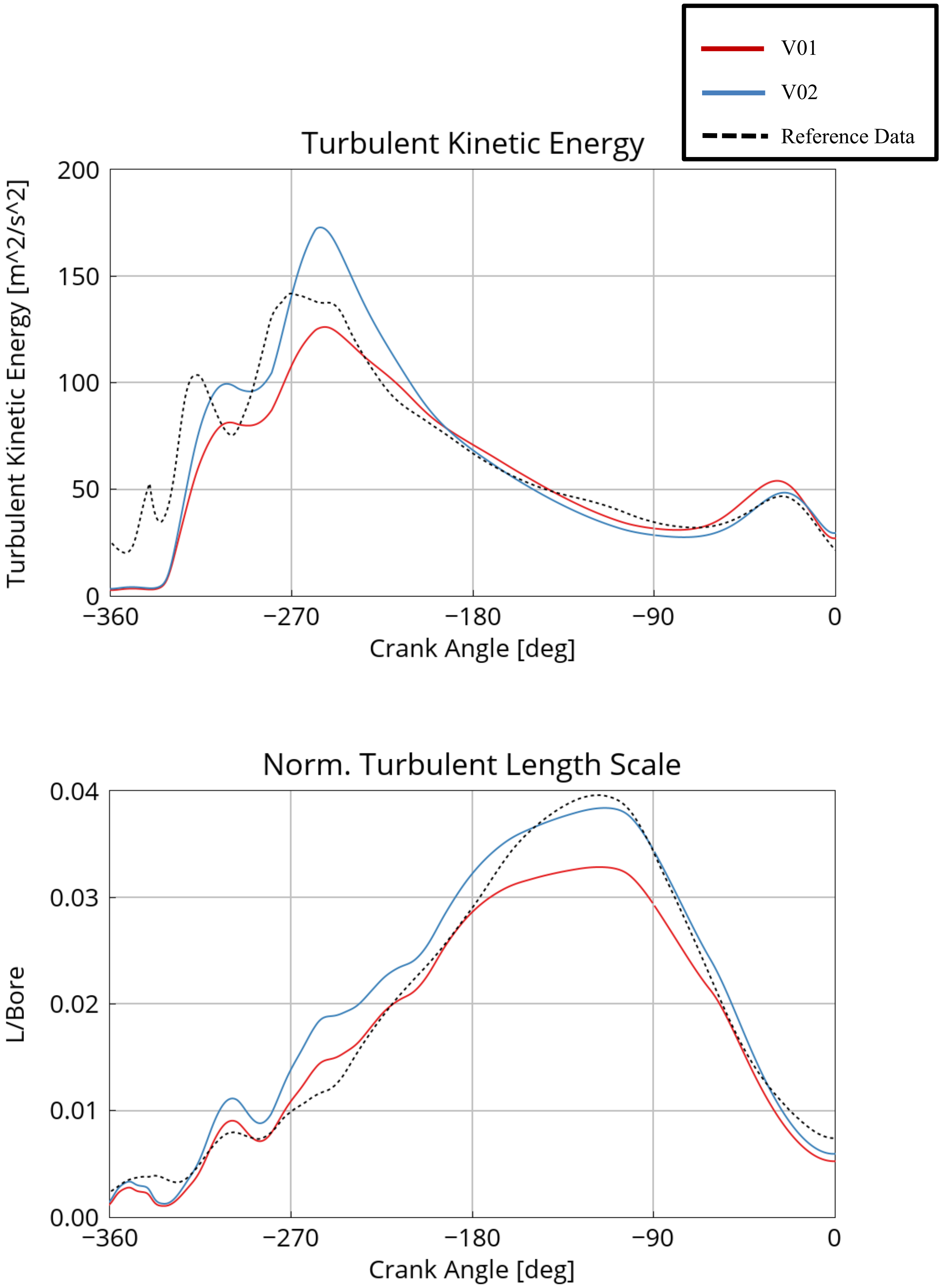

Figure 32: Optimized turbulence profiles for 2500 rpm x 10 bar BMEP

For this operating point, the increase in the Spray/Jet Term Multiplier results in a slight overestimation of the peak TKE value. Nevertheless, the optimization provides a more accurate prediction of the turbulence peak preceding ignition. As for the LS, a noticeable improvement is observed in the reproduction of the profile, particularly after BDC.

Case 3: 2000 rpm x 6 bar BMEP

Figure 33 illustrates the results for the third operating condition.

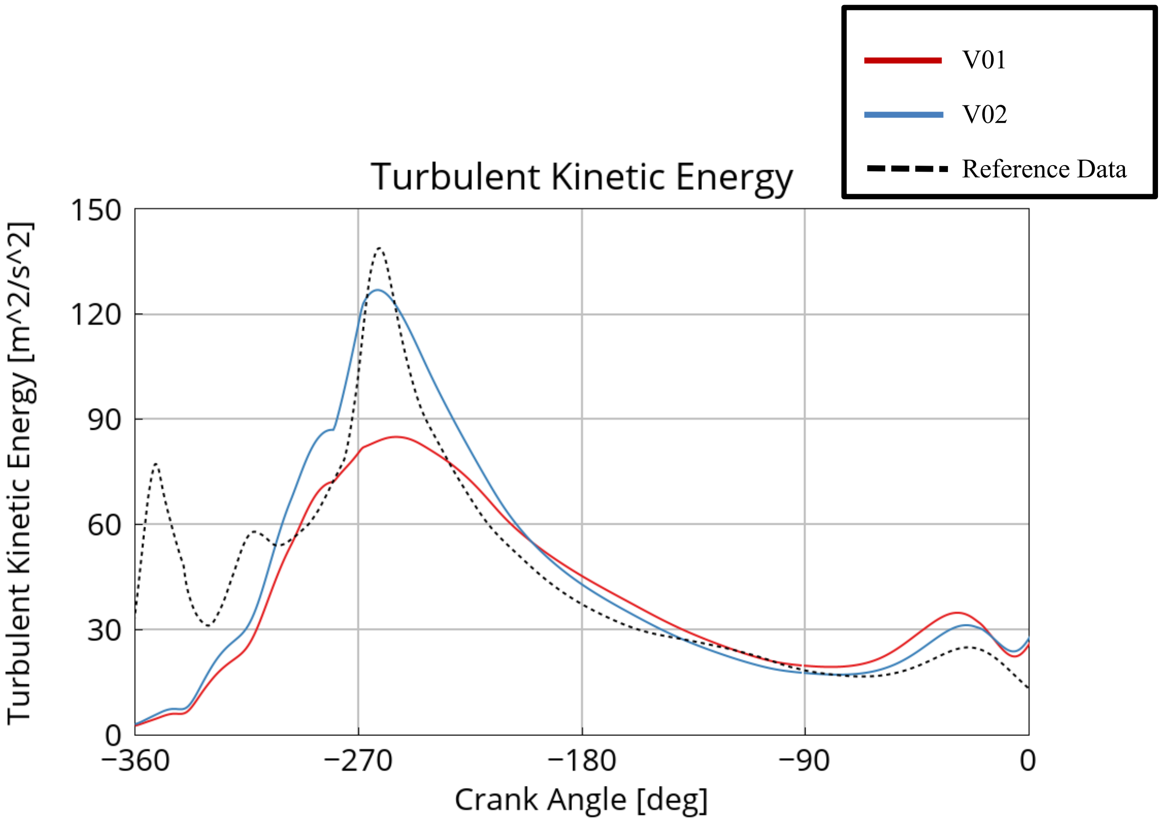

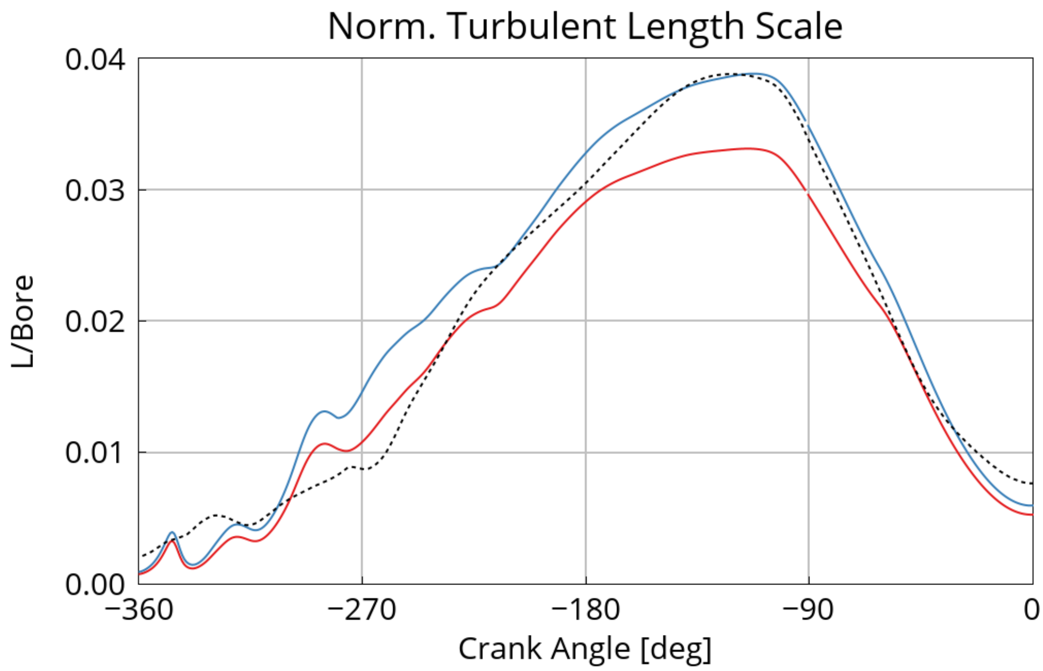

Figure 33: Optimized turbulence profiles for 2000 rpm x 6 bar BMEP

The calibrated LS profile follows a trend consistent with that observed for the other operating conditions, while a similar improvement is achieved for the TKE during the compression stroke. Moreover, compared with the previous operating condition, the higher Spray/Jet Term Multiplier enables a more accurate prediction of the TKE peak for this case.

The comparison between the pressure trace predicted by the TPA model and the reference data reveals only minor deviations throughout the engine cycle, with a precise correlation particularly during the compression stroke. All the operating conditions considered exhibit good agreement between the simulation results and the provided dataset, especially in terms of Peak Firing Pressure (PFP) phasing and slopes of the compression and expansion polytropic curves. The most significant deviations are confined to the final stage of the expansion stroke and can be attributed to the simplified modelling of the heat transfer between the burned gases and the cylinder walls. Overall, the results confirm the robustness of the model over a wide range of operating conditions, providing a reliable basis for the subsequent turbulence calibration.

The optimized TPA model, evaluated by means of the TKE and LS curves, shows a significant improvement in the prediction of the in-cylinder turbulence evolution, particularly during the intake and compression strokes. The integration of the optimized turbulence parameters into the engine model further enhanced the predictive capabilities of the Digital Twin by refining the simulation of the combustion process.

4.3 Intake Flow Analysis Results

The aim of this section is to present the results of the flow bench analysis performed on the 3D engine model by comparing the experimental discharge coefficients provided by IFPEN with those obtained from the CFD simulations carried out in CONVERGE Studio.

The 3D CFD simulations enable a detailed analysis of the flow through the intake ports, allowing the inlet and outlet air mass flow rates to be accurately evaluated. Given the adoption of aggressive Miller strategies to reduce the effective compression ratio with respect to the geometric CR, thereby limiting the end-of-compression temperature, it is essential to determine not only the forward discharge coefficients but also the reverse CDs, in order to characterize the backflow phenomenon associated with the LIVC strategy.

The different configurations developed for the single-cylinder 3D engine model made it possible to evaluate the air mass flow rate through the measurement region at various valve lifts, as reported in Table 29.

Valve Lift (L) [mm]	
	0.2
Low Lift	*0.5*
	1
	2
	3
Medium Lift	*4*
	6
	8
High Lift	*10*
	11

Table 29: Valve lifts for CDs calculation

About the forward discharge coefficients, the mass flow rate profiles through the measurement region, obtained from the CFD simulations by imposing a pressure drop of 5000 Pa between the intake manifold and the bottom of the liner, are presented in Figure 34.

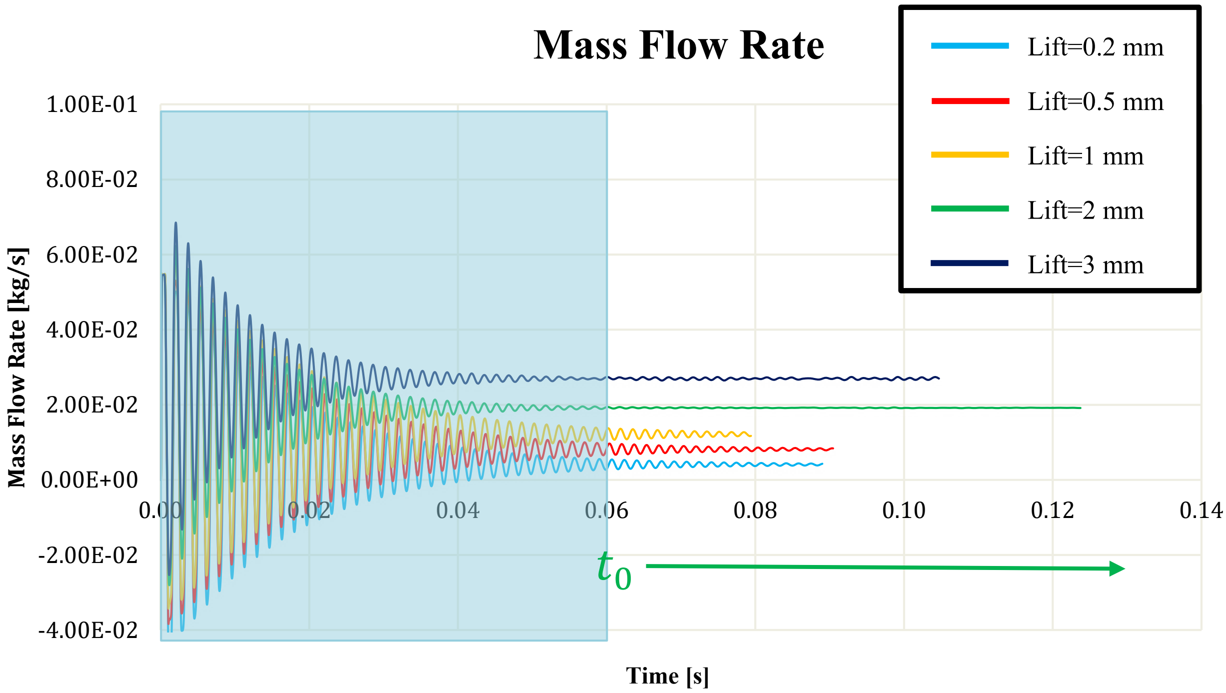

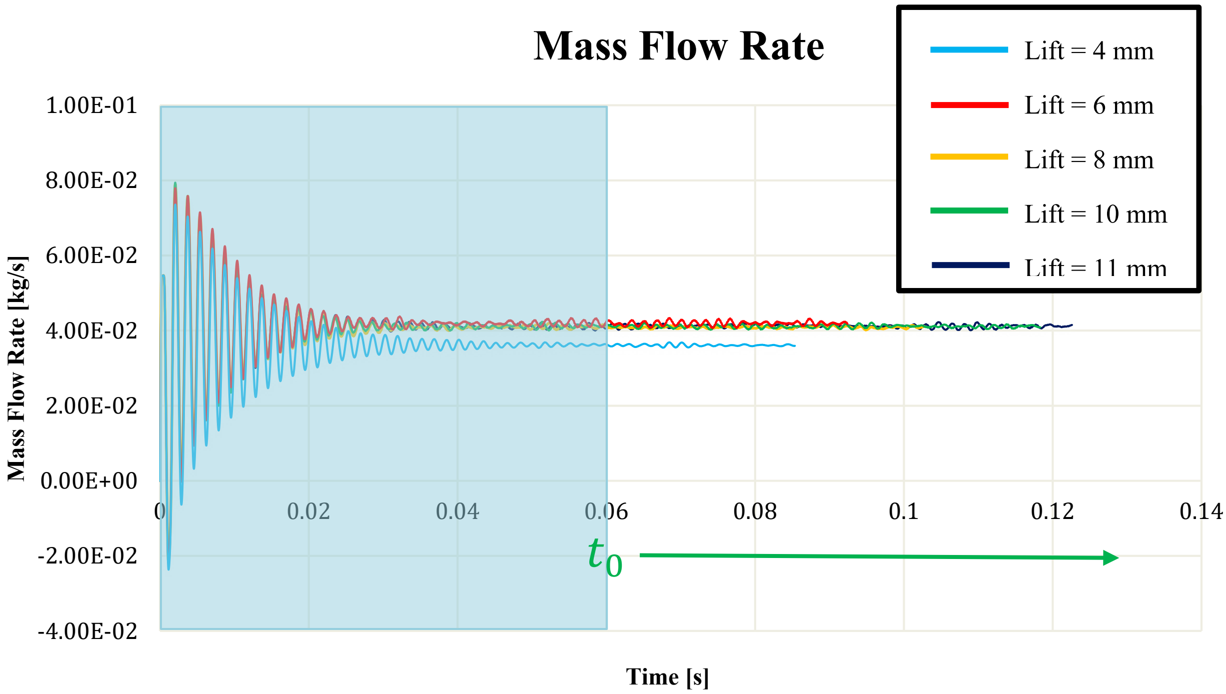

Figure 34: Mass Flow Rates for forward CDs

The results indicate that the air mass flow rate through the measurement region increases with valve lift up to approximately 6 mm, beyond which it remains nearly unchanged. This behaviour is attributed to the geometry of the intake ports, which limits the air flow into the cylinder beyond a certain valve lift.

In addition, the initial phases of the simulations are characterized by a transitional stage with high oscillations, reflecting the fact that the numerical solution has not yet reached convergence. For this reason, the mass flow rate was averaged, for each valve lift, over the time interval from $t_0 = 0.06$s to the end of the simulation. The resulting mean mass flow rates are reported in Table 30 as a function of the valve lift-to-reference diameter ratio (L/D).

Lift [mm]	L/D [-]	Mass Flow Rate [kg/s]
0	*0*	*0*
0.2	*0.008*	*0.004*
0.5	*0.020*	*0.008*
1	*0.040*	*0.012*
2	*0.081*	*0.019*
3	*0.121*	*0.027*
4	*0.161*	*0.036*
6	*0.242*	*0.042*
8	*0.323*	*0.041*
10	*0.403*	*0.041*
11	*0.444*	*0.041*

Table 30: Mean Mass Flow Rate through the measurement region

Once the mean flow rates had been determined, the discharge coefficients were calculated using the formulations presented in the previous chapter.

$$CD = \frac{\dot{m}}{A_R * \rho_{is} * U_{is}} \quad (8)$$

$$A_R = \frac{\pi * D_{REF}^2}{4} \quad (9)$$

The resulting values were compared with the corresponding experimental coefficients provided by IFPEN and previously implemented in the engine Digital Twin, as reported in Table 31.

Lift [mm]	L/D [-]	Forward CD [-]	IFPEN CD [-]
0	*0*	*0*	*0*
0.2	*0.008*	*0.040*	-
0.5	*0.020*	*0.081*	-
1	*0.040*	*0.121*	*0.122*
2	*0.081*	*0.190*	*0.192*
3	*0.121*	*0.267*	*0.263*
4	*0.161*	*0.357*	*0.346*
6	*0.242*	*0.416*	*0.396*
8	*0.323*	*0.405*	*0.390*
10	*0.403*	*0.407*	*0.383*
11	*0.444*	*0.408*	*0.381*

Table 31: Forward CDs values

Figure 35 compares the experimental and simulated discharge coefficient curves as a function of the L/D ratio.

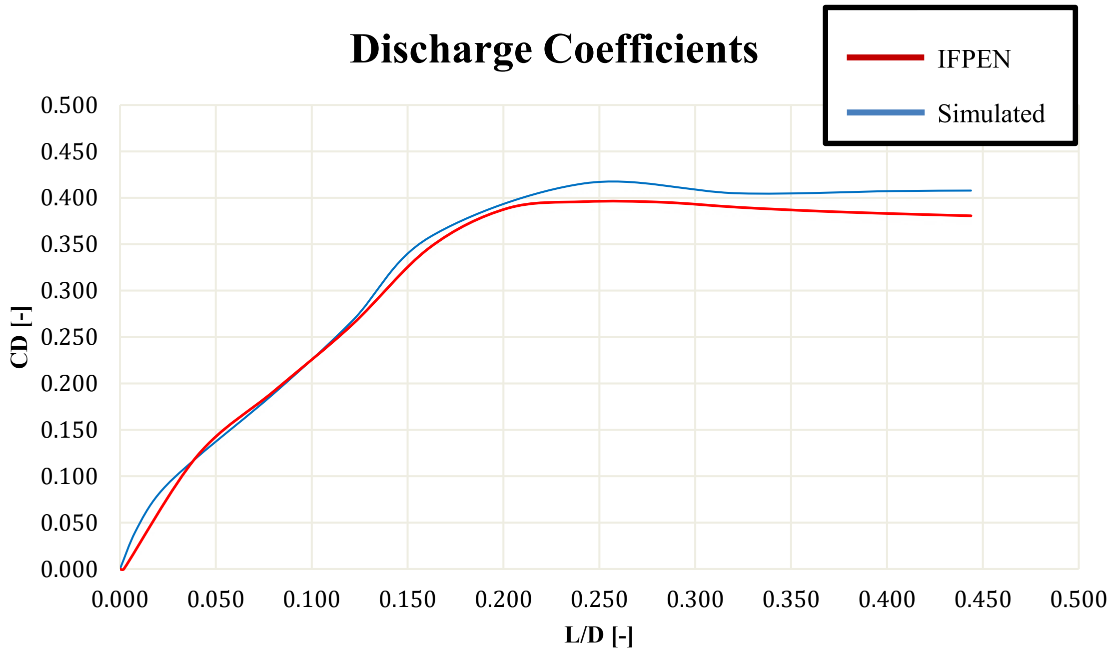

Figure 35: Forward CDs profiles

Similarly to the air mass flow rate through the measurement region, the discharge coefficients also reach their maximum value at intermediate valve lifts and then remain nearly constant as the lift increases.

The results indicate that the experimental data previously implemented in the model underestimated the forward discharge coefficients, particularly at medium-to-high valve lifts. Furthermore, the CFD simulations performed for valve lifts below 1 mm extended the dataset available for the engine Digital Twin, by providing discharge coefficients in a range where no experimental data were previously available, thereby improving the predictive accuracy of the engine model during the initial stages of the intake process.

The reverse discharge coefficients, required to characterize the backflow phenomenon associated with the Miller strategies, were determined using the same procedure adopted for the forward conditions. The different model configurations, each corresponding to one of the valve lifts listed in Table 29, provided the mass flow rate profiles from the cylinder to the intake plenum, as shown in Figure 36.

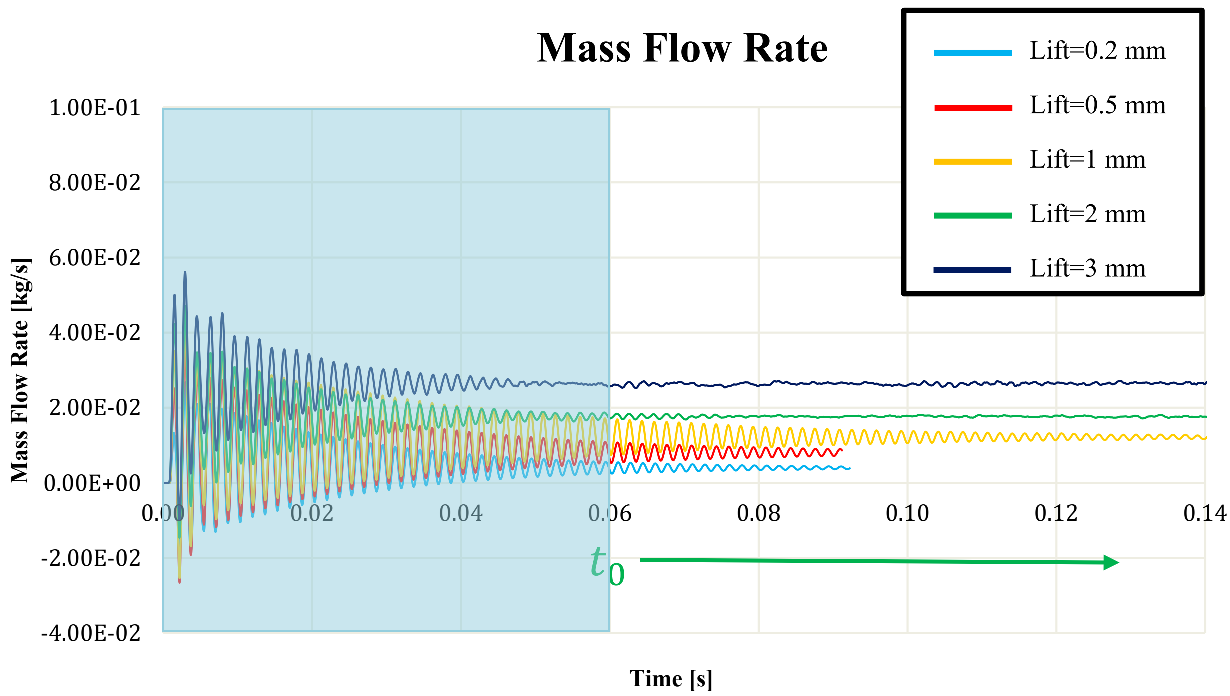

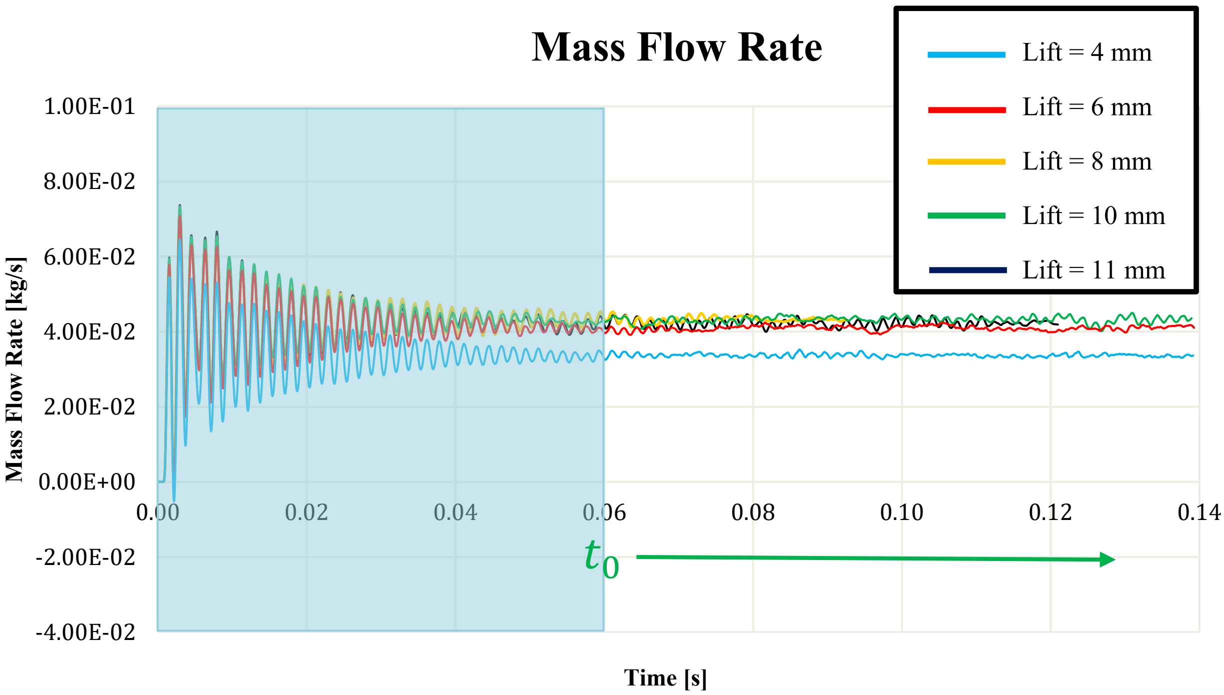

Figure 36: Mass Flow Rates for reverse CDs

Similarly to the forward discharge coefficients, the mass flow rate through the measurement region under reverse conditions increases with valve lift up to approximately 6 mm, beyond which it approaches a nearly constant value.

Compared with the forward CDs, the reverse simulations exhibit less stable flow rate profiles with larger oscillation amplitudes. This behaviour is mainly attributed to the geometry of the intake ports, which is designed to guide the flow efficiently under forward conditions while minimizing fluid-dynamic losses. Under reverse conditions, by contrast, the flow becomes more disturbed, resulting in a longer time for the numerical solution to reach convergence.

Nevertheless, the mean mass flow rate, calculated after excluding the initial transient characterized by the largest oscillations, remains sufficiently accurate. For each valve lift, it is comparable to the corresponding value obtained under forward conditions, as reported in Table 32.

Lift [mm]	L/D [-]	Forward Mass Flow Rate [kg/s]	Reverse Mass Flow Rate [kg/s]
0	*0*	*0*	*0*
0.2	*0.008*	*0.004*	*0.004*
0.5	*0.020*	*0.008*	*0.008*
1	*0.040*	*0.012*	*0.012*
2	*0.081*	*0.019*	*0.018*
3	*0.121*	*0.027*	*0.026*
4	*0.161*	*0.036*	*0.034*
6	*0.242*	*0.042*	*0.041*
8	*0.323*	*0.041*	*0.043*
10	*0.403*	*0.041*	*0.043*
11	*0.444*	*0.041*	*0.042*

Table 32: Intake valves Mass Flow Rate values

The reverse discharge coefficients, computed from the mean air mass flow rates, are listed in Table 33.

Lift [mm]	L/D [-]	Forward CD [-]	Reverse CD [-]
0	*0*	*0*	*0*
0.2	*0.008*	*0.040*	*0.039*
0.5	*0.020*	*0.081*	*0.080*
1	*0.040*	*0.121*	*0.122*
2	*0.081*	*0.190*	*0.175*
3	*0.121*	*0.267*	*0.261*
4	*0.161*	*0.357*	*0.334*
6	*0.242*	*0.416*	*0.405*
8	*0.323*	*0.405*	*0.429*
10	*0.403*	*0.407*	*0.428*
11	*0.444*	*0.408*	*0.419*

Table 33: Intake valves discharge coefficients values

Figure 37 compares the forward and reverse discharge coefficients obtained from the CFD simulations.

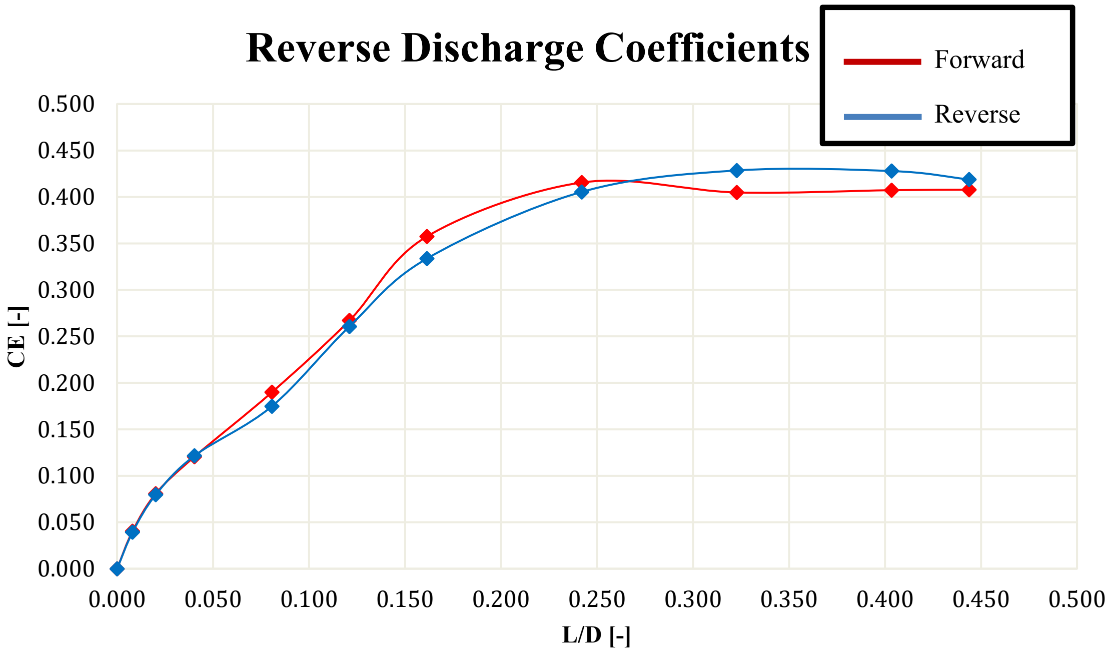

Figure 37: Discharge coefficients profiles

The reverse discharge coefficients have similar values to those obtained under forward conditions. In particular, they are slightly higher at medium-to-high valve lifts, whereas the differences become almost negligible at low valve lifts.

Since the backflow phenomenon occurs during the final stage of the intake process, when the valve lift is low, it is essential to determine the reverse discharge coefficients for lifts below 1 mm. Extending the simulations to this operating range therefore enabled a more accurate characterization of the backflow phenomenon, improving its representation within the engine Digital Twin.

The analysis of the discharge coefficients obtained from the 3D CFD simulations, together with their comparison with the experimental values, provides a more accurate characterization of the flow through the intake ports. In particular, at medium-to-high valve lifts, the calculated coefficients are in close agreement with the experimental measurements provided by IFPEN. Furthermore, the coefficients obtained for valve lifts below 1 mm provide a more detailed description of the initial and final stages of the intake process, improving the representation of the backflow phenomenon and the estimation of the trapped air mass inside the cylinder.

4.4 Conclusions

This chapter discussed the results of the numerical simulations performed on the engine model to assess the ability of the Digital Twin to reproduce the actual engine behaviour under different operating conditions.

First, the capability of the TPA model to accurately reconstruct the in-cylinder turbulence evolution during the cycle phases preceding ignition was evaluated. The results demonstrate good agreement between the reference and simulated data, regardless of engine speed, load, or charge dilution level. The accurate prediction of the TKE and LS profiles during the compression stroke enabled a more detailed description of the air–fuel mixing process, thereby enhancing the predictive capabilities of the Digital Twin.

Subsequently, the results of the flow bench analysis were examined. The CFD simulations extended the characterization of the discharge coefficients to valve lifts below 1 mm, improving the representation of the initial and final stages of the intake process. Under forward conditions, the results showed that the experimental dataset previously implemented in the Digital Twin underestimated the discharge coefficients by a maximum of 6% at high lifts. Furthermore, the reverse-flow simulations revealed significant backflow even at low valve lifts, confirming the importance of accurately characterizing this operating range to improve the representation of the intake process.

Overall, the results demonstrate that the proposed methodologies enable the engine behaviour to be reliably reproduced over a wide range of operating conditions. The integration of the TPA model with the CFD simulations enhanced the predictive capabilities of the Digital Twin by refining the simulation of the combustion process.

5 Vehicle Virtual Test Rig Results

5.1 Introduction

The aim of this chapter is to present the results obtained from the development of the vehicle virtual test rig described in Chapter 3 by comparing the simulation results with the experimental dataset provided by IFPEN. The objective of the analysis is to assess the model's ability to reproduce the behaviour of the hybrid powertrain under representative operating conditions and to evaluate its accuracy against the reference data.

To this end, the simulation results were compared with the experimental measurements acquired during roller bench tests conducted according to the WLTP procedure. For the C SUV-class PHEV demonstrator considered in this study, the speed profile of the analysed WLTC is reported in Figure 38.

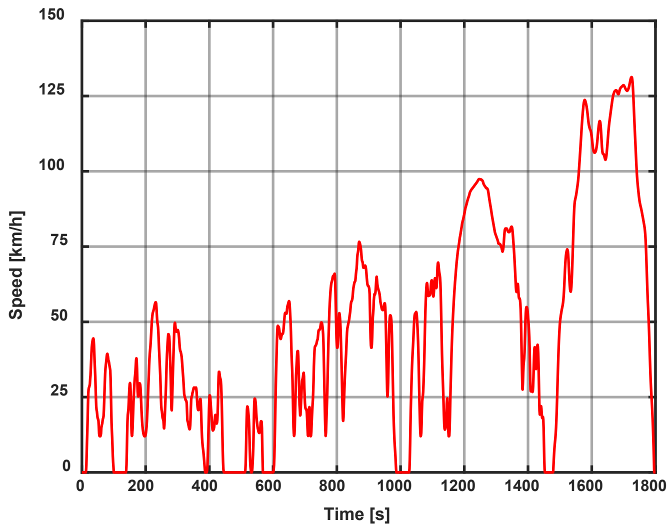

Figure 38: WLTC speed profile for a C SUV-class PHEV

This speed profile makes it possible to analyse the dynamic behaviour of the vehicle over a wide range of operating conditions, from an initial phase characterized by low speeds and frequent stops, representative of urban driving, to a final phase with higher speeds, typical of motorway operation.

The presentation of the results follows the main stages of the development of the Virtual Test Rig and the implementation of the Equivalent Consumption Minimization Strategy. First, the ability of the model to accurately follow the speed profile prescribed by the WLTP procedure is assessed. Subsequently, the calibration and validation results of the Virtual Test Rig are presented through a comparison with the experimental data acquired during a WLTC performed in Charge Sustaining mode. Particular attention is devoted to fuel consumption, average CO_2 emissions, and the evolution of the battery State of Charge throughout the driving cycle, as these parameters are fundamental for evaluating the energy and environmental performance of the PHEV demonstrator.

Overall, the analysis of the results makes it possible to assess the reliability of the Virtual Test Rig in reproducing vehicle behaviour, while also evaluating the contribution of the energy management strategy to optimizing the overall performance of the hybrid powertrain.

5.2 ECMS Implementation Results

Before proceeding with the calibration and validation phases of the Virtual Test Rig, the correct configuration of the vehicle model must be verified. To this end, the model capability to reproduce the speed profile prescribed by the WLTP procedure was assessed. The target speed profile was implemented in the model through the VehDriverAdvanced template.

Unlike a backward solution, in a forward simulation the driver template uses the target speed as a reference to determine the throttle, brake, and clutch commands required to follow the driving cycle. Therefore, the accurate reproduction of the speed profile is a fundamental requirement for ensuring the reliability of the subsequent analyses of the vehicle dynamic behaviour.

Figure 39 compares the speed profile obtained from the simulations with the corresponding reference curve provided by IFPEN.

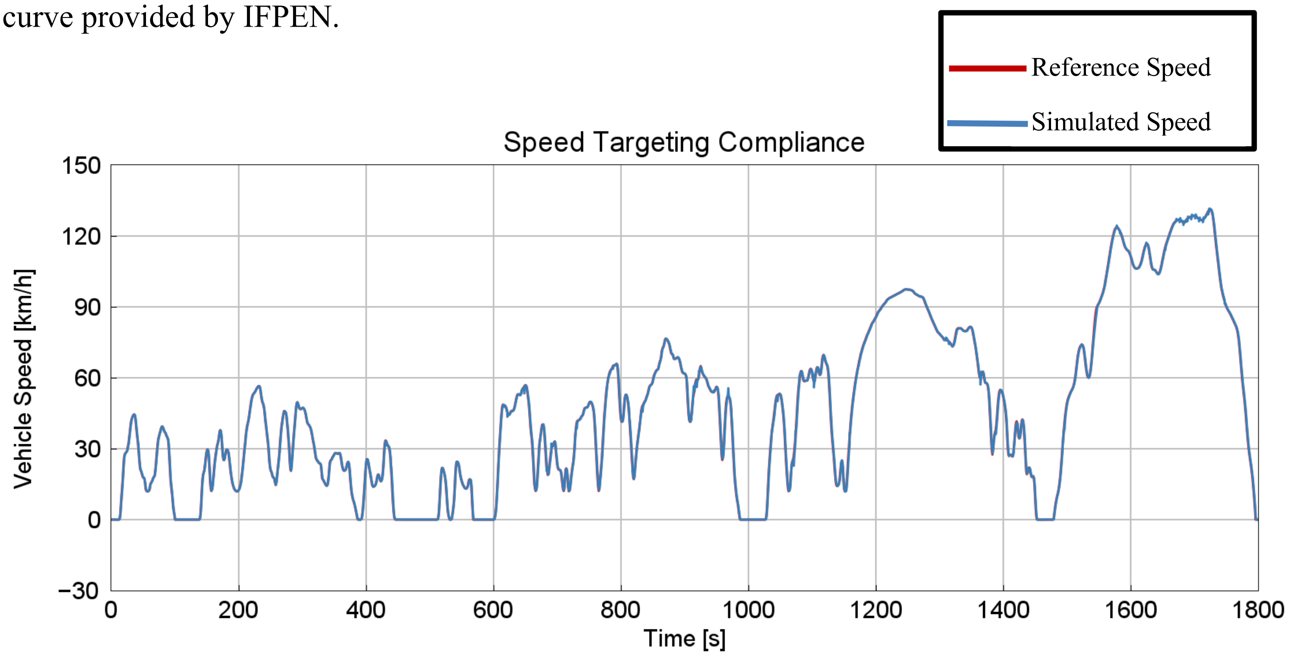

Figure 39: Simulated speed profile

The simulated speed profile shows excellent agreement with the target profile throughout the entire driving cycle, confirming the model's ability to accurately reproduce the WLTC prescribed by the regulations. The corresponding wheel torque request is shown in Figure 40.

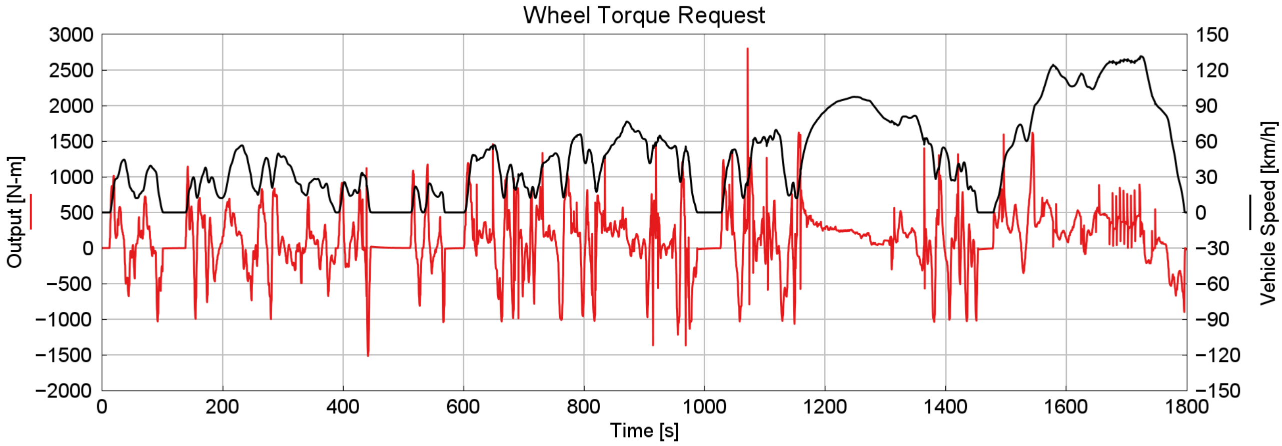

Figure 40: Wheel Torque Request

The obtained results are consistent with the speed profile. In particular, during acceleration phases, the requested wheel torque assumes positive values, providing the tractive force required to increase the vehicle speed, whereas during deceleration phases it becomes negative. A few minor exceptions can nevertheless be observed. For example, at the beginning of the final deceleration phase just after 1720 s, the requested wheel torque remains temporarily positive despite the decrease in vehicle speed. This behaviour is mainly caused by the transients associated with engine shutdown and gear shifts, whose overall effect is negligible over the entire driving cycle.

Having verified the model's ability to accurately reproduce the speed profile prescribed by the WLTP, the calibration of the Virtual Test Rig could then be carried out. The objective of this phase was to obtain a battery State of Charge at the end of the driving cycle consistent with the experimental value measured by IFPEN, while maintaining the same initial SOC.

WLTC – SOC Values	
Initial SOC	*22.6%*
Final SOC	*19.8%*

Table 34: Initial and final SOC values provided by IFPEN

The implementation of an ECMS-based control strategy introduces two key calibration parameters: the equivalence factor and the penalty function exponent. Following an extensive simulation campaign, the parameter values yielding the closest match between the simulated and experimental battery State of Charge at the end of the driving cycle were selected.

ECMS Calibration Parameters	
Equivalence Factor (s) [-]	*2.05*
Penalty Function Exponent (α) [-]	*1*

Table 35: Equivalence factor and penalty function exponent calibrated values

The resulting penalty function exhibits a piecewise linear trend as a function of the battery State of Charge, with a breakpoint at the target SOC. The target value was set equal to the initial SOC, since the WLTC considered in this study was performed in CS mode.

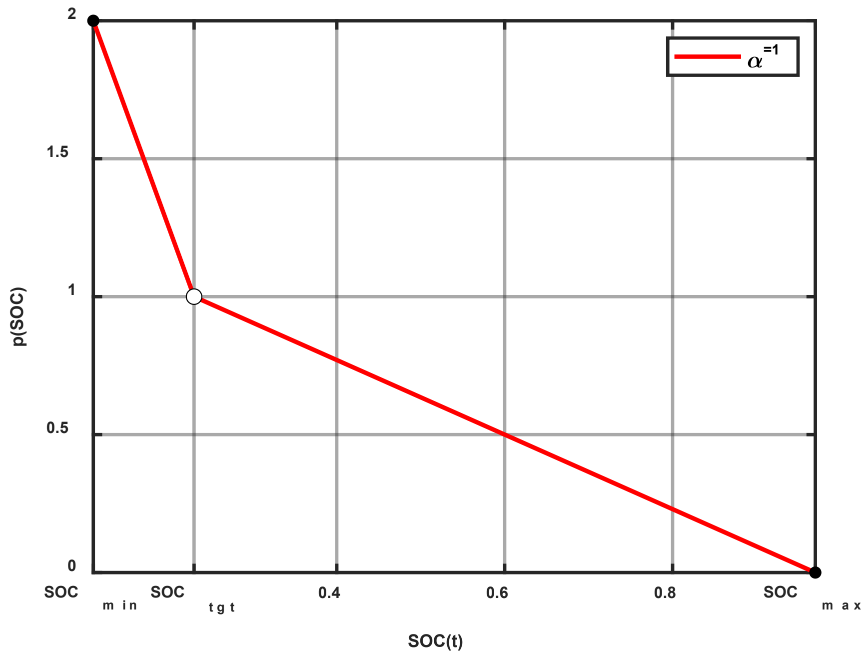

Figure 41: Penalty Function for alpha=1

After updating the calibration parameter values, the cost function and the penalty function are formulated as follows.

$$\dot{m}_{eqv} = \dot{m}_f + 2.05 * \frac{P_{batt}}{Q_{LHV}} * p \quad (10)$$

$$p(SOC) = 1 - \left(\frac{\max(SOC(t) - SOC_{tgt}, 0)}{SOC_{max} - SOC_{tgt}} + \frac{\min(SOC(t) - SOC_{tgt}, 0)}{SOC_{tgt} - SOC_{min}} \right)^1 \quad (11)$$

$$where \begin{cases} \dot{m}_{eqv}\ , \dot{m}_f\ , P_{batt}\ , SOC(t)\ , p(SOC)\ are\ obtained\ from\ the\ simulations \\ Q_{LHV},\ SOC_{max},\ SOC_{min}\ and\ \ SOC_{tgt}\ are\ numerical\ values \end{cases}$$

The numerical values of the parameters used in Equations (10) and (11) are listed in Table 36.

WLTC – CS mode	
$\boldsymbol{Q_{LHV}}$ *[MJ/kg]*	*41.51*
SOC_{max} *[%]*	*97*
SOC_{min} *[%]*	*11*
$\boldsymbol{SOC_{tgt}}$ *(in CS mode) [%]*	*23*

Table 36: ECMS main parameters

Figure 42 shows the evolution of the battery State of Charge throughout the WLTC simulation performed in Charge Sustaining mode, together with the vehicle operating mode.

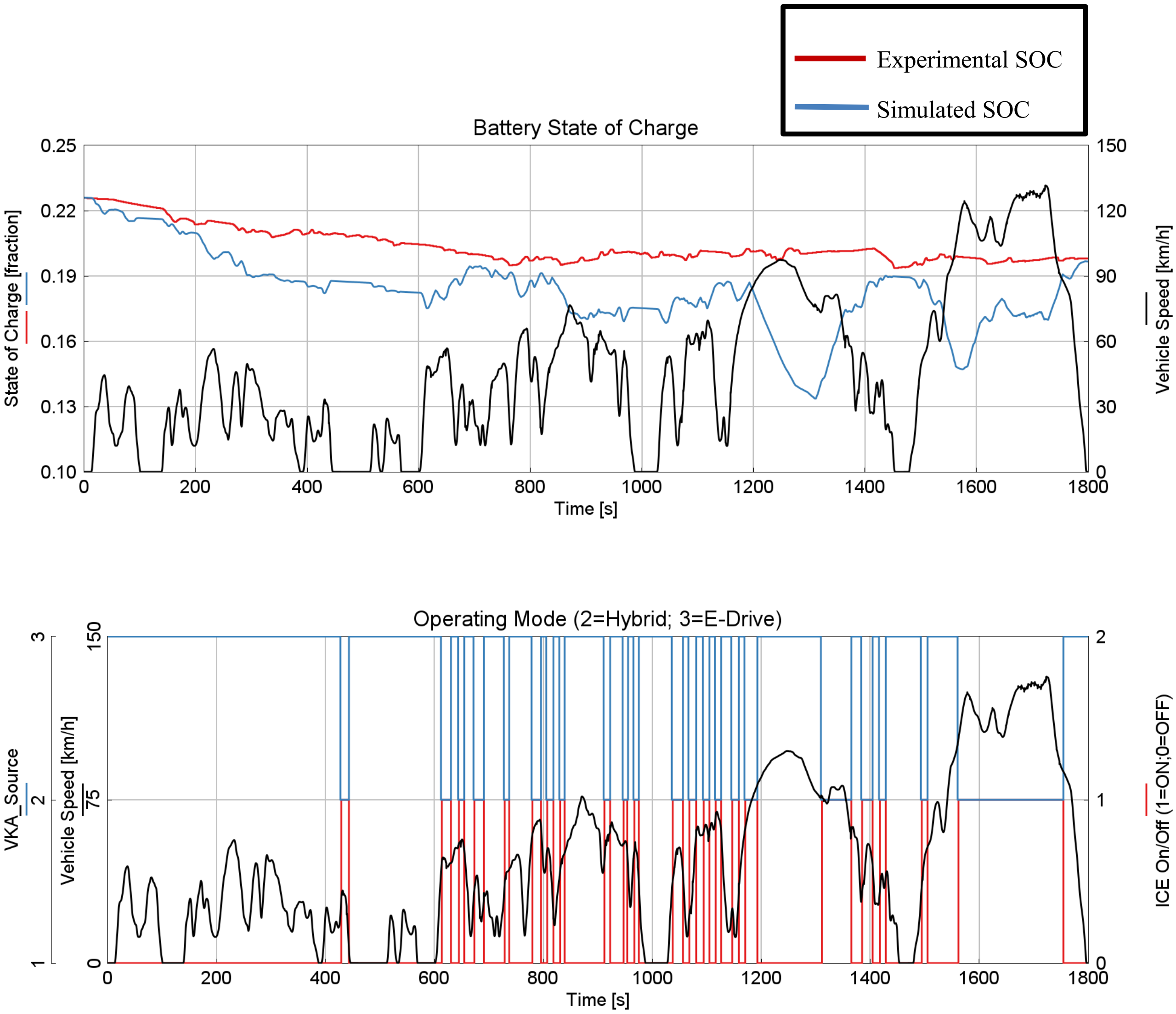

Figure 42: Battery SOC and vehicle operating mode

Compared with the experimental trend, the SOC obtained from the simulations remains lower throughout the entire driving cycle, with a maximum deviation of approximately 6%. However, the final value matches the one measured by IFPEN, confirming the correct calibration of the model. The differences observed in the SOC profile are mainly attributable to the vehicle operating strategy selected by the ECMS, which differs from the one adopted during the experimental roller bench tests.

During the initial phase of the cycle, the vehicle operates mainly in electric mode, resulting in a more pronounced SOC decrease compared with the experimental measurements. Similarly, in the time interval between approximately 1200 s and 1300 s, the internal combustion engine remains switched off, causing a further reduction in battery SOC. This energy is subsequently recovered both through regenerative braking and by operating the internal combustion engine under high-efficiency conditions, thus limiting fuel consumption. In the final part of the WLTC, the hybrid operating mode enables an additional energy recovery that, combined with regenerative braking, allows the SOC to be restored to the final value experimentally measured.

Moreover, Figure 42 highlights a slight delay between the activation of the internal combustion engine and the VKA_Source signal, which represents the operating mode selected by the surrogate model through the backward state optimization (electric mode when the signal is equal to 3 and hybrid mode when it is equal to 2). This delay is generated by the engine start-up transient, which ends when the Starter State condition is exceeded, corresponding to an engine speed below 900 rpm. To account for this behaviour, a Torque template was implemented, providing a torque contribution of 30 Nm, conventionally selected as approximately half of the maximum torque of the P0 electric machine. The effect of this component is illustrated in Figure 43.

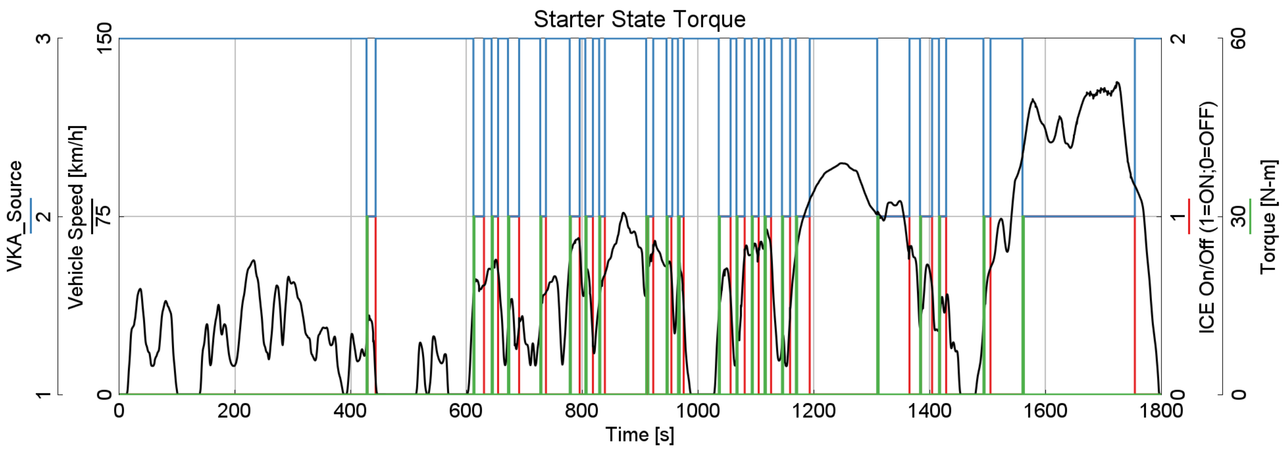

Figure 43: Starter Torque

The torque provided by the corresponding template is solely intended to ensure the start-up of the internal combustion engine and, therefore, is set to zero as soon as the ICE exits the Starter State phase.

In addition to the vehicle operating mode, the other Optimal Control Signals determined through the backward state optimization performed by the surrogate model concern the torque profiles of both the internal combustion engine and the two electric machines, which are reported below.

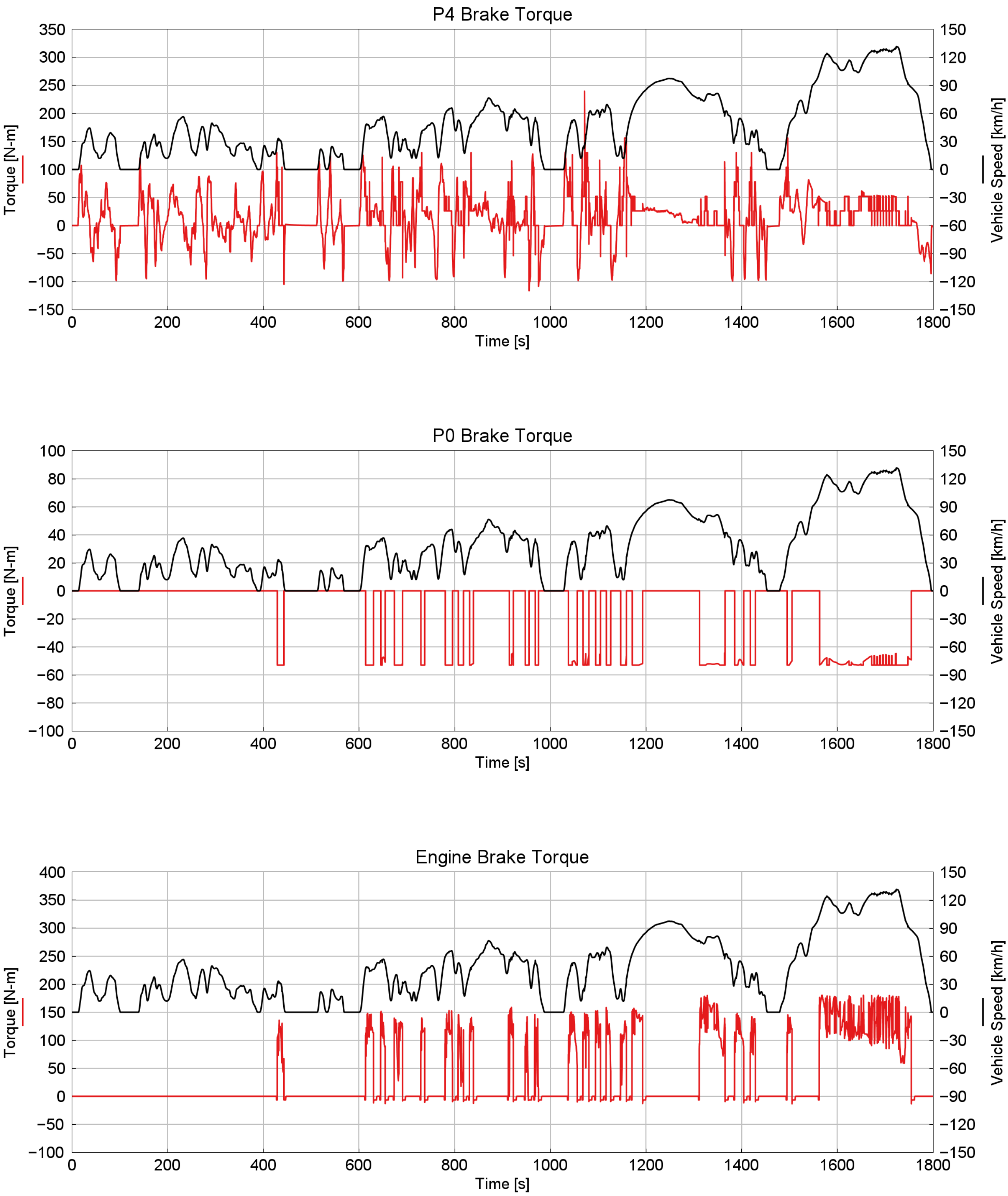

Figure 44: ICE, P0 and P4 Brake Torque profiles

During electric operating conditions, the P4 electric machine acts as the prime mover, representing the only source of torque delivered to the wheels. Consequently, positive torque values result in vehicle acceleration, whereas negative values lead to deceleration and enable energy recovery through regenerative braking. When the vehicle operates in hybrid mode, the P4 electric machine provides torque to the wheels in addition to the internal combustion engine. At the same time, the activation of the ICE enables energy recovery through the P0 electric machine. The negative torque values of the internal combustion engine are mainly associated with engine start-up and shutdown transients, and their effect on the simulation reliability is considered negligible.

The torque profiles of the two electric machines are also subject to two different operating constraints. The first is imposed by their respective torque-speed characteristic curves, whereas the second depends on the battery State of Charge. The VKA template implemented in the surrogate model ensures compliance with both constraints by modulating the torque request whenever required. In particular, the torque of the P0 electric machine is limited by its lower torque boundary, defined by its characteristic curve, which constrains the maximum energy recovery achievable during hybrid operation, as shown in Figure 45.

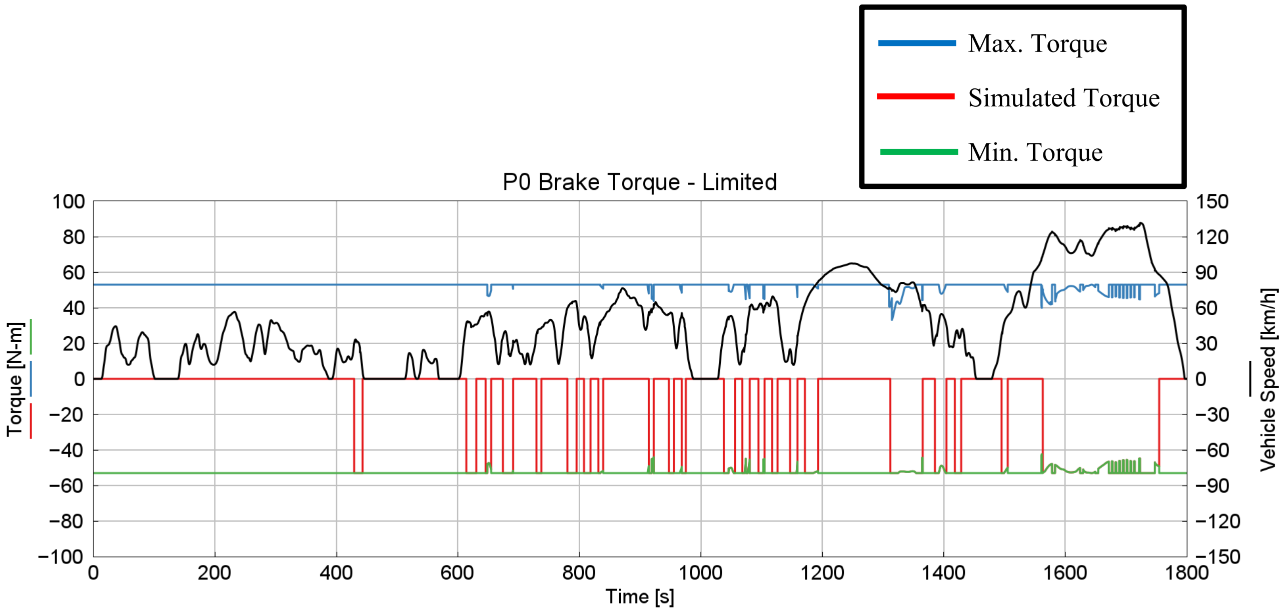

Figure 45: P0 Brake Torque and its limits

Conversely, the torque of the P4 electric machine is limited by the low battery State of Charge, which reduces the maximum achievable traction torque.

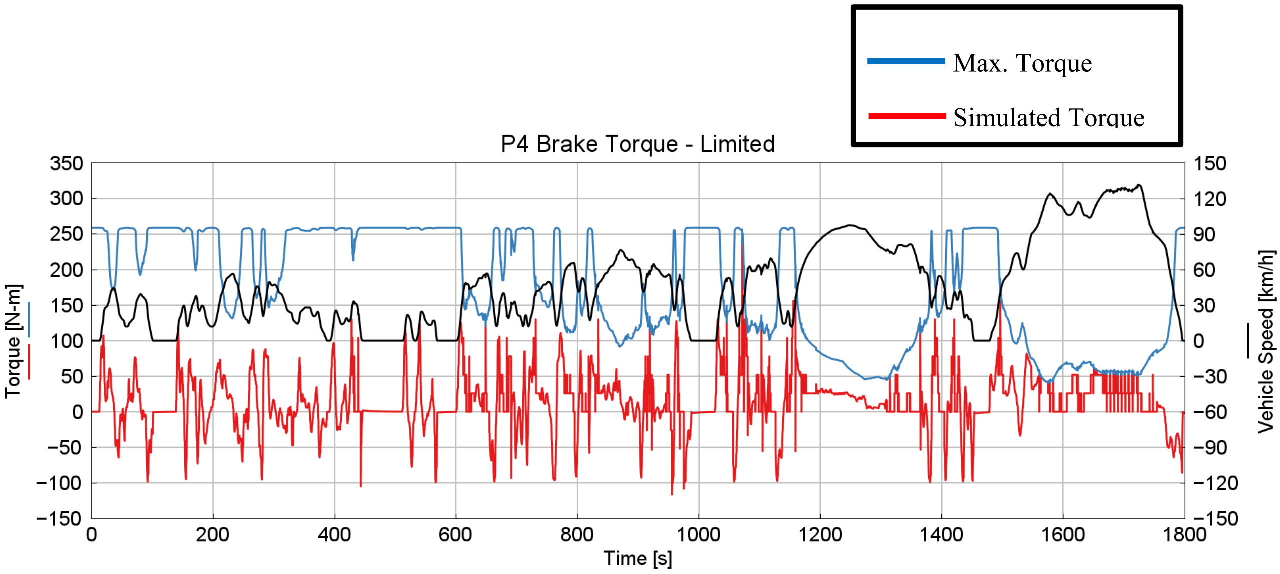

Figure 46: P4 Brake Torque and its upper limit

Regarding the transmission system, the gear shift profile obtained from the simulations is reported in Figure 47.

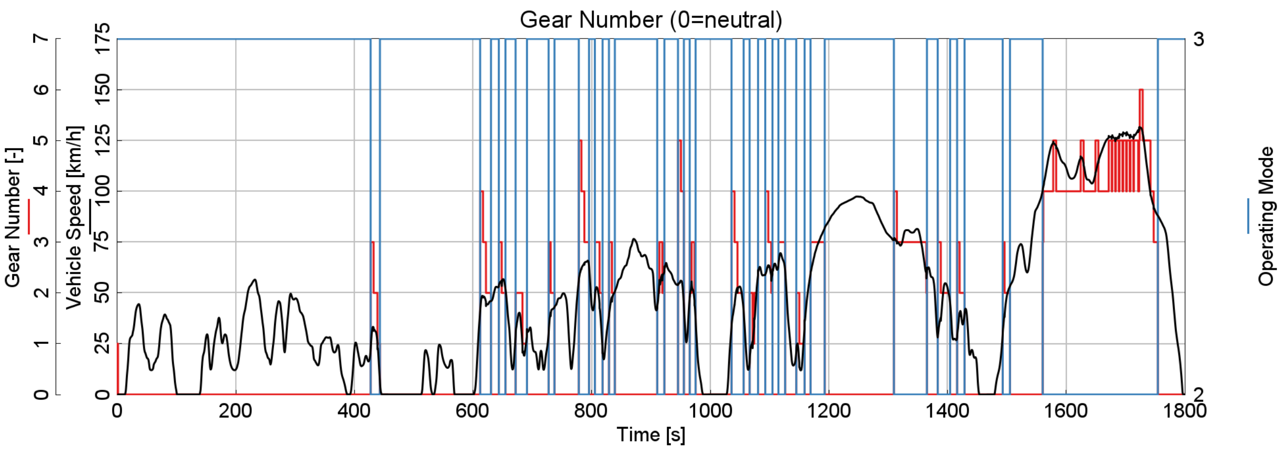

Figure 47: Gear Number profile

Since the vehicle under study is a PHEV with a P0 P4 hybrid architecture, neutral gear was imposed during electric operation, as the wheel torque is provided exclusively by the P4 electric machine, which is connected to the rear axle. During hybrid operation, instead, the correct implementation of the control strategy can be observed. In particular, when the internal combustion engine is active, only one gear per shift is allowed, avoiding physically unrealistic operating conditions, such as excessively high torque demands on the ICE caused by multiple simultaneous gear changes. The obtained results are consistent with the speed profile prescribed by the WLTP procedure and allow the ICE rotational speed to be maintained below the maximum limit of 5000 rpm, as shown in Figure 48.

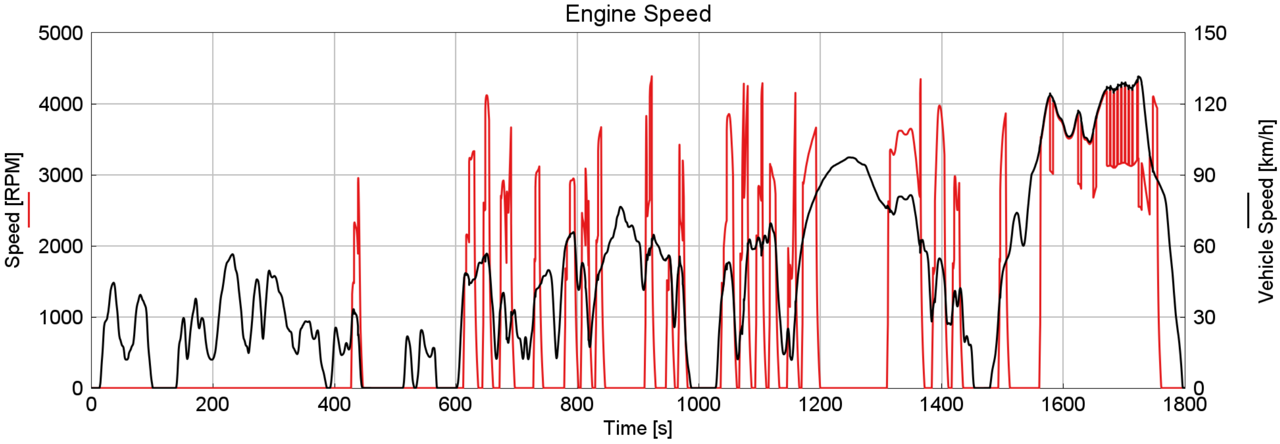

Figure 48: ICE Speed

The results show relatively high engine speed values, with peaks above 4000 rpm. This allows the internal combustion engine to operate under high-efficiency conditions, contributing to the reduction of fuel consumption over the driving cycle.

Starting from the ICE brake torque, the corresponding BMEP values can be derived, as reported in Figure 49.

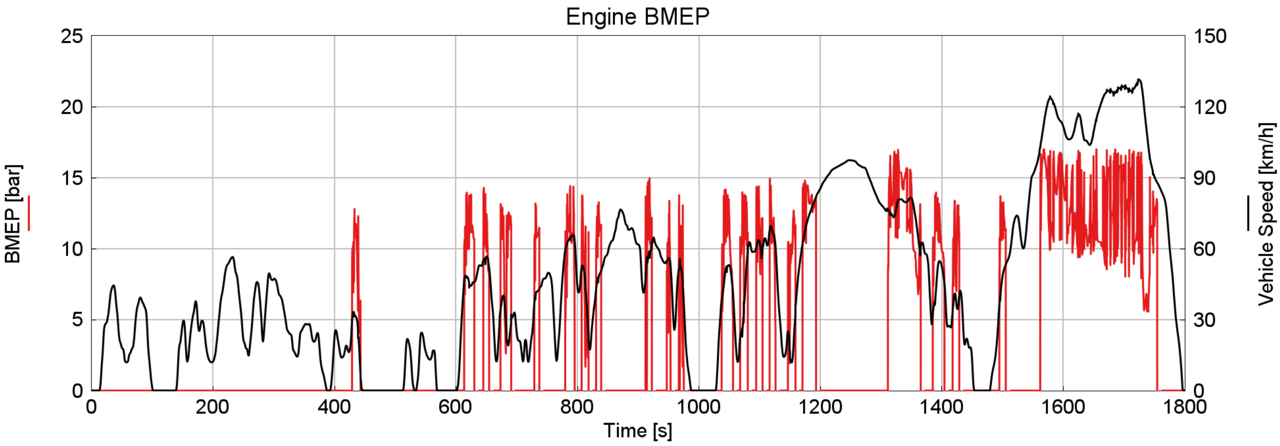

Figure 49: ICE BMEP

It is therefore possible to evaluate the Brake Specific Fuel Consumption (BSFC) as a function of the engine speed and the corresponding BMEP values. The BSFC is defined by the following relationship.

$$BSFC = \frac{1000 * \dot{m}_f}{BT * \omega} \quad (12)$$

$$
where \begin{cases} BSFC \text{ } is \text{ } the \text{ } Brake \text{ } Specific \text{ } Fuel \text{ } Consumption \text{ } [\frac{g}{kWh}] \\ \dot{m}_f \text{ } is \text{ } the \text{ } fuel \text{ } flow \text{ } rate \text{ } [\frac{g}{h}] \\ BT \text{ } is \text{ } the \text{ } ICE \text{ } Brake \text{ } Torque \text{ } [Nm] \\ \omega \text{ } is \text{ } the \text{ } engine \text{ } speed \text{ } [\frac{rad}{s}] \end{cases}
$$

The distribution of the engine operating points on the BSFC map is shown in Figure 50.

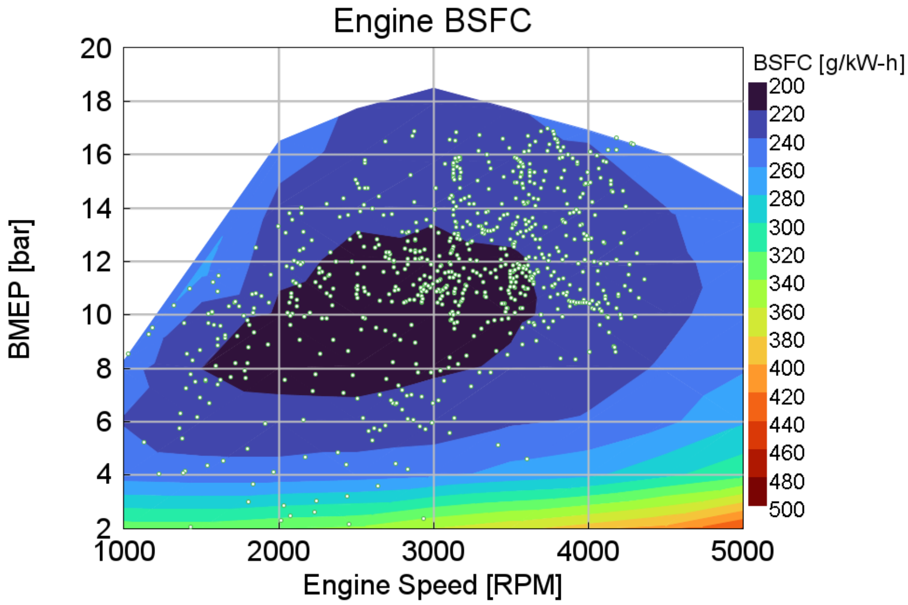

Figure 50: ICE BSFC Map

The operating points obtained from the simulations are mainly located within the regions of the map characterized by the lowest BSFC values. The main exceptions are represented by the low-load points, which are primarily associated with engine shutdown transients and the final shift to sixth gear, the latter being required due to the maximum engine speed limit imposed on the ICE. The points corresponding to high-load and medium-high engine speed conditions, although located further from the minimum BSFC region, still fall within operating areas characterized by high efficiency and low fuel consumption.

After verifying the correct calibration of the ECMS strategy, aimed at obtaining a final SOC value consistent with the experimental data provided by IFPEN, the model validation phase could be carried out. This phase focused on the comparison between simulated and experimental results in terms of average fuel consumption and average distance specific CO_2 emissions over the entire driving cycle. The obtained values are reported in Table 37.

Virtual Test Rig Validation	Experimental Data	Simulated Data
Average Fuel Consumption [L/100km]	*7.28*	*7.29*
Average Distance Specific CO_2 [g/km]	*165*	*166*

Table 37: Fuel Consumption and CO_2 emissions

The analysis of the results shows that the model is able to accurately estimate both fuel consumption and carbon dioxide emissions, achieving values in good agreement with those measured during the experimental roller bench tests. Although the implementation of the ECMS strategy enabled the optimization of the energy management, the simulations did not highlight any reduction in fuel consumption nor CO_2 emissions compared with the reference PHEV demonstrator. Nevertheless, the obtained results are considered satisfactory, especially given that the model is still at an early stage of the development process.

Overall, the simulations demonstrate that the Virtual Test Rig is able to reliably reproduce the behaviour of the PHEV demonstrator over the entire driving cycle prescribed by the WLTP procedure. The implementation of the ECMS strategy provides a good correlation with the experimental data, confirming the capability of the Virtual Test Rig to optimize energy management and estimate vehicle fuel consumption and CO_2 emissions.

5.3 Conclusions

This chapter presented the results related to the development, calibration, and validation of the Virtual Test Rig of the PHEV demonstrator within the PHOENICE project.

First, the analysis of the speed profile and the wheel torque request enabled the assessment of the correct implementation of the 0D map-based and 1D vehicle model within the simulation platform. The accurate reproduction of the speed profile prescribed by the WLTP procedure confirms the reliability of the model in reproducing regulatory driving cycles.

Subsequently, the implementation of an ECMS-based energy management strategy allowed the calibration of the vehicle model through a backward state optimization. The use of a specific cost function and penalty function, capable of accounting for asymmetrical SOC constraints with respect to the target value, enabled the calibration of the equivalence factor and penalty function exponent with the aim of obtaining a battery State of Charge at the end of the WLTC performed in Charge Sustaining mode consistent with the experimental data. The values identified for the two parameters through a trial-and-error procedure demonstrate the effectiveness of the Virtual Test Rig in reproducing the dynamic behaviour of the vehicle throughout the entire driving cycle, identifying the energy management strategy capable of achieving the experimentally measured SOC value at the end of the simulation.

The analysis of the torque profiles, BMEP, and engine speed further highlights the capability of the ECMS strategy to identify operating points characterized by high efficiency. The ICE operating points are mainly distributed close to the minimum BSFC curve or, in any case, within regions of the map characterized by low specific fuel consumption, confirming the correct management of power distribution between the internal combustion engine and the two electric machines.

Overall, the Virtual Test Rig proved to be a reliable tool for analysing the behaviour of the PHEV demonstrator during the driving cycle prescribed by the WLTP procedure. The good correlation between the numerical results and the experimental data confirms the validity of the adopted approach and provides a solid basis for the subsequent development of more advanced control strategies and for the extension of the model to additional vehicle operating scenarios.

6 Conclusions

The present thesis work was carried out within the framework of the European PHOENICE project, aimed at developing a Plug-in Hybrid Electric Vehicle demonstrator capable of reducing fuel consumption and emissions under real driving conditions while maintaining high levels of efficiency and performance. In this context, the main objective of the activity was the development of a simulation environment, consisting of the engine Digital Twin and the vehicle Virtual Test Rig, capable of reproducing the behaviour of the hybrid powertrain and supporting the implementation of energy management strategies.

The first part of the work focused on the optimization of the engine Digital Twin through the calibration of the Three Pressure Analysis model. Starting from the data obtained from 3D CFD simulations and from the dataset provided by the Politecnico di Torino, the capability of the model to reproduce the evolution of in-cylinder turbulence during the phases preceding combustion onset was analysed. The calibration activity allowed the identification of the turbulence parameters with the greatest influence on the prediction of the Turbulent Kinetic Energy and the Normalized Turbulent Length Scale, improving the correlation between the 1D model results and the reference data. The integration of the optimized parameters into the engine Digital Twin enhanced the predictive capability of the model, providing a more accurate description of the combustion process.

Subsequently, in order to further improve the representation of engine behaviour, a flow characterization activity was carried out through 3D CFD simulations of the single-cylinder model. This analysis allowed the determination of the intake valve discharge coefficients under both forward and reverse conditions, extending the available experimental dataset and characterizing the flow behaviour in the intake ports also at low valve lift values. The introduction of the new coefficients into the engine model enabled a more detailed description of the initial and final intake phases, including the backflow phenomenon associated with the Miller strategy based on Late Intake Valve Closing. The overall activities contributed to the optimization of the Digital Twin, enabling the reliable reproduction of engine behaviour over a wide range of operating conditions and refining the simulation of the combustion process.

The second part of the work concerned the development of the Virtual Test Rig of the PHEV demonstrator through the integration of powertrain, battery, and control system models within the GT-SUITE platform. The vehicle model was calibrated and validated by comparison with the experimental data provided by IFPEN, acquired during WLTC tests performed on a roller bench. The implementation of an energy management strategy based on the Equivalent Consumption Minimization Strategy allowed the optimization of power distribution between the internal combustion engine and the electric machines, calibrating the control parameters to achieve a final battery State of Charge consistent with the experimental value in Charge Sustaining mode. The results obtained highlighted the capability of the Virtual Test Rig to reproduce the dynamic and energetic behaviour of the vehicle, providing a reliable estimation of fuel consumption and CO_2 emissions throughout the driving cycle.

Despite the results achieved, the work presents some limitations. First, the vehicle model is based on a 0D and 1D map-based representation of the system, which does not allow a detailed evaluation of the mass and the heat transport in the thermal management system. Furthermore, the validation of the Virtual Test Rig was mainly performed through the comparison of fuel consumption and CO_2 emissions, without including additional energetic or thermal powertrain quantities.

Considering these aspects, possible future developments include an extension of the vehicle model validation, the integration of a thermal management system, and the introduction of an updated fast-running engine model, in order to evaluate the potential of the Digital Twin within the Virtual Test Rig in more extensive simulation scenarios. Another relevant area of interest concerns the development of more advanced energy management strategies and the application of the model to different driving cycles and operating conditions.

In conclusion, the work demonstrates how an approach based on the integration of highly detailed physics-based models can represent an effective tool for the development and optimization of next generation hybrid propulsion systems. The developed engine Digital Twin and vehicle Virtual Test Rig provide a reliable platform for powertrain performance analysis and for the assessment of new control strategies, contributing to the objectives of the PHOENICE project towards more efficient and low emission mobility, in line with the European regulatory framework.

Bibliography

[1] European Commission, “Proposal for a Regulation of the European Parliament and of the Council on type-approval of motor vehicles and engines and of systems, components and separate technical units intended for such vehicles, with respect to their emissions and battery durability (Euro 7) and repealing Regulations (EC) No 715/2007 and (EC) No 595/2009,” COM(2022) 586 final, 10 Nov. 2022.

[2] European Parliament and Council of the European Union, “Regulation (EU) 2024/1257 of the European Parliament and of the Council of 24 April 2024 on type-approval of motor vehicles and engines and of systems, components and separate technical units intended for such vehicles, with respect to their emissions and battery durability,” Official Journal of the European Union, 8 May 2024.

[3] European Economic and Social Committee, “'Fit for 55': delivering the EU's 2030 Climate Target on the way to climate neutrality,” COM(2021) 550 final, 24 Feb. 2022.

[4] European Parliament and Council of the European Union, “Regulation (EU) 2023/851 of the European Parliament and of the Council of 19 April 2023 amending Regulation (EU) 2019/631 as regards strengthening the CO_2 emission performance standards for new passenger cars and new light commercial vehicles in line with the Union’s increased climate ambition,” Official Journal of the European Union, OJ L 110, 25 Apr. 2023.

[5] J. Dornoff and F. Rodríguez, “Euro 7: The new emission standard for light- and heavy-duty vehicles in the European Union,” ICCT, Policy Update, Mar. 2024.

[6] G. Trentadue et al., “On-road emissions and energy efficiency assessment of a plug-in hybrid electric vehicle,” European Commission, Joint Research Centre, Report JRC105088, 2019.

[7] P. Plötz et al., “From lab-to-road: real-world fuel consumption and CO_2 emissions of plug-in hybrid electric vehicles,” Environmental Research Letters, vol. 16, no. 5, Art. no. 054078, 2021.

[8] L. Serrao, S. Onori, and G. Rizzoni, “A Comparative Analysis of Energy Management Strategies for Hybrid Electric Vehicles,” Journal of Dynamic Systems, Measurement, and Control, vol. 133, no. 3, Art. no. 031012, 2011.

[9] J. B. Heywood, Internal Combustion Engine Fundamentals, 2nd ed., McGraw-Hill Education, Oct. 2018.

[10] B. Hu, S. Akehurst, and C. Brace, “Novel approaches to improve the gas exchange process of downsized turbocharged spark-ignition engines: A review,” International Journal of Engine Research, vol. 17, no. 6, 2016.

[11] L. Teodosio, V. De Bellis, and F. Bozza, “Fuel Economy Improvement and Knock Tendency Reduction of a Downsized Turbocharged Engine at Full Load Operations through a Low-Pressure EGR System,” SAE International Journal of Engines 2015-01-1244, 2015.

[12] T. G. Leone and M. Pozar, “Fuel Economy Benefit of Cylinder Deactivation – Sensitivity to Vehicle Application and Operating Constraints,” SAE Technical Paper 2001-01-3591, SAE International Fall Fuels & Lubricants Meeting & Exhibition, 2001.

[13] K. Fridrichová, et al., “Overview of the Potential and Limitations of Cylinder Deactivation,” Renewable and Sustainable Energy Reviews, vol. 146, Art. no. 111196, 2021.

[14] R. Stanglmaier and C. Roberts, "Homogeneous Charge Compression Ignition (HCCI): Benefits, Compromises, and Future Engine Applications," SAE Technical Paper 1999-01-3682, 1999.

[15] K. Epping et al.,"The Potential of HCCI Combustion for High Efficiency and Low Emissions," SAE Technical Paper 2002-01-1923, 2002.

[16] E. Nakai et al., “Mazda SkyActiv-X 2.0L Gasoline Engine,” in 28th Aachen Colloquium Automobile and Engine Technology, 2019.

[17] T. Tahtouh, F. Millo, L. Rolando, G. Castellano et al., “A Synergic Use of Innovative Technologies for the Next Generation of High Efficiency Internal Combustion Engines for PHEVs: The PHOENICE Project,” SAE Technical Paper 2023-01-0224, 2023.

[18] T. Tahtouh, M. André, F. Millo, L. Rolando et al., “Development of a Digital Twin to Support the Calibration of a Highly Efficient Spark Ignition Engine,” SAE Technical Paper 2023-01-1215, 2023.

[19] T. Tahtouh et al., “A Methodology to Develop a Sustainable, High Efficiency Hybrid Propulsion System: The PHOENICE Project,” FISITA World Congress, 2023.

[20] L. Rolando, F. Millo, G. Castellano, T. Tahtouh, M. Andre, and F. Bocchieri, “A Numerical Model for the Virtual Calibration of a Highly Efficient Spark Ignition Engine,” Powertrains, Energy and Lubricants International Meeting, JSAE, 2023.

[21] M. Zagun, “Holistic Optimization of Energy Consumption of a Hybrid Powertrain with an ‘Equivalent Fuel Consumption Minimization Strategy’ Algorithm”, University Federation SouthWest Germany, Dec. 2020.